UNIVERSIDADE DE SÃO PAULO

FACULDADE DE CIÊNCIAS FARMACÊUTICAS

Programa de Pós-Graduação em Ciência dos Alimentos

Área de Bromatologia

English content starting on page 13

Effects of fungal- and plant-derived non-starch polysaccharides in macrophages

Victor Costa Castro-Alves

Tese para obtenção do grau de

DOUTOR

Orientador:

Prof. Tit. João Roberto Oliveira do Nascimento

São Paulo

2017

UNIVERSIDADE DE SÃO PAULO
FACULDADE DE CIÊNCIAS FARMACÊUTICAS
Programa de Pós-Graduação em Ciência dos Alimentos
Área de Bromatologia

Effects of fungal- and plant-derived non-starch polysaccharides in macrophages

Versão Original encontra-se no Serviço de Pós-Graduação da FCF/USP

Victor Costa Castro-Alves

Tese para obtenção do grau de
DOUTOR

Orientador:
Prof. Tit. João Roberto Oliveira do Nascimento

São Paulo
2017

Autorizo a reprodução e divulgação total ou parcial deste trabalho, por qualquer meio convencional ou eletrônico, para fins de estudo e pesquisa, desde que citada a fonte.

Ficha Catalográfica

Elaborada pela Divisão de Biblioteca e

Documentação do Conjunto das Químicas da USP

C355e

Castro-Alves, Victor Costa
Effects of fungal- and plant-derived non-starch polysaccharides in macrophages / Victor Costa Castro-Alves. - São Paulo, 2017.
94 p.

Tese (doutorado) - Faculdade de Ciências Farmacêuticas da Universidade de São Paulo. Departamento de Alimentos e Nutrição Experimental.
Orientador: Nascimento, Jo?o Roberto Oliveira do

1. immune system. 2. lipids. 3. polysaccharides. 4. chayote. 5. Pleurotus albidus. I. T. II. Nascimento, João Roberto Oliveira do, orientador.

Victor Costa Castro-Alves

Effects of fungal- and plant-derived non-starch polysaccharides on macrophages

Comissão Julgadora

da

Tese para obtenção do grau de Doutor

_____

Prof. João Roberto Oliveira do Nascimento

Orientador/ Presidente

_____

1° Examinador

_____

2° Examinador

_____

3° Examinador

_____

4° Examinador

São Paulo, _____ de 2017

To my mom, dad, brother, sister and wife

ACKNOWLEDGEMENTS

[redacted]

[redacted]

[redacted]

[redacted]

[redacted]

I am also acknowledge to the scholarship provided by the National Council for Scientific and Technological Development (CNPq; Grant #140839/2014-3; March 2014/June 2016) and by the São Paulo Research Foundation (FAPESP; Grant #2016/05083-0; Since July 2016).

I am acknowledge to the Nuclear Magnetic Resonance facility at Brazilian Biosciences National Laboratory (LNBio, CNPEM/MCTI, Campinas, Brazil) for the use of the nuclear magnetic resonance spectrometers (Proposal RMN #20318 and RMN #21463) and to the Laboratory for Surface Science (LNNano, CNPEM/MCTI) for the use of the atomic force microscopes (Proposal AFM #21276).

The Food Research Center (FoRC), CEPID-FAPESP (Research, Innovation and Dissemination Centers, São Paulo Research Foundation) funded this research (Grant #2013/07914-8).

RESUMO

CASTRO-ALVES, V. C. **Effects of fungal- and plant-derived non-starch polysaccharides in macrophages.** Tese (Doutorado em Ciências). Programa de Pós-Graduação em Ciência dos Alimentos, Faculdade de Ciências Farmacêuticas, Universidade de São Paulo, SP, Brasil, 94 p, 2017.

O consumo de polissacarídeos não-amido (PNA) de fungos e plantas tem sido associado a redução do risco de doenças cardiovasculares. Além de promoverem efeitos físicos no trato gastrointestinal e serem utilizados como substratos pela microbiota intestinal, os PNA podem interagir com células do sistema imune, como macrófagos, cruciais no reparo tecidual, metabolismo lipídico, e na defesa do organismo contra patógenos. Entretanto, os efeitos em macrófagos dependem da estrutura do PNA. Recentemente, foi observado que o chuchu (*Sechium edule*) e o fungo *Pleurotus albidus* são fontes de PNA com potencial efeito sobre macrófagos. Assim, foram avaliados os efeitos dos PNA do chuchu fresco e cozido em macrófagos. Além disso, foi otimizado um método para extração de polissacarídeos de cogumelo, e avaliada a estrutura e os efeitos biológicos dos PNA do *P. albidus* em macrófagos. Foi observado que os PNA do chuchu regulam a secreção de citocinas e o processo de fagocitose por macrófagos, e alterações na composição de PNA durante o cozimento tem um impacto em seus efeitos biológicos. Além disso, os PNA do chuchu induzem o efluxo de colesterol e regulam a expressão de genes necessários para a ativação do inflamassoma NLRP3 em macrófagos previamente tratados com cristais de colesterol. Também foi demonstrado que o método otimizado de extração de PNA de cogumelos reduz em até pela metade o tempo de extração normalmente empregado. Além disso, foi verificado que o *P. albidus* é fonte para extração de glicanos com efeitos em macrófagos. Os resultados também sugerem que os glicanos obtidos do *P. albidus* inibem em diferentes níveis a inflamação induzida por lipídeos e a formação de células espumosas, com efeitos significativos sobre a ativação do inflamassoma NLRP3. Tais diferenças parecem estar associadas à estrutura dos glicanos. Por fim, os resultados sugerem que os benefícios dos PNA do chuchu estão além dos seus efeitos físicos sobre o trato gastrointestinal, e que os PNA do *P. albidus* promovem benefícios que podem ser relevantes para explorar sua utilização como um alimento ou fonte para extração de ingredientes funcionais.

Palavras-chave: chuchu, lipídeos, *Pleurotus albidus*, polissacarídeos, sistema imune.

ABSTRACT

CASTRO-ALVES, V. C. **Effects of fungal- and plant-derived non-starch polysaccharides in macrophages.** Thesis (Doctoral degree in Science). Graduate Program in Food Science, Scholl of Pharmaceutical Sciences, University of São Paulo, SP, Brazil, 94 p., 2017.

The consumption of fungal- and plant-derived non-starch polysaccharides (NSP) have been associated with reduced risk of cardiovascular diseases and cancer. In addition to promote physiochemical effects on the gastrointestinal tract and serve as substrate for the intestinal microbiota to produce short-chain fatty acids, NSP can interact with immune system cells including macrophages, which are crucial for tissue repair, lipid metabolism and host defense against foreign substances and pathogens. However, the effects of NSP in macrophages depends on their structure. Recently, it was showed that the chayote (*Sechium edule*) and the fungus *Pleurotus albidus* are promising sources of NSP with potential immunomodulatory effects in macrophages. In this study, it was explored the effects of cooking on the composition of NSP from chayote and evaluated their biological effects in macrophages. Furthermore, it was optimized a method for the extraction of mushroom NSP and characterized the structure and biological effects of NSP from *P. albidus* in macrophages. Results showed that the NSP from chayote pulp regulate cytokine secretion and phagocytosis by macrophages, and minor changes in composition during cooking influences their effects in macrophages. Furthermore, NSP from chayote induces cholesterol efflux and inhibits the expression of genes required for NLRP3 inflammasome activation in macrophages previously exposed to cholesterol crystals. Then, it was showed that the optimized method for the extraction of NSP from mushroom reduces by up to half the extraction time commonly required. Furthermore, results showed that *P. albidus* is source of easily extractable glucans with biological effects in macrophages. Results also suggest that glucans from *P. albidus* inhibit lipid-induced inflammation and foam-cell formation at distinct levels, with significant effects on NLRP3 inflammasome activation. Taken together, the results suggest that the benefits of chayote NSP is beyond their physical properties on the gastrointestinal tract, and that the *P. albidus* NSP offers potential health benefits that might be of relevance as a functional food ingredient.

Keywords: chayote, immune system, lipids, *Pleurotus albidus*, polysaccharides.

LIST OF FIGURES

Figure 1 Schematic diagram of samples used in the study…….. 30

Figure 2 Cultivation of the basidiome from *Pleurotus albidus*……... 31

Figure 3 Profile and composition of chayote polysaccharides…….…... 44

Figure 4 Effects of polysaccharides from chayote on cell proliferation and toxicity…..… 46

Figure 5 Effects of chayote polysaccharides in macrophages exposed or unexposed to LPS or zymosan…….……..……..... 47

Figure 6 Effects of SeR in macrophage-like cells previously exposed or unexposed to cholesterol crystals (CC)……... 49

Figure 7 Effects of SeR on the expression of genes related with lipid efflux in macrophage-like cells previously exposed to cholesterol crystals (CC)..…..... 50

Figure 8 Effects of SeR in macrophage-like cells previously exposed to cholesterol crystals (CC) with phagocytosis blocked…….. 51

Figure 9 Effects of SeR on NLRP3 inflammasome activation in macrophage-like cells previously exposed to cholesterol crystals (CC)……..……. 53

Figure 10 Effects of SeR on priming of the NLRP3 inflammasome in macrophage-like cells previously exposed to cholesterol crystals (CC) or LPS..……..……... 54

Figure 11 Optimization steps and comparison of polysaccharides obtained with the original and the optimized method……..……..…. 56

Figure 12 Best tree of maximum likelihood analysis of *Pleurotus* species from Latin America……..... 57

Figure 13 Basidiome, yield of the submerged culture and profile of polysaccharides from *P. albidus*……..…. 59

Figure 14 Nuclear magnetic resonance (NMR) spectra of the polysaccharide from the cold water extract (PaCW) from the basidiome of *P. albidus*……..…….… 60

Figure 15 Nuclear magnetic resonance (NMR) spectra of the exopolysaccharide (PaEX) from the submerged culture of *P. albidus*…….……... 61

Figure 16 Nuclear magnetic resonance (NMR) spectra of the polysaccharide from the hot water extract (PaHW) from the basidiome of *P. albidus* ……..... 62

Figure 17 Nuclear magnetic resonance (NMR) spectra of the endopolysaccharide (PaEN) from the submerged culture of *P. albidus*…….. 63

Figure 18 Nuclear magnetic resonance (NMR) spectra of the polysaccharide from the hot alkali extract (PaHA) from the basidiome of *P. albidus*……...… 64

Figure 19 Effects of polysaccharides from *P. albidus* in macrophages …… 65

Figure 20 Effects of glucans from *P. albidus* in human macrophage-like cells previously exposed or not to modified LDL (acLDL) or cholesterol crystals (CC)……..…. 67

Figure 21 Effects of glucans from *P. albidus* on the expression of genes related to NLRP3 inflammasome activation and lipid efflux in human macrophage-like cells previously exposed to modified LDL (acLDL) or cholesterol crystals (CC)…..... 68

Figure 22 Effects of glucans from *P. albidus* on caspase-1-induced cell death in human macrophage-like cells exposed to cholesterol crystals (CC)……..…..……..... 70

Figure 23 Effects of polysaccharides from raw chayote (SeR) on lipid efflux and NLRP3 inflammasome in macrophage-like cells previously exposed to cholesterol crystals (CC)…….....… 75

LIST OF ABBREVIATIONS

ABCA1	ATP-binding cassette transporter A1
acLDL	acetylated low-density lipoprotein
AOAC	Association of Official Analytical Chemists
ASC	Adaptor protein apoptosis-associated speck-like protein containing a CARD
ATCC	American Type Culture Collection
ATP	Adenosine triphosphate
BCA	Bicinchoninic acid assay
BSA	Bovine serum albumin
CARD	Caspase activation and recruitment domain
CBA	Cytometric Bead Array
CC	Cholesterol crystals
CLCASP1	Cleaved caspase-1
COSY	Correlation spectroscopy
CytD	Cytochalasin D
DCFDA	2',7'-dichlorodihydrofluorescein diacetate
DF	Dietary fiber
DMEM	Dulbecco's modified Eagle's medium
EMMPRIN	Extracellular matrix metalloproteinase inducer
FAO	Food and Agriculture Organization
FBS	Fetal bovine serum
FFAR2	Free fatty acid receptor 2
FFAR3	Free fatty acid receptor 3
FI	Fluorescence intensity
FTIR	Fourier transform infrared spectroscopy
Glyb	Glyburide\Glibenclamide
GPR41	G protein–coupled receptor 41
GPR43	G protein–coupled receptor 43
HMBC	Heteronuclear multiple-bond correlation spectroscopy
HPAEC	High-performance anion exchange chromatography
HPSEC	High-performance size-exclusion chromatography
HSQC	Heteronuclear single quantum coherence

IL-1β	Interleukin 1 beta
IL-6	Interleukin 6
ITS	Internal transcriber space
LAL	Limulus amebocyte lysate
LDH	Lactate dehydrogenase
LPS	Lipopolysaccharide
LXRα	Liver X receptor alpha
Md	Media
MEA	Malt extract agar
MMP	Matrix metallopeptidase
MNP	Mean number of particles
MTT	3-(4,5-dimethylthiazol-2-yl)-2,5-diphenyltetrazolium bromide
MW	Molecular weight
MWCO	Molecular weight cut-off
MWD	Multiple wavelength detector
NLRP3	Nod-like receptor family pyrin domain containing protein 3
NMR	Nuclear magnetic resonance
NO	Nitric oxide
NSP	Non-starch polysaccharide
OD	Optical density
OM	Oyster mushroom
PaCW	Polysaccharides from the cold water extract of *Pleurotus albidus* basidiome
PAD	Pulse amperometric detector
PaEN	Endopolysaccharides from the submerged culture of *Pleurotus albidus*
PaEX	Exopolysaccharides from the submerged culture of *Pleurotus albidus*
PaHA	Polysaccharides from the hot alkaline extract of *Pleurotus albidus* basidiome
PaHW	Polysaccharides from the hot water extract of *Pleurotus albidus* basidiome
PDA	Potato dextrose agar
PI	Phagocytic index
PP	Percentage of phagocytosis
PPARγ	Peroxisome proliferator-activated receptor gamma
PRR	Pattern recognition receptor
qPCR	Quantitative polymerase chain reaction

RID	Refractive index detector
ROESY	Rotating-frame Overhauser spectroscopy
ROS	Reactive oxygen species
RPMI	Roswell Park Memorial Institute
SCFA	Short-chain fatty acid
SDS-PAGE	Sodium dodecyl sulfate polyacrylamide gel electrophoresis
SeC	Polysaccharides from cooked chayote (*Sechium edule*) pulp
SeH	Polysaccharides from hot aqueous extract of chayote (*Sechium edule*) pulp
SeR	Polysaccharides from raw chayote (*Sechium edule*) pulp
Sorb	Sorbitol
SR-A	Scavenger receptor A
TLR	Toll-like receptor
TNF-α	Tumor necrosis factor alpha
TOCSY	Total correlation spectroscopy
Tx	Triton X-100
UNG	Uracil-N glycoslyase

TABLE OF CONTENTS

1. INTRODUCTION..... 21

1.1. Dietary fiber: definition and physiological effects…..... 21

1.1.1. Direct effects of non-starch polysaccharides in macrophages…..... 22

1.1.2. Plant- and fungal-derived non-starch polysaccharides with potential effects on macrophage function…..... 24

1.2 Thesis outline…… 25

2. OBJECTIVE…..... 27

2.1. General objective..... 27

2.2. Specific objectives..... 27

3. MATERIAL AND METHODS..... 29

3.1. Materials..... 29

3.2. Samples..... 29

3.2.1. Production and identification of the basidiome from Pleurotus albidus….. 30

3.2.2. Production of submerged culture from Pleurotus albidus…..... 32

3.3. Extraction of polysaccharides..... 32

3.3.1. Extraction of polysaccharides from chayote fruit…..... 32

3.3.2. Optimization of extraction of polysaccharides from mushroom basidiome.. 33

3.3.3. Extraction of polysaccharides from the basidiome of Pleurotus albidus….. 34

3.3.4. Extraction of polysaccharides from the submerged culture of Pleurotus albidus…..... 34

3.4. Characterization of polysaccharides..... 34

3.4.1. General methods..... 34

3.4.2. Fourier transform infrared (FTIR) and 1D- and 2D-nuclear magnetic resonance (NMR) spectroscopy…..... 36

3.5. Endotoxin contamination..... 37

3.6. Preparation of cholesterol crystals (CC)…..... 37

3.7. Cell culture..... 37

3.7.1. Cell lines and treatment..... 37

3.7.2. Viability..... 38

3.7.3. Cytotoxicity..... 38

3.7.4. Detached cell counting..... 39

3.7.5. Cytokine secretion..... 39
3.7.6. Nitric oxide (NO) secretion..... 39
3.7.7. Reactive oxygen species (ROS) production..... 39
3.7.8. Phagocytosis of zymosan particles..... 40
3.7.9. Western blot..... 40
3.7.10. Quantitative real-time polymerase chain reaction (qPCR)..... 40
3.8. Statistical analysis..... 41
4. RESULTS..... 43
4.1. Effects of polysaccharides from raw and cooked chayote pulp in macrophages..... 43
4.2. Effects of polysaccharides from chayote on lipid-induced inflammation and foam cell formation……... 48
4.3. Optimization of extraction of polysaccharides from mushroom basidiome……... 55
4.4. Structure and effects of polysaccharides from the basidiome and submerged culture of *P. albidus* in macrophages..... 57
4.5. Effects of polysaccharides from *P. albidus* on lipid-induced inflammation and foam cell formation..... 66
5. DISCUSSION..... 71
5.1. Effects of polysaccharides from raw and cooked chayote pulp on macrophages..... 71
5.2. Effects of polysaccharides from chayote on lipid-induced inflammation and foam cell formation..... 73
5.3. Optimization of extraction of polysaccharides from mushroom basidiome……... 75
5.4. Structure and effects of polysaccharides from the basidiome and submerged culture of *P. albidus* in macrophages..... 76
5.5. Effects of polysaccharides from *P. albidus* on lipid-induced inflammation and foam cell formation..... 78
6. CONCLUSION..... 81
REFERENCES..... 83
APPENDIX A – Overview of activities (Student's sheet)..... 93

1. INTRODUCTION

Our diet has strong impact in our health and wellbeing. Thus, there is increasing interest in the study of food compounds that promote benefits beyond its basic nutritional. In this regard, the consumption of plant- and fungal-derived dietary fiber (DF) have been associated with reduced risk of cardiovascular diseases and cancer (1). DF promote benefits through several mechanisms. In this study, the effects of DF were focused in macrophages, which are cells crucial for tissue repair, lipid metabolism and host defense against foreign substances and pathogens.

1.1 Dietary fiber: definition and physiological effects

Defining DF has been both challenging and controversial because DF can be identified neither by a unique chemical entity nor by a group of related compounds and different DF may have one or more physiological function or health benefits. Despite issues on definition, mostly of DF is composed by monosaccharides linked together by glyosidic linkages, which are resistant to digestion and absorption in the human small intestine—with complete or partial fermentation in the large intestine by the gut microbiota (2). The starch, which is the main energy reserve in plants, is not considered a DF—except the resistant starches—since it can be absorbed in the human small intestine after hydrolysis. In contrast, non-starch polysaccharides (NSP) from fungal (e.g. mannan and β-glucan) and plant sources (e.g. hemicellulose and pectin), which generally have a structural function on source organisms, are not digested by human enzymes in the small intestine and therefore are not absorbed, being defined as a DF.

The consumption of DF promotes benefits through several mechanisms. DF affects absorption in the small intestine, thereby attenuating postprandial blood glucose and lipid levels. DF also delays gastric emptying, maintaining levels of satiety and contributing towards weight loss. However, the effects of DF were beyond physical effects on the gastrointestinal tract. The gut microbiota use DF to produce short-chain fatty acids (SCFA), which induce development of epithelial cells, maintaining the epithelial integrity and therefore host protection. SCFA also induce the growth of commensal bacteria and enhance mucus production, which limit the access of pathogenic bacteria to the gut (3,4). Furthermore, recent studies focused on the effects of SCFA on the short-chain free fatty acid receptors FFAR2/GPR43 and FFAR3/GPR41 in immune system cells (5). However, increased attention

have been focused on the investigation of another important mechanism that is not related to the production of SCFA: the direct effect of DF on immune system cells, especially phagocytes such as macrophages (6).

1.1.1 Direct effects of non-starch polysaccharides in macrophages

It is universally accepted that blood monocytes can be recruited to tissues where they give rise to transient macrophage populations. However, tissue resident macrophages also proliferate in specific conditions (7,8). Regardless if the macrophage is monocyte-derived or tissue resident, it interact with others cells mainly through secretion and perception of cytokines and chemokines, playing crucial roles ranging from development and repair, to lipid metabolism and innate immune responses against foreign materials or pathogens (9).

Since interest on finding alternative ways to regulate macrophage function is increasing, it has been extensively studied the direct effects of NSP in macrophages (6). Among the several types of fungal-derived NSP (e.g. heteropolymers, mannan and α-glucans), β-glucans were regarded as the main responsible for biological effects in macrophages. Notably, β-glucans obtained from distinct fungal species or extraction methods differ in size and structure and their physiochemical properties and biological effects change accordingly (10). Thus, there is a need for the investigation of the structure and biological effects of glucans from fungal species whose effects in macrophages is not yet known.

Plant-derived NSP also interact with macrophage receptors. However, several NSP from plant-derived foods have been neither chemically characterized nor evaluated for effects in macrophages. Since the structure of NSP differ according to the source or even within the same tissue from a species, it is also important characterize plant-derived NSP and evaluate their potential biological effects in macrophages. The complex structure of fungal- and plant-derived NSP allow the identification of several mechanisms by which they can interact with macrophages through different pattern recognition receptors (PRRs) including toll-like receptors (e.g. TLR2, TLR4), c-type lectin receptors (e.g. dectin-1, mannose receptor) and scavenger receptors (e.g. CD36, SR-A), thereby inducing a broad spectrum of responses (6).

Recently, it was shown that arabinogalactans enhance the macrophage phagocytic activity and host immune response against *Mycobacterium tuberculosis* in mice (11). Interestingly, nasal administration of a similar polysaccharide from acai (*Euterpe oleracea*) berry enhances macrophage resistance and increased the survival of mice with pulmonary infections (12). Furthermore, pectin and β-glucan enhanced phagocytic activity and induced

phenotypic changes in macrophages, respectively, and both NSP were shown to reduce the growth of tumors in mice (13,14). Several studies suggest that at least part of effects from NSP in response to pathogens and cancer cells is related to NSP-induced changes on cytokine and chemokine profile in macrophages, as showed for fucoidan, β-glucan, inulin, mannan and xyloglucan (15–17). These findings emphasize the need for study the relation between the chemical structure and effects of NSP. Notably, effects of NSP in macrophages were beyond of enhance the response against pathogens and cancer cells and cytokine profile. NSP also regulate lipid metabolism in macrophages (18–21).

Macrophages promote modified lipoprotein uptake mainly through scavenger receptors allowing reverse cholesterol transport (22), which is important to maintain low levels of highly reactive modified lipoproteins. However, during hypercholesterolemia, increased levels of modified low-density protein (mLDL) and the formation of cholesterol crystals (CC) acts as pro-inflammatory signals for macrophages, impairing the reverse cholesterol transport to liver. The increased intracellular lipid content lead to the formation of pro-inflammatory lipid-laden macrophages, called foam cells (23). Furthermore, intracellular nucleation of mLDL and phagocytosis of CC promotes NLRP3 (Nod-like receptor protein 3) inflamasome activation (24) and therefore pro-inflammatory cytokine and chemokine secretion, reactive oxygen species (ROS) production and caspase-1-induced cell death, contributing towards a pro-inflammatory microenvironment, which is an important risk factor for atherosclerosis (25). The enhanced exposure of monocytes to mLDL also promote epigenetic histone modifications, which induces a long-lasting macrophage phenotype with increased mRNA levels of pro-inflammatory cytokines and matrix-degrading proteins, such as metalloproteinases (26).

In the past few years, it have been shown that some NSP inhibit foam-cell formation and lipid-induced inflammation through reduction of lipid influx and/or enhancement of lipid metabolism and efflux (18–21). Despite further studies are needed, effects of NSP on lipid metabolism in macrophages promote potential health benefits that may reduce risk of diseases and disorders associated with hypocholesterolemia.

1.1.2 Plant- and fungal-derived non-starch polysaccharides with potential effects in macrophage function

Although some plant- and fungal-derived NSP have effects in macrophages clearly defined, it is noteworthy that several NSP from food sources were not been evaluated for their effects in macrophages.

Recently, our research group showed that chayote—a fruit from *Sechium edule* (Jacq.) Swartz widely consumed in Latin America, especially in Brazil—is source of NSP including homogalacturonans and rhamnogalacturonans highly substituted with arabinan, galactan and arabinogalactans (27). Notably, NSP with a similar composition to those found on chayote enhanced the innate immune response against tumors, reduced the adverse effects of chemotherapy in animal models and showed immumodulatory effects in macrophages (28,29). Thus, the study of NSP from chayote fruit in macrophages will expand the understanding of how chayote consumption promote health benefits. Furthermore, as chayote fruit is usually consumed after cooking and heating, the processing might solubilize or degrade NSP (30). Thus, the composition and effects of NSP from both the cooked chayote fruit and from the hot aqueous extract obtained after heating should be explored.

Among the fungal sources of NSP with potential effects in macrophages, there is an increasing interesting on the study of mushrooms from *Pleurotus* species, also called oyster mushrooms (OM). OM are one of the most consumed class of edible mushrooms worldwide (31). The increased interest in the study of OM is attributed not only to its nutritive and biological effects, but also to their potential for bioremediation and bioconversion of agricultural residues (32). However, although some native OM have potential commercial relevance, their health effects were poorly explored (33).

Pleurotus albidus (Berk.) Pegler, a South American species of OM, have been proposed for commercial production due to its high biological efficiency in culture conditions and the qualities of its edible basidiome (33,34). Furthermore, *P. albidus* can be used for bioconversion of residual substrates as it mycelium can be easily cultivated on agricultural waste producing relatively large amount of biomass (35). Cultivation of *P. albidus* may also contribute to a reduction in the environmental impact of the biofuel industry because of its high efficiency in bioconversion of the vinasse, which is a by-product of sugarcane fermentation during alcohol production (36). However, the potential health effects of NSP from the mycelium and basidiome of *P. albidus* remain poorly understood. Besides, a systemic review of articles published until 2016 revealed more than 40 studies in which was

evaluated the effects of NSP—especially β-glucans—from OM in macrophages, and *P. albidus* was not the source of NSP in neither of these studies (personal information). Thus, the study of the mycelium and basidiome of *P. albidus* as a source of biologically active NSP is needed.

In this study, both chayote fruit and the fungus *P. albidus* were explored as source of biologically active NSP with potential biological effects in macrophages. Firstly, it was investigated the effects of cooking on the composition and effects of polysaccharides from chayote pulp in macrophages. Then, polysaccharides from chayote were also evaluated in in human macrophage-like cells unexposed or exposed to cholesterol crystals. Furthermore, to explore the composition and structure of polysaccharides from the basidiome of *P. albidus*, it was optimized a method for the extraction of mushroom polysaccharides. Then, polysaccharides from both the basidiome and the submerged culture of the mycelium from *P. albidus* were characterized and investigated for their effects in macrophages. Finally, it was investigated the effects of polysaccharides from *P. albidus* on foam cell formation and lipid-induced inflammation in human macrophage-like cells.

1.2 Thesis outline

Section 3 describes all material and methods used in this Thesis.

The Results (**section 4**) were separated into five sub-sections; each one covering a specific objective of the Thesis. **Section 4.1** detailed the results from the evaluation of effects of polysaccharides from raw and cooked chayote pulp in macrophages, which was published in the *Food Research International* (doi: 10.1016/j.foodres.2016.01.017) (37). Then, it was described the results from the evaluation of polysaccharides from chayote on lipid-induced inflammation and foam cell formation in human macrophage-like-cells (unpublished results; **section 4.2**). In **section 4.3**, it was described the results from the optimization of extraction of polysaccharides from mushroom basidiome, which was published in the *Food Analytical Methods* (doi: 10.1007/s12161-016-0406-9) (38). **Section 4.4** describes the characterization and evaluation of biological effects of polysaccharides from the basidiome and submerged culture of *P. albidus*, which was published in the *International Journal of Biological Macromolecules* (doi: 10.1016/j.ijbiomac.2016.11.059) (39). Then, it was described the effects of polysaccharides from *P. albidus* on lipid-induced inflammation and foam cell formation (submitted; **section 4.5**).

The Discussion (**section 5**) was separated in five sub-sections (**sections 5.1** to **5.5**), each one covering the discussion about results described in **sections 4.1** to **4.5**. The main findings of the study along with a general conclusion are included in Conclusion (**section 6**). The bibliography, numbered and formatted in Vancouver style, were included in **References section**.

2. OBJECTIVE

2.1 General objective

Evaluate the effects of non-starch polysaccharides from chayote fruit and the fungus *Pleurotus albidus* in macrophages.

2.2 Specific objectives

a) Evaluate the effects of polysaccharides from raw and cooked chayote in macrophages;

b) Evaluate the effects of polysaccharides from chayote on lipid-induced inflammation and foam cell formation in human macrophages-like cells;

c) Optimize a method for the extraction of mushroom polysaccharides;

d) Characterize the polysaccharides from the basidiome and submerged culture of *P. albidus* and evaluate their effects in macrophages;

e) Evaluate the effects of polysaccharides from *P. albidus* on lipid-induced inflammation and foam cell formation in human macrophage-like cells.

3. MATERIAL AND METHODS

3.1 Materials

Yeast extract, peptone and agar were purchased from BD Biosciences (Franklin Lakes, USA). Potato dextrose agar (PDA) and malt extract were purchased from Kasvi (Curitiba, Brazil). Dulbecco's modified Eagle (DMEM) and Roswell Park Memorial Institute 1640 media (RPMI) containing penicillin (100 UI/mL) and streptomycin (100 µg/mL) and heat-inactivated fetal bovine serum (FBS) were purchased from Cultilab (Campinas, Brazil). Heat-stable α-amylase from *Bacillus licheniformis*, amyloglucosidase from *Aspergillus niger* and endopolygalacturonase from *A. aculeatus* were purchased from Megazyme International (Wicklow, Ireland). Trypan blue dye was purchased from Bio-Rad (Hercules, USA). Sodium hydroxide (NaOH), acetylated low-density lipoprotein (acLDL), RIPA buffer and Halth protease inhibitor cocktail were purchased from Thermo (Waltham, USA). Water was from a Milli-Q purification system from Millipore (Bedford, MA). Unless stated otherwise, other reagents and chemicals were from Sigma-Aldrich (St. Louis, USA).

3.2 Samples

Chayote fruits from the green variety and ready to be consumed were purchased in a local market (São Paulo, Brazil). The fruits from two independent samplings (each one containing at least 8 fruits) weighing 450–500 g were firm, fresh in appearance, free of foreign smell and taste and with no apparent defects in shape or skin, being classified as “extra” according to FAO guidelines (40).

The basidiome from *Pleurotus ostreatus* used to optimize the method for the extraction of mushroom polysaccharides was purchased in a local market (São Paulo, Brazil). Three independent samplings containing approximately 500 g of fresh mushroom were used. The basidiome from *P. albidus* was collected from *Araucaria angustifólia* (Bertol.) Kuntze trunk in Serra da Bocaina (Rio de Janeiro, Brazil). The tissue culture from the collected basidiome was used to produce two samplings and the submerged culture was produced using the mycelium deposited at the collection from the Algae, Cyanobacteria and Fungi Culture Collection of the Botanic Institute of São Paulo (accession CCIBt4244).

As shown in **Figure 1**, the basidiome of *P. ostreatus* were used only to optimize the method for the extraction of mushroom polysaccharides, whereas chayote fruits and the mycelium and basidiome of *P. albidus* were used as source for the extraction of polysaccharides with potential effects in macrophages.

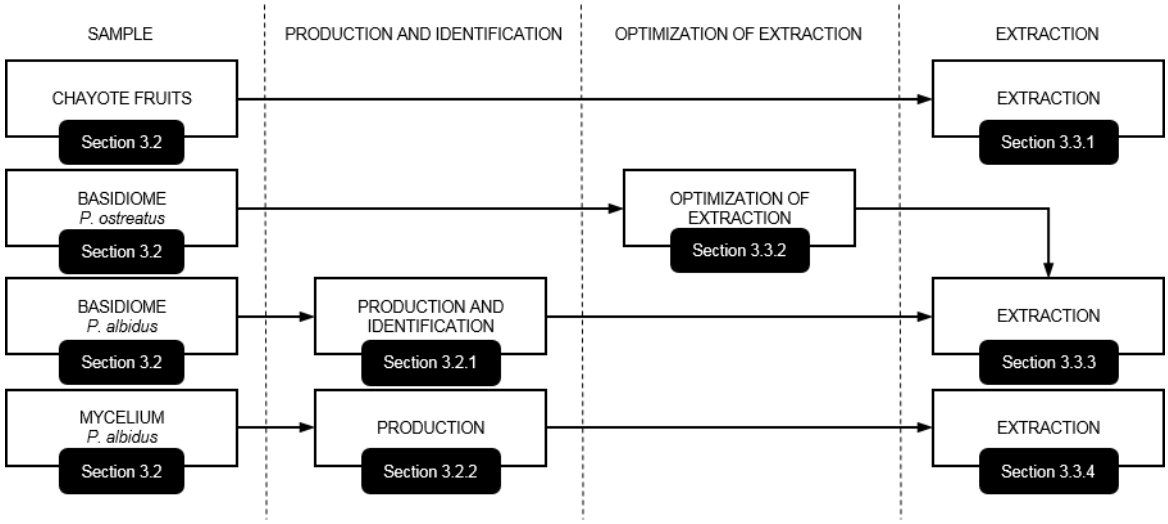

Figure 1. Schematic diagram of samples used in the study. Information about the samples and methods can be found at indicated sections (in black). Chayote fruits were used for the extraction of polysaccharides from raw (SeR) and cooked chayote pulp (SeC) and from the hot water extract obtained during cooking (SeH). The basidiome of *Pleurotus ostreatus* was used to optimize the method for the extraction of mushroom polysaccharides. The basidiome of *P. albidus* was produced in polyethylene bags for the extraction of polysaccharides from the cold (PaCW) and hot water (PaHW) and hot alkali extract (PaHA). Finally, the mycelium of *P. albidus* was produced in submerged culture for the extraction of endo- (PaEN) and exopolysaccharides (PaEX).

3.2.1 Production and identification of the basidiome from Pleurotus albidus

The mycelium from the collected basidiome was cultured in PDA (25 °C; 7 d). Then, mycelial discs from the culture were used for spawn production in wheat grain. The wheat grain was soaked overnight in tap water, drained, autoclaved and inoculated with mycelial discs (25 °C; 15 d) to produce the spawn. Then, polyethylene bags containing *Brachiaria brizantha* (Hochst.) Stapf. hay were humidified, sterilized and inoculated with the spawn (2% w/w). The spawn run was performed in a mushroom house with controlled light (500 lux) and temperature (25 °C). Three days after primordia initiation (approximately 20 d after

inoculation of the spawn), the basidiome was collected, freeze-dried and deposited at Herbarium SP from Botanic Institute of São Paulo (acession SP466412). Images of production of the basidiome are shown in **Figure 2**. The morphological and molecular identification of the basidiome is described below. The extraction of polysaccharides from basidiome is described in **section 3.3.3**.

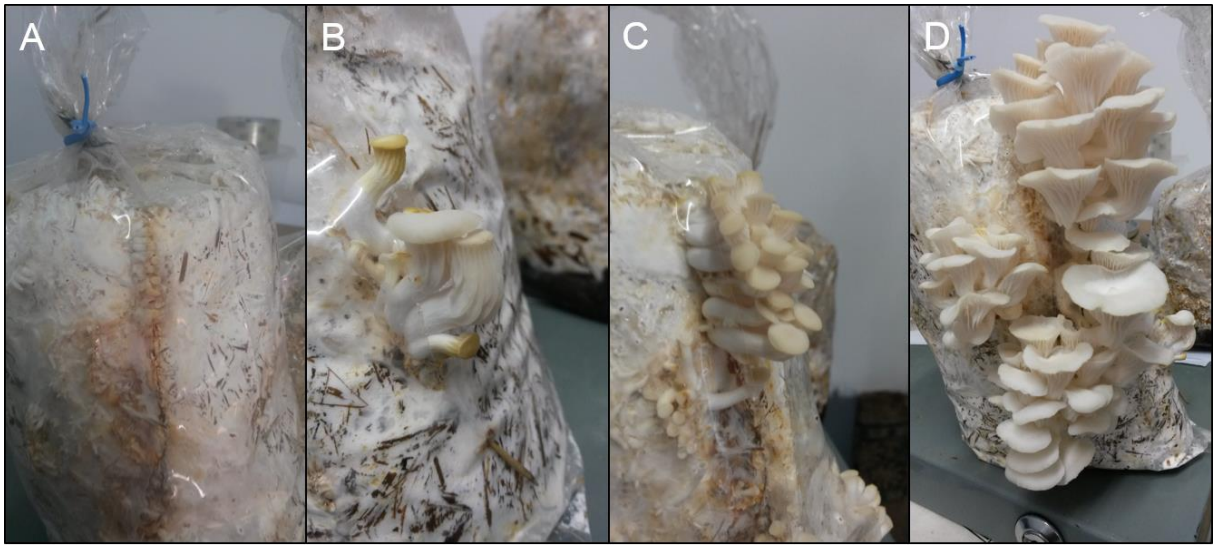

Figure 2. Cultivation of the basidiome from *Pleurotus albidus*. Polyethylene bags containing *Brachiaria brizantha* (Hochst.) Stapf. Hay were inoculated with mycelial discs of *P. albidus*. **(A)** Approximately 20 d after inoculation, small mushrooms—primordia—came up naturally on the surface of the substrate inside the polyethylene bag. Then, the polyethylene bag was cut close to the primordia to allow the growth of the basidiome. Images were representative of **(B)** 1 d, **(C)** 2 d and **(D)** 3 d after primordia initiation (photos: Daniel Gomes, São Paulo Agency for Agribusiness Technology).

To perform the morphological identification, the freeze-dried basidiome was wetted with 70% ethanol, rehydrated in 5% potassium hydroxide and examined by light microscopy. The complete description was compared to previous report (41). For molecular identification, DNA was used. ITS1F and ITS4 primer sets (42,43) were used for polymerase chain reaction (PCR) (44). The Internal Transcribed Spacer (ITS) sequence generated was deposited in GenBank (accession KX538950) and a maximum likelihood analysis was performed using RAxML servers with the same parameters—in addition to the sequence herein generated—previously described (44).

3.2.2 Production of submerged culture from Pleurotus albidus

The production of submerged culture was performed using mycelial discs of *P. albidus* stored in distilled water similar as previously described (45). Discs cultured in malt extract agar (MEA; 30 g/L malt extract, 3 g/L peptone, 15 g/L agar) were incubated (25 °C; 7 d). Then, mycelial discs were used for spawn production as described for basidiome production (**section 3.2.1**). After incubation, the spawn was inoculated (1% w/v) in culture broth (20 g/L glucose, 2 g/L yeast extract, 2 g/L peptone, 1 g/L sodium phosphate monobasic, 0.5 g/L magnesium sulphate) and incubated on an orbital shaker (120 rpm; 28 °C; 12 d) (45). Samples from the submerged culture were taken at different times for analysis of the biomass and content of endo- and exopolysaccharides. The extraction of endo- and exopolysaccharides from submerged culture is described in **section 3.3.4**.

3.3 Extraction of polysaccharides

3.3.1 Extraction of polysaccharides from chayote fruit

Polysaccharides from raw and cooked chayote pulp were obtained similar as previously described (27). Furthermore, the hot aqueous extract obtained after heating was retained to evaluate polysaccharides in the cooking water. Briefly, fruits were peeled and halved. One-half of fruit pulps was frozen in N_2 and freeze-dried. The other halves were cut into cubes (2 cm^3) and cooked in boiling water (1:2 w/v) until softening occurred (46). The firmness of fresh and cooked pulp was analyzed at different cooking times. The softening was confirmed using a TA-TX2*i*/5 texture analyzer (Stable Micro Systems, Goldaming, England) equipped with a 3 mm diameter puncture probe at 2 mm/s for 5 mm after the probe contact. After complete softening, the material was filtered (22-25 µm Miracloth; Calbiochem, La Jolla, USA) and washed with water. Both the hot water extract from cooking and the drained water from the cooked material were pooled to constitute the hot water extract. The cooked fruit was frozen in N_2 and freeze-dried, whereas the hot water extract was concentrated under vacuum at ambient temperature, frozen in N_2 and stored at -80°C. After freeze-drying, the raw and cooked pulp were milled (A10, IKA, Staufen, Germany), passed thought a 60-mesh (260 µm) sieve and incubated in chloroform:methanol (1:1; 70°C; 30 min) to remove lipids and inactivate enzymes. Extracts were filtered in a sintered-glass funnel and washed with acetone. Remaining solids from the raw and the cooked fruit and the hot water extract were hydrolyzed

in 50 mM sodium phosphate buffer with α-amylase (pH 6.0; 3,000 U/mL; 90 °C; 1 h) and amyloglucosidase (pH 4.5; 3,300 U/mL on soluble starch; 60 °C; 90 min) to hydrolyze starch. Then, the material was centrifuged and supernatants were collected. Ethanol was added to the supernatants to a concentration of 80% ethanol overnight to precipitate the water-soluble polysaccharides. After centrifugation, supernatants were collected, concentrated under vacuum at ambient temperature and separated for oligosaccharide analysis. Precipitates—which corresponded to the water-soluble NSP—were washed with ice-cold 80% ethanol, solubilized in water, dialyzed against water (MWCO 12-14 kDa; Spectrum Labs, Los Angeles, USA), frozen in N_2 and freeze-dried. Then, optical micrographs (light microscopy) of the extracts dispersed in Lugol's iodine staining were analyzed to confirm the complete removal of starch. The water-soluble polysaccharides from the raw and cooked chayote and from the hot aqueous extract were named SeR, SeC and SeH, respectively.

3.3.2 Optimization of extraction of polysaccharides from mushroom basidiome

The method described by Palacios et al. (47) was used as the reference. Modifications were performed at individual steps and results were compared to the original method. Briefly, freeze-dried mushroom was incubated with methanol (60 °C; 8 h) and submitted to successive extractions of 24 h with water at 25 °C, water at 100 °C and 1 M NaOH at 100 °C. After removing proteins using trichloroacetic acid, supernatants were precipitated with 80% ethanol and washed with acetone to yield crude polysaccharides.

First, a reduction of the time necessary to obtain the mushroom crude extract was tested. The freeze-dried mushroom was incubated at 70 ºC for 2 h, instead of 8 h, and a chloroform:methanol mixture (1:1) was substitute for methanol. After incubation, the solid was washed with acetone and centrifuged. Finally, the supernatant was discarded and the precipitate was dried under a N_2 stream, resulting in the crude extract. Furthermore, shorter incubation times of crude extract with water at 25°C, water at 100°C and 1 M NaOH at 100°C were tested. As a way to reduce possible β-elimination reactions, the addition of 20 mM sodium borohydride in the hot alkali solution was also tested. In this test, 1 M potassium hydroxide was used instead of 1 M sodium hydroxide and the results were compared after extraction for 24 h (original method). The following steps to obtain polysaccharides were performed according to the original method. Then, proposed modifications were all combined in one procedure and polysaccharides obtained were compared to those of the original method. Finally, polysaccharides were also submitted to additional cycles of extraction for 24

h with cold and hot water, and hot alkaline solution to assess their stability to the optimized method.

3.3.3 Extraction of polysaccharides from the basidiome of Pleurotus albidus

Extraction of polysaccharides from the cold (PaCW) and hot water (PaHW) and hot alkali (PaHA) extract from the basidiome of *P. albidus* were based on the optimization described in **section 3.3.2**.

3.3.4 Extraction of polysaccharides from the submerged culture of Pleurotus albidus

Polysaccharides from the submerged culture were extracted similar as previously described (45). The submerged culture was centrifuged to separate the mycelium and supernatant. The endopolysaccharides from the mycelium were extracted with water (100 °C; 2 h). After extraction, the material was centrifuged and the supernatant was collected. Ethanol was added to the supernatant to a concentration of 70% ethanol to precipitate the polysaccharides, which were separated after centrifugation. Then, polysaccharides were washed with acetone and solubilized in water. After removing proteins using trichloroacetic acid, the supernatant was neutralized, dialyzed (MWCO 3.5 kDa; Spectrum Labs) and freeze-dried to yield the endopolysaccharides.

The exopolysaccharides from the supernatant of submerged culture was precipitated with ethanol, separated after centrifugation and purified as described for the endopolysaccharides. Endo- and exopolysaccharides obtained from the submerged culture of *P. albidus* were named PaEN and PaEX, respectively.

3.4 Characterization of polysaccharides

3.4.1 General methods

Proximate composition of mushroom crude extract was based on AOAC International official methods (48). Briefly, moisture was removed by oven dehydration (95 °C; 12 h) (AOAC method 925.45); ash was determined after incineration of sample (550 °C; 8 h) (AOAC method 960.52). Protein was determined by the micro-Kjeldahl method (AOAC method 960.52) using a conversion factor of 4.38 to quantify the nitrogen percentage in the

mushroom crude extract (49). Lipids were extracted with diethyl ether under reflux (16 h) using a Soxhlet extractor (AOAC method 920.39). Total dietary fiber was determined using the enzymatic-gravimetric method (AOAC method 985.29). Available carbohydrate in the mushroom crude extract was calculated by difference.

Polysaccharide fractions were evaluated for total sugars using the phenol-sulfuric acid assay (50). Glucose was used as the standard. Proteins were determined using the Bradford (51,52), fluorescamine (53) or bicinchoninic acid (BCA) assay (Pierce BCA Protein Assay kit; Thermo) depending on the availability. Bovine serum albumin (BSA) was used as the standard. Amino acids profile was determined similar as previously described (54). Briefly, polysaccharides or BSA (standard) were hydrolyzed with 6 M hydrochloric acid (110°C; 20 h) on a heating block (Reacti-Therm stirring/heating module; Pierce, Rockford, USA). Then, the supernatant was neutralized with 50% w/w NaOH and analyzed by high performance anion-exchange chromatography coupled to a pulsed amperometric detector (HPAEC-PAD) using an ICS-5000 system (Dionex, Sunnyvalle, USA), equipped with an AminoPac PA10 column (250 × 2 mm; Dionex). A mixture of 21 L-amino acids plus glycine was used as the standard. The monosaccharide composition of polysaccharide fractions were determined after hydrolysis of polysaccharide with 2 M thrifluoroacetic acid and evaporation under N_2 flow. The residue was reconstituted in water and analysis was performed through HPAEC-PAD in an DX 500 system (Dionex), equipped with a CarboPac PA10 column (250 × 4 mm) (55). Neutral sugars (arabinose, fucose, galactose, glucose, mannose, rhamnose and xylose) and uronic acids (galacturonic and glucuronic acid) were used as standards. Oligosaccharides were analyzed by HPAEC-PAD (56) in a DX-500 system (Dionex), equipped with a CarboPac PA100 column (250 × 4 mm) (Dionex). Monosaccharide (glucose), disaccharide (maltose) and a mixture of malto-oligosaccharides containing maltoriose to maltoheptaose were used as standards. Homogeneity and average molecular weight of polysaccharide fractions were analysed by high-performance size-exclusion chromatography coupled with refractive index and multiple wavelength detector (HPSEC-RID/MWD). Analysis was performed in an Infinity system (Agilent, Santa Clara, USA) equipped with two PL aquagel-OH mixed-M columns or PL aquagel-OH 60, 50, 40 and 30 columns (300 × 7.5 mm; Agilent) connected in series, depending on the availability. The MWD was set at 280 nm. Dextran series (5-2,000 kDa) was used as standard. The triple helical conformation of polysaccharides was determined by the bathochromic shift of polysaccharides when mixed with Congo red (CR) in alkali diluted solutions (57). Relative homogalacturonan content was analyzed after hydrolysis of polysaccharides with endopolygalacturonase and quantification of reducing end

groups released using the 2-cyanoacetamide method (58). Briefly, polysaccharides or polygalacturonic acid (standard) were incubated in 50 mM sodium acetate buffer (pH 5.0; 25 °C) with endopolygalacturonase (2 U/mL). Samples were taken at different times and incubated with 0.025% 2-cyanoacetamide and 50 mM borate buffer (pH 9.0). The solution was heated (100°C; 5 min), ice-cooled and the absorbance was measured at 274 nm. Results represent the equivalent of reducing end groups released using a standard curve of galacturonic acid.

3.4.2 Fourier transform infrared (FTIR) and 1D- and 2D-nuclear magnetic resonance (NMR) spectroscopy

Polysaccharides were powderized with KBr and pressed into pellets for FTIR analysis. Spectrum was recorded using a Frontier FTIR spectrometer (PerkinElmer, Waltham, USA) in the frequency range of 4,000 to 400 cm^{-1} and resolution of 4 cm^{-1}. Results represent the mean of 32 scans per sample.

1D- and 2D-NMR were performed similar to that previously described (59). Polysaccharides were deuterium-exchanged three times by freeze-drying and further dissolved in D_2O. Depending on the availability, NMR spectra were recorded using an Inova 500 MHz spectrometer system (Varian, Palo Alto, USA) or an Inova 600 MHz spectrometer system (Varian) equipped with a 5-mm inverse cryoprobe with field z-gradient, both operating at 599.88 and 150.84 MHz for ^{1}H and ^{13}C, respectively. Temperature was maintained constant at 313 K (39.85 °C) for all acquisitions. 3-(Trimethylsilyl)propionic-2,2,3,3-d4 acid sodium salt was used as internal reference (0.0 ppm). For 1D acquisition, the parameters were as follows: ^{1}H spectral width of 7,000 Hz with 32 K data points 64 transients and relaxation delay 2 s; ^{13}C spectral width of 37,718.1 Hz with 64 K data points, 10,000 transients and 3 s relaxation delay. The gradient experiments implemented in the Chempack package of Vnmrj 3.2 software for 2D acquisition were used and the parameters were as follows: COSY with spectral width in both dimension of 7,000 Hz, 512 *t*1 increments, 4k data points in *t*2, 16 transients and 2 s relaxation delay; TOCSY with spectral width in both dimension of 7,000 Hz, 512 *t*1 increments, 4k data points in *t*2, 32 transients, mixing time of 100 ms and 2 s relaxation delay; HSQC was acquired with 256 *t*1 increments, 4k data points in *t*2, 64 transients, 2 s relaxation delay, spectral width 7,000 Hz for ^{1}H and 30,165.9 Hz (200 ppm) for ^{13}C; HMBC with 256 *t*1 increments, 4k data points in *t*2, 128 transients, 2 s relaxation delay, spectral width 7,000 Hz for ^{1}H and 36,199.1 Hz (240 ppm) for ^{13}C; ROESY with spectral

width in both dimension of 7,000 Hz, 512 *t*1 increments, 4k data points in *t*2, mixing time of 200 ms, 32 transients and 2 s relaxation delay. The NMR spectra were processed using NMRPipe scripts (60), Vnmrj 3.2 (Varian) and SpinWorks 3.0 software (RMN Laboratory, University of Manitoba, Winnipeg, Canada). Images were analyzed using MestReC 4.7 (MestreLab Research, Santiago de Compostela, Spain) and NMRViewJ 9.1 software (One Moon Scientific, Westfield, USA).

3.5 Endotoxin contamination

Polysaccharide fractions were tested for endotoxin contamination before cell culture assays. The Limulus amebocyte lysate (LAL) QCL-1000 assay kit (Lonza, Walkersville, USA) was used according to the manufacturer's instructions. Briefly, polysaccharides were solubilized in LAL reagent water (Lonza), mixed or not with β-G-Blocker (Lonza) and incubated with the LAL and the chromogenic substrate. Finally, the reaction was stopped and the absorbance was measured at 410 nm. LPS with defined endotoxin units were used as standards.

3.6 Preparation of cholesterol crystals (CC)

CC were prepared as previously described (61). Cholesterol was dissolved in 95% ethanol (60 °C; 10 min). The solution was filtered while still warm and vacuum dried (30 °C; 48 h). After cholesterol crystallisation, the material was autoclaved and powdered to yield crystals with size of 1-5 μm. CC were tested negative for endotoxin (LAL QCL-1000 assay kit, Lonza) and stored at -22 °C until analysis.

3.7 Cell culture

3.7.1 Cell lines and treatment

The RAW 264.7 and Caco-2 cell lines (American Type Culture Collection, ATCC; Manassas, USA) were cultured in DMEM (10% FBS). The THP-1 cell line (Rio de Janeiro Cell Bank; Rio de Janeiro, Brazil) was cultured in RPMI (10% FBS). Cells were maintained in a humidified atmosphere with 5% CO_2 at 37°C. The ATCC guidelines for the maintenance of cells were followed. The RAW 264.7 and Caco-2 cell lines were allowed to grow until they

reached a confluence between 70 and 90%; Trypan blue dye was used to ensure a viability of at least 90% before plating. The THP-1 cell line was allowed to grow until it suspension reached approximately 8.0×10^5 cell/mL; Trypan blue dye was used to ensure a viability of at least 95% before differentiation. To induce THP-1 monocyte differentiation into a macrophage-like phenotype that resemble properties of mature macrophages, cells were seeded in RPMI containing PMA (100 ng/mL) for 24 h, and then replaced for RPMI without PMA for a further 48 h, resulting in macrophage-like cells with increased adherence and loss of proliferative activity (62). No significant loss of viability (< 10%) was observed after PMA treatment. Since cell density and treatment differ among experiments, the detailed information about each experiment is shown in the figure captions of Results (**section 4**).

3.7.2 Viability

Cell viability was evaluated using the 3-(4,5-dimethylthiazol-2-yl)-2,5-diphenyltetrazolium bromide (MTT) (63). Results from MTT assay was confirmed using the crystal violet assay (64) depending on the availability. For the MTT assay, the supernatant was removed and cells were washed with phosphate-buffered saline (PBS) and incubated with 0.1 mg/mL MTT (37 °C; 3 h). Then, formazan crystals were solubilized with dimethyl sulfoxide (DMSO). In the crystal violet assay, cells were washed with PBS and incubated with 0.2% crystal violet (2% ethanol in PBS) (37 °C; 30 min). Then, cells were washed with PBS and the crystal violet was solubilized with 33% acetic acid. In both MTT and crystal violet assays, the absorbance was measured at 540 nm. The viability of cells (%) was expressed when compared to the control.

3.7.3 Cytotoxicity

The lactate dehydrogenase (LDH) released into the supernatant was evaluated using the Cytotoxicity Detection Kit (Roche Diagnostics, Mannheim, Germany) according to the manufacturer's instructions. Briefly, the supernatant was mixed with the substrate solution and incubated (25°C; 30 min). Then, the stop solution was added and the absorbance was measured at 490 nm. The cytotoxicity (%) was expressed as the amount of LDH released when compared to cells treated with a lysis solution (Roche Diagnostics).

3.7.4 Detached cell counting

Detached cell detection was performed similar as previously described (59). The supernatant was collected and cells were partially de-clumped using a sterile filter (0.45 µL; Millipore). The number of cells in the supernatants was counted on a Neubauer's chamber using a Primo Vert inverted microscope (Carl Zeiss, Oberkochen, Germany). Results represent the number of detached cells per well.

3.7.5 Cytokine secretion

Supernatant from cells were collected and stored at -80 °C until analysis. Cytokine secretion was evaluated through enzyme-linked immunosorbent assay (ELISA) using OptEIA kits (IL-1β and TNF-α; BD Biosciences) or flow cytometry (FACSVerse flow cytometer, BD Biosciences) using Cytometric Bead Array (CBA) kits (IL-6 and TNF-α; BD Biosciences) depending on the availability. For ELISA, supernatant was incubated with the capture antibody for IL-1β or TNF-α. After incubation, the detection antibody and the enzyme reagent was added. Then, the plate was incubated with the substrate reagent. After incubation, the stop solution was added and absorbance was measured at 450 nm (subtracted from 570 nm). For flow cytometry, antibody-coated beads for cytokines were mixed with culture supernatants and to detector antibodies. After incubation, beads fluorescence was analysed. FCAP array software (BD Biosciences) was used for quantification. Recombinant human cytokines were used as standards.

3.7.6 Nitric oxide (NO) secretion

The NO secretion was evaluated similar as previously described (65). Equal volumes of supernatant from cells and Griess reagent were incubated in the dark for 10 min. Finally, the absorbance was measured at 570 nm. Sodium nitrite was used as standard.

3.7.7 Reactive oxygen species (ROS) production

ROS production was evaluated using 2',7'-dichlorodihydrofluorescein diacetate (DCFDA). Cells were seeded on a clear bottom black plate. After treatment, the supernatant was removed and cells were incubated with 25 µM DCFDA (37 °C; 45 min). After

incubation, cells were washed with PBS and fluorescence was measured (excitation/emission = 485/535 nm) using a Synergy H1 Hybrid Reader (Biotek, Winoosky, USA).

3.7.8 Phagocytosis of zymosan particles

Phagocytosis was performed as previously described (66). Cells were seeded on a plate containing glass coverslips (13 mm diameter). After treatment, cells were incubated with zymosan particles (10 particles per cell) and phagocytosis was allowed to proceed (37 °C; 1 h). After washing with PBS, coverslips were fixed with 4% paraformaldehyde and stained with May-Grünwald reagent. At least 50 macrophages were analyzed on each coverslip using a CBA optical microscope (Olympus, Tokyo, Japan). Phagocytosis was determined as the percentage of phagocytosis (PP), the mean number of particles per cell (MNP) and the phagocytic index (PI = PP × MNP).

3.7.9 Western blot

Cells were lysed with RIPA buffer supplemented with Halth protease inhibitor cocktail (Thermo). Proteins from lysate were quantified using the Pierce BCA Protein assay kit (Thermo). Then, 25 μg of protein/sample was resolved on 12% SDS-PAGE gels and proteins were transferred to a nitrocellulose membrane. The membrane was blocked with 3% BSA and probed with monoclonal antibodies against β-actin (1:1,000) and to active caspase-1 (p20) (1:500) or cathepsin B (1:500) (Cell Signaling, Danvers, USA). After incubation with HRP-conjugated secondary antibody (1:5,000; Cell Signaling), fluorescence of protein bands was acquired using the Clarity Western ECL substrate (Bio-Rad) on an Image Quant 400 system (GE Healthcare, Chicago, USA). Density of protein bands was determined using the ImageJ software and normalized against the levels of β-actin.

3.7.10 Quantitative real-time polymerase chain reaction (qPCR)

RNA from cell was extracted using the RNeasy Mini Kit (Qiagen, Venlo, Netherlands) according to the manufacturer's instructions. RNA was purified using the Turbo DNA-free kit (Thermo) and the quality of RNA was assessed both by agarose gel electrophoresis and absorbance (A_{260}/A_{230} between 1.9 and 2.0). cDNA synthesis was performed using the High-capacity cDNA Reverse Transcription Kit (Thermo). qPCR analysis was performed using a

QuantStudio 7 real-time PCR system (Thermo) using the TaqMan Universal Master Mix II, no UNG (Thermo) and hydrolysis probes (FAM/MGB, TaqMan; Thermo) for reference and target genes according to the manufacturer's instructions. Probes for β-actin (*ACTB*; Hs01060665_g1) and ribosomal protein L37a (*RPL37A*; Hs01102345_m1) genes were used both to optimize the amount of cDNA template and to analyze reference genes (67). Probes for peroxisome proliferator activated receptor gamma (*PPARγ*; Hs0115513_m1), liver X receptor alpha (*NR1H3*; Hs00172885_m1), extracellular matrix metalloproteinase inducer (*EMMPRIN*; Hs00936295_m1), matrix metalloproteinase 9 (*MMP-9*; Hs00957562_m1), NLR family pyrin domain containing 3 (*NLRP3*; Hs00918082_m1), caspase-1 (*CASP1*; Hs003548836_m1) and interleukin 1 beta (*IL1B*; Hs01555410_m1) were used for target genes. The geometrical mean of cycle threshold (Ct) values from reference genes (68) was used to calculate relative expression using the ΔΔCt method (69). Results represent fold change expression when compared to cells incubated only with RPMI.

3.8 Statistical analysis

The results represent the mean ± standard deviation (SD) of at least three independent experiments, unless stated otherwise in the figure captions of Results (**section 4**). Analysis was performed in Prism 5.0 software (GraphPad, San Diego, USA) using Student's t-test (to asses differences between two groups) and one-way ANOVA with Tukey's (to assess differences between all groups) or Dunnett's (to assess differences between the control and two or more groups) post hoc tests. Significance was set at $p < 0.05$.

4. RESULTS

4.1 Effects of polysaccharides from raw and cooked chayote pulp in macrophages

As shown in **Figure 3A**, pulp firmness confirmed the complete softening of chayote pulp after 20 min of cooking. Polysaccharides from raw (SeR) and cooked chayote (SeC) and from the hot aqueous extract (SeH) yielded 12, 10 and 2% on a dry-weight basis, respectively. Fractions were composed by carbohydrates (> 99%) and proteins comprised less than 0.1% (not shown), which was confirmed after hydrolysis and analysis of amino acids profile (**Figure 3B**). No endotoxin contamination (not shown) and starch was detected among the polysaccharides (**Figure 3C**). Size-exclusion chromatography profile revealed that SeR was separated in high- (340 kDa) and low-MW (46 kDa) fractions. SeC and SeH showed a similar profile; however, SeC had a slightly higher proportion (69%) of high-MW polysaccharides, whereas SeH had a lower proportion (59%) (**Figure 3D**). Furthermore, polysaccharides were mainly composed of galactose, arabinose and galacturonic acid (**Figure 3E**). Galactose was the main sugar in SeR and SeC, but the proportion in SeC was significantly higher. In contrast, arabinose was the main sugar in SeH. Furthermore, higher proportions of homogalacturonans (galacturonic acid-rich fractions) in SeR and SeH was confirmed after hydrolysis with endopolygalacturonase and quantification of reducing end groups released (**Figure 3F**). No oligosaccharides were detected on the supernatants obtained during the precipitation of chayote polysaccharides (**Figure 3G**).

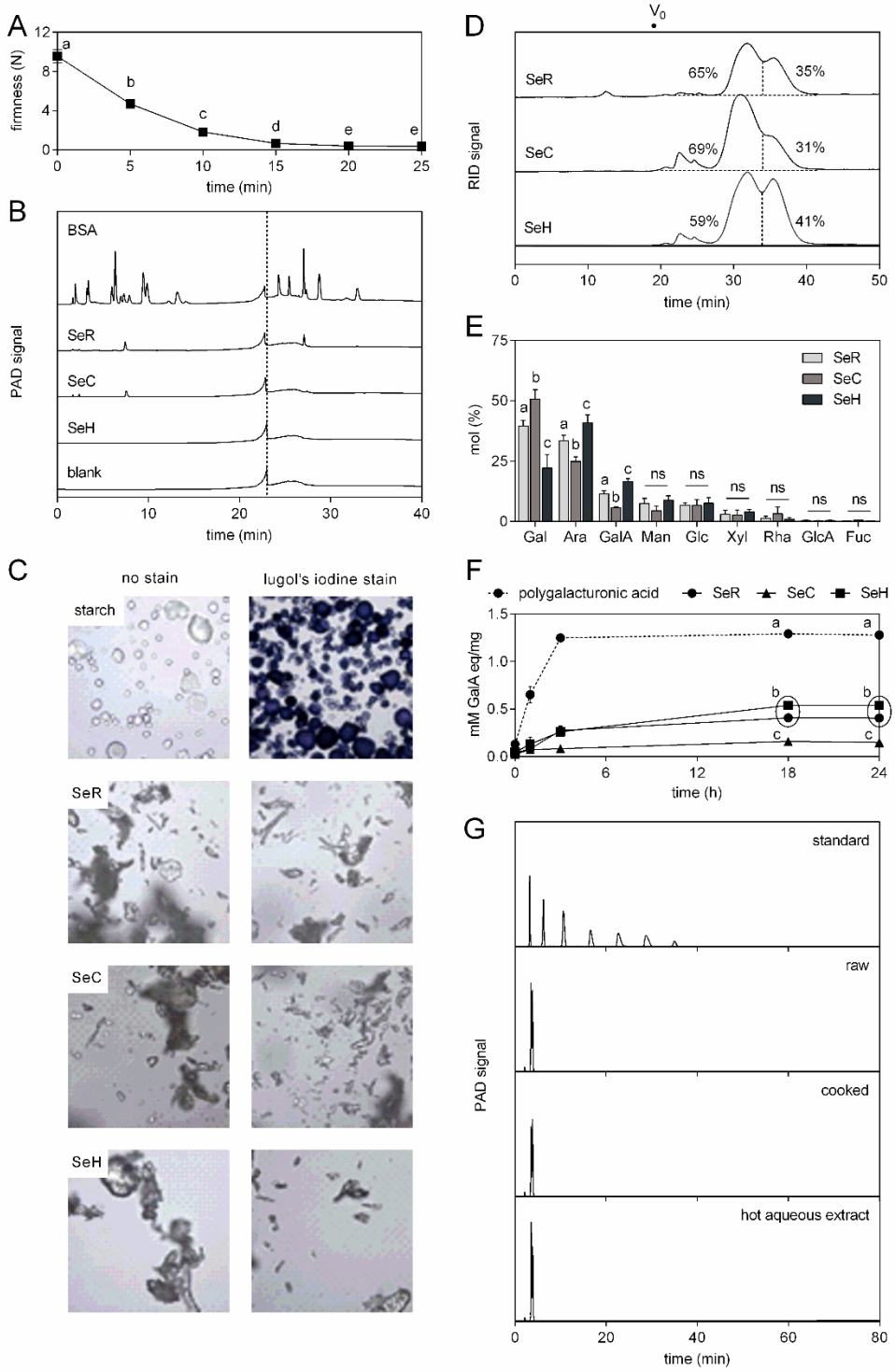

Figure 3. Profile and composition of chayote polysaccharides. (**A**) Firmness of chayote pulp at different cooking times. (**B**) Amino acids profile of bovine serum albumin (BSA) and polysaccharides (2 mg) from the raw (SeR) and cooked chayote pulp (SeC) and from hot aqueous extract (SeH) after hydrolysis. The peak at approximately 23 min (dashed line) is a response of the pulse amperometric detector (PAD) to changes in the mobile phase. (**C**) Optical micrographs (400 × magnification) of starch from chayote tuberous roots (standard) and polysaccharides without (left) or with lugol's iodine satin (right). (**D**) Size-exclusion

chromatography profile of polysaccharides detected using the refractive index detector (RID). No peaks were detected when the multiple wavelength detector was set at 280 nm (not shown). (**E**) Monosaccharide composition of polysaccharides. (**F**) Reducing end groups released by polygalacturonic acid (standard) and polysaccharides (1 mg/mL) after incubation with endopolygalacturonase. (**G**) Oligosaccharide profiling of standards (glucose and maltose to maltoheptaose) and supernatants obtained during the precipitation of polysaccharides. Gal: Galactose; Ara: Arabinose; GalA: Galacturonic acid; Man: Mannose; Glu: Glucose; Xyl: Xylose; Rha: Rhamnose; GlcA: Glucuronic acid; Fuc: Fucose; V_0: Void volume. Different letters represent significant differences; ns: No significant difference (ANOVA with Tukey's as post hoc test, $p < 0.05$). Images were representative of two independent samplings. Results represent the mean ± SD of three independent experiments.

As shown in **Figure 4A**, SeR up to 100 µg/mL had positive effects on the MTT assay, suggesting effects of SeR on macrophage proliferation. In contrast, SeR at 400 µg/mL had significantly lower values than control, which was the only effect of SeC. The results of SeH were similar to those of SeR. Furthermore, effects on the MTT assay were more evident in macrophages previously exposed to LPS. SeR had no negative effect in LPS-pretreated macrophages. Differences between SeR and SeH (100 µg/mL; 24 h) in untreated and LPS-pretreated macrophages were confirmed by the crystal violet assay (**Figure 4B**).

Notably, polysaccharides had no effect when tested on the Caco-2 cell line (**Figure 4C**). Furthermore, no differences in both LDH release and the number of detached macrophages were observed between the control and polysaccharides, regardless the concentration (**Figure 4D**).

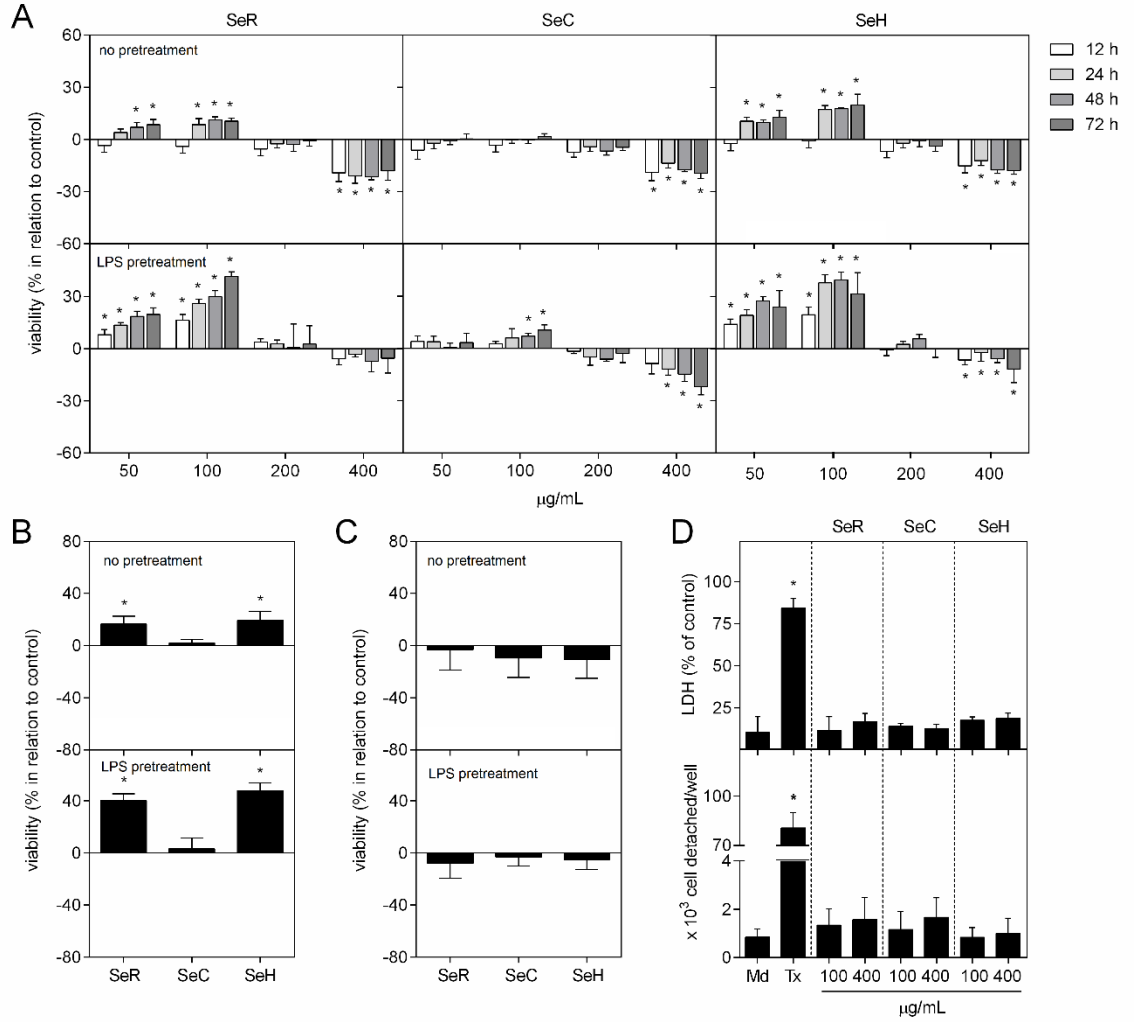

Figure 4. Effects of polysaccharides from chayote in cell proliferation and toxicity. (**A**) RAW 264.7 macrophages (2.0 × 10^4 cell/well; 96-well plate) without (top) or with LPS pretreatment (1 µg/mL; 1 h) (bottom) were incubated with polysaccharides from the raw (SeR) and cooked (SeC) chayote pulp and from hot aqueous extract (SeH) (50-400 µg/mL; 12-72 h) and evaluated through the MTT assay. (**B**) RAW 264.7 macrophages (2.0 × 10^4 cell/well; 96-well plate) without (top) or with LPS pretreatment (1 µg/mL; 1 h) (bottom) were incubated with chayote polysaccharides (100 µg/mL; 24 h) and evaluated through the crystal violet assay. (**C**) Caco-2 cells (2.0 × 10^4 cell/well; 96-well plate) without (top) or with LPS pretreatment (1 µg/mL; 1 h) (bottom) were incubated with chayote polysaccharides (100 µg/mL; 24 h) and evaluated through the MTT assay. Percentage change was expressed when compared to those of untreated macrophages (control). (**D**) Lactate dehydrogenase (LDH) release from RAW 264.7 macrophages (2.0 × 10^4 cell/well; 96-well plate) (top) and the number of detached macrophages (1.0 × 10^5 cell/well; 6-well plate) (bottom) after incubation with chayote polysaccharides (100 and 400 µg/mL; 24 h). The cytotoxicity (%) was expressed as the amount of LDH released by macrophages when compared to cells treated with a lysis

solution (Roche). Md: media; Tx: 0.2% Triton X-100 (cell death control); *: significant difference when compared to the control (ANOVA with Dunnett's as post hoc test; $p < 0.05$). Results represent the mean ± SD of three independent experiments.

As shown in **Figure 5A**, although chayote polysaccharides induced TNF-α secretion in macrophages, only SeR and SeH reduced TNF-α secretion in macrophages previously exposed to LPS and zymosan. Notably, chayote polysaccharides had no effect on IL-6 secretion in macrophages, but reduced its secretion in LPS-pretreated macrophages (**Figure 5B**). SeR and SeH also inhibited IL-6 secretion in macrophages previously exposed to zymosan. Chayote polysaccharides also induced NO secretion in macrophages, but only SeR and SeH inhibited LPS- and zymosan-induced NO secretion (**Figure 5C**). Regarding the phagocytic activity of macrophages using zymosan particles, SeR reduced the percentage of phagocytosis (**Figure 5D**), the mean number of particles per cell (**Figure 5E**) and therefore the phagocytic index (**Figure 5F**). SeR also reduced the phagocytic index in macrophages previously exposed to LPS. Similar effects were observed for SeH, but not for SeC.

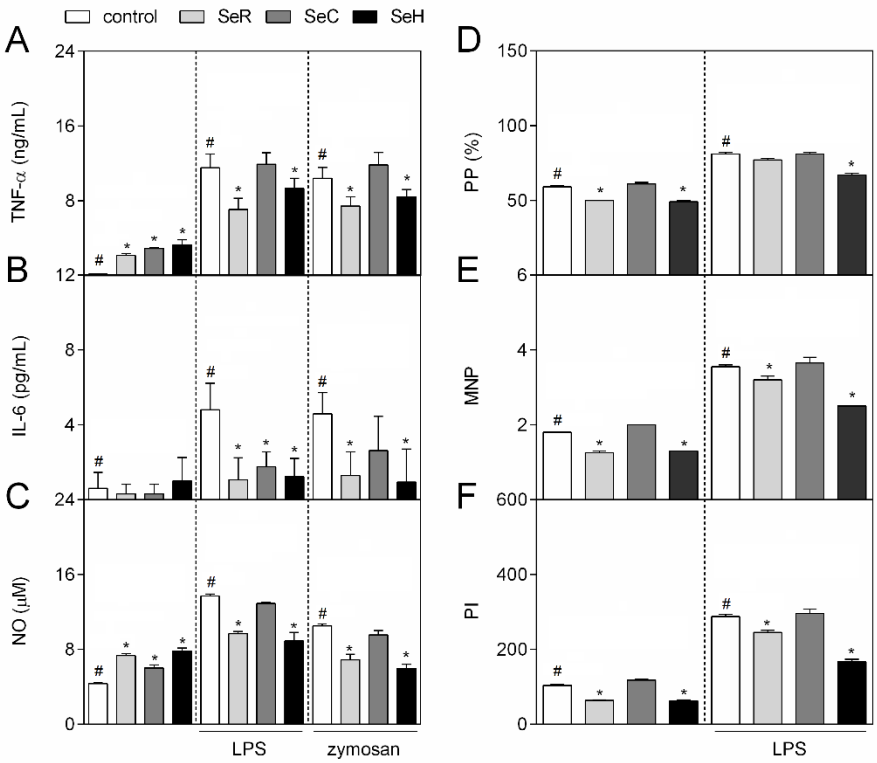

Figure 5. Effects of chayote polysaccharides in macrophages exposed or unexposed to LPS or zymosan. RAW 264.7 macrophages (2.0×10^4 cell/well; 96-well plate) were previous exposed or not to LPS (1 μg/mL; 1 h) or zymosan (50 μg/mL; 1 h) and incubated further with

polysaccharides from the raw (SeR) and cooked chayote pulp (SeC) and from hot aqueous extract (SeH) (100 μg/mL; 24 h). Then, macrophages were evaluated for **(A)** tumor necrosis factor alpha (TNF-α) and (**B**) interleukin-(IL-) 6 secretion. **(C)** RAW 264.7 macrophages (1.0 × 10^5 cell/well; 24-well plate) were previously exposed or not to LPS (1 μg/mL; 1 h) or zymosan (50 μg/mL; 1 h) and incubated with chayote polysaccharides (100 μg/mL; 24 h). Then, macrophages were evaluated for nitric oxide (NO) secretion. (**D**) RAW 264.7 macrophages (1.0 × 10^5 cell/well; 24-well plate containing coverslips) were previously exposed or not to LPS (1 μg/mL; 1 h) and incubated with chayote polysaccharides (100 μg/mL; 24 h). Then, phagocytosis of zymosan particles (10 particles/cell) was allowed (37 °C; 1 h). Results represent the percentage of phagocytosis (PP), (**E**) the mean number of particles per cell (MNP) and (**F**) the phagocytic index (PI = PP × MNP). *: Significant difference when compared to the control (#) (ANOVA with Dunnett's as post hoc test; $p < 0.05$). Results represent the mean ± SD of three independent experiments.

4.2 Effects of polysaccharides from chayote on lipid-induced inflammation and foam cell formation

The results from size-exclusion chromatography in **section 4.1** revealed that polysaccharides from the raw (SeR) and cooked (SeC) chayote and from the hot water extract obtained after cooking (SeH) have the same polysaccharide profile, differing only in their proportion of high- and low-MW polysaccharide fractions. Thus, SeR was chosen to explore the effects of chayote polysaccharides on lipid-induced inflammation and foam cell formation because of its higher yield of extraction than SeC and SeH. Furthermore, since the RAW 264.7 cell line is defective in the production of the apoptosis-associated speck-like protein containing a caspase recruitment domain (ASC), which is necessary for NLRP3 inflammasome assembling (70), the human monocytic THP-1 cell line was differentiated into a macrophage-like cell type and used instead of the RAW 264.7 cell line.

SeR (200 and 400 μg/mL) induced IL-1β secretion, but had no effect on the viability and ROS accumulation in macrophage-like cells with no pre-treatment (**Figure 6A**). In contrast, when SeR was tested in cells previously exposed to CC (**Figure 6B**), this polysaccharide fraction (400 μg/mL) inhibited loss of viability, ROS accumulation and IL-1β secretion in CC-pretreated cells.

Notably, SeR (400 μg/mL) also reduced the intracellular lipid content in macrophages previously exposed to CC (**Figure 6C**). To explore whether SeR induces lipid efflux,

macrophages previously treated with CC for 120 min to increase intracellular lipid content were subsequently incubated in CC-free media with SeR for a further 24 h. As shown in **Figure 6D**, SeR (400 µg/mL) significantly reduced the intracellular lipid content when compared to untreated cells (control).

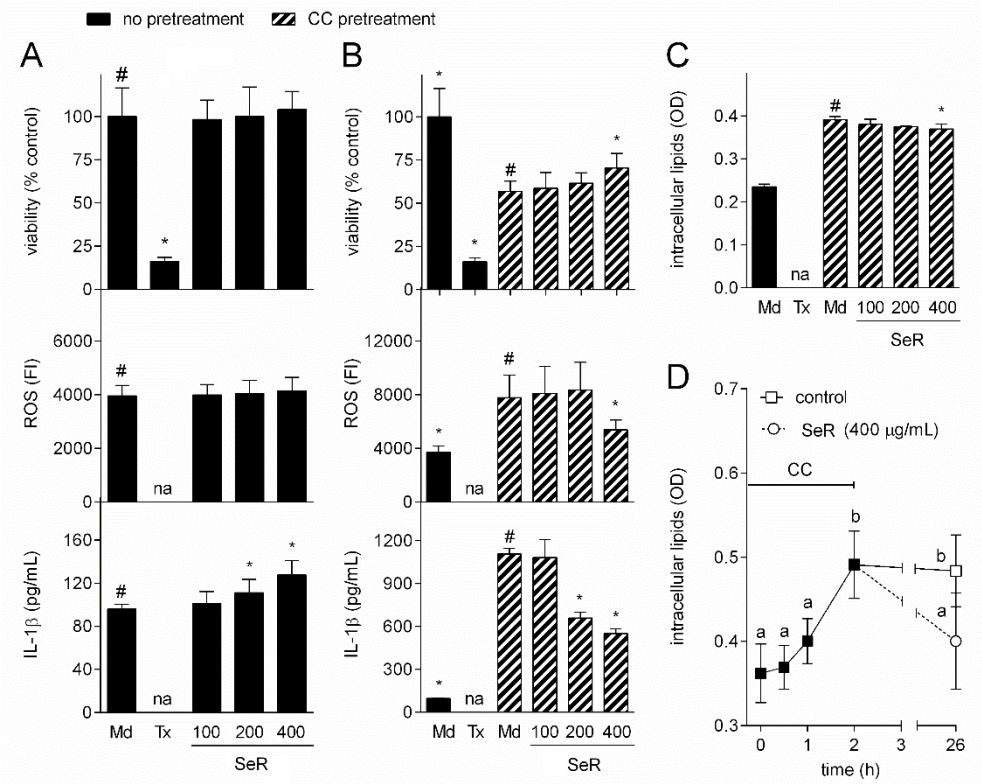

Figure 6. Effects of SeR in macrophage-like cells previously exposed or unexposed to cholesterol crystals (CC). (**A**) Macrophage-like THP-1 cells were incubated with polysaccharides from raw chayote (SeR; 100, 200 and 400 µg/mL) for 24 h and evaluated for viability, reactive oxygen species (ROS) accumulation and interleukin (IL)-1β secretion. (**B**) Macrophage-like THP-1 cells were treated with CC (1 mg/mL) and incubated with SeR (100, 200 and 400 µg/mL) for 24 h. Then, cells were evaluated for viability, ROS accumulation, IL-1β production and (**C**) intracellular lipid content. **(D)** Macrophage-like THP-1 cells were treated with CC (1 mg/mL) for 120 min. Then, cells were incubated in CC-free media with SeR (400 µg/mL) for a further 24 h and evaluated for intracellular lipid content. Md: Media; Tx: 0.2% Triton X-100 (cell death control); FI: Fluorescence intensity; OD: Optical density; na: Not analysed. *: Significant difference when compared to control (#) (ANOVA with Dunnett's post hoc test; $p < 0.05$). Different letters located above the bars represent significant difference (ANOVA with Tukey's post hoc test; $p < 0.05$). Results represent the mean ± SD of at least three independent experiments.

Since SeR significantly reduced intracellular lipid content in CC-pretreated cells, whether SeR induces genes involved on lipid efflux was also investigated. Despite SeR (400 μg/mL) having no effect on PPARγ (**Figure 7A**), it enhanced LXRα gene expression (**Figure 7B**), which is related to cholesterol efflux in macrophages. Furthermore, SeR (400 μg/mL) reduced both EMMPRIN (**Figure 7C**) and MMP-9 gene expression (**Figure 7D**), which are negatively regulated by LXRα agonists. Thus, SeR seems to induce lipid efflux in macrophage-like cells through an LXRα-dependent manner.

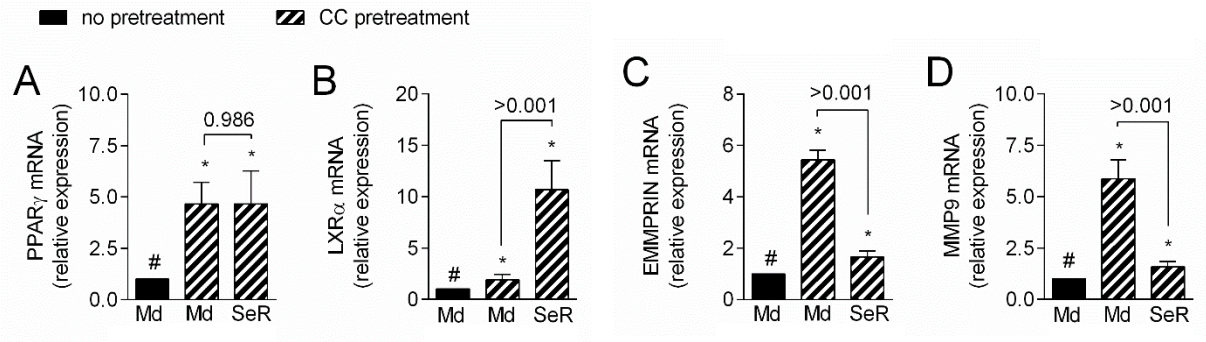

Figure7. Effects of SeR on the expression of genes related with lipid efflux in macrophage-like cells previously exposed to cholesterol crystals (CC). Relative mRNA expression of (**A**) peroxisome proliferator activated receptor gamma (PPARγ), (**B**) liver X receptor alpha (LXRα), (**C**) extracellular matrix metalloproteinase inducer (EMMPRIN) and (**D**) matrix metallopeptidase 9 (MMP9) in macrophage-like THP-1 cells previous exposed to CC for 30 min and incubated with polysaccharides from raw chayote (SeR; 400 μg/mL) for a further 24 h. The geometrical mean of the cycle threshold (Ct) values of β-actin and ribosomal protein L37 were used to calculate the relative expression of target genes using the ΔΔCt method. The number located above the bars represents the p value (Student's t test). *: Significant difference when compared to control (#) (ANOVA with Dunnett's post hoc test; $p < 0.05$). Identical significant differences were observed when ΔCt values was used instead of ΔΔCt. Results represent the mean ± SD of at least three independent experiments.

Since the data presented above indicated that SeR induces lipid efflux in CC-pretreated cells, it was assessed if this mode of action is also responsible for the inhibitory effects of SeR on cell death and IL-1β secretion in CC-pretreated cells. To accomplish this, the phagocytosis inhibitor cytochalasin D (CytD) was used at 0.25 mM, which blocked phagocytosis of CC and had no effect on the other parameters evaluated (**Figure 8A**).

Notably, SeR (400 µg/mL) decreased the loss of viability, ROS accumulation and IL-1β ssecretion even when CytD (0.25 mM) had previously blocked CC phagocytosis (**Figure 8B**), ruling out the possibility that induction of lipid efflux by SeR is the main responsible for its inhibitory effects in CC-pretreated cells.

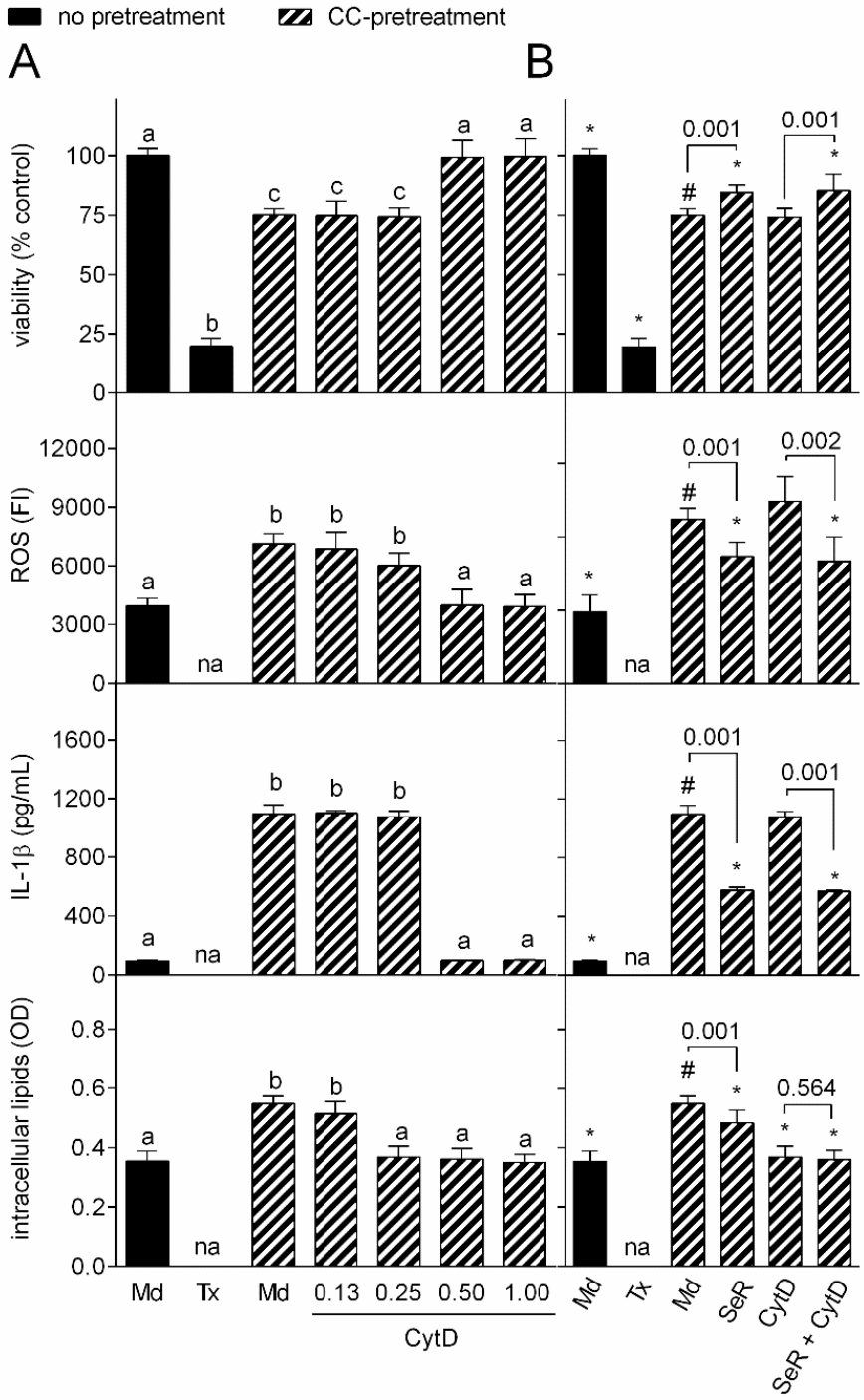

Figure 8. Effects of SeR in macrophage-like cells previously exposed to cholesterol crystals (CC) with phagocytosis blocked. (**A**) Macrophage-like THP-1 cells were incubated

with cytochalasin D (CytD; 0.13, 0.25, 0.50 and 1.00 µM) for 30 min and treated with CC (1 mg/mL) for a further 30 min. Then, cells were incubated for 24 h and evaluated for viability, reactive oxygen species (ROS) accumulation, interleukin (IL)-1β secretion and intracellular lipid content. (**B**) Macrophage-like THP-1 cells were incubated with 0.25 µM cytochalasin D (CytD) for 30 min and treated with CC (1 mg/mL) for a further 30 min. Then, cells were incubated with polysaccharides from raw chayote (SeR; 400 µg/mL) for 24 h and evaluated for viability, ROS accumulation, IL-1β secretion and intracellular lipid content. Md: Media; Tx: 0.2% Triton X-100 (cell death control); FI: Fluorescence intensity; OD: Optical density; na: Not analysed. Different letters located above the bars represent significant difference (ANOVA with Tukey's post hoc test; $p < 0.05$). The number located above the bars represents the p value (Student's t test). *: Significant difference when compared to control (#) (ANOVA with Dunnett's post hoc test; $p < 0.05$). Results represent the mean ± SD of at least three independent experiments.

CC induces priming and activation of the NLRP3 inflamasome, thereby upregulating IL-1β and NLRP3 gene expression and enhancing active caspase-1-mediated cell death and IL-1β secretion (71). To confirm the effects of SeR on NLRP3 inflammasome activation, active caspase-1 was measured in macrophage-like cells previously exposed to CC. Notably, SeR (400 µg/mL) strongly inhibited CC-induced active caspase-1 (**Figure 9A**), which suggests that SeR inhibits NLRP3 inflammasome activation.

The trigger of K^+ efflux and leakage of the lysosomal cysteine protease cathepsin B are needed to CC-induced NLRP3 inflammasome assembling and therefore caspase-1 activation (61). Since SeR inhibited active caspase-1 in macrophage-like cells previously exposed to CC, it was investigated the effects of SeR on K^+ efflux and cathepsin B levels in CC-pretreated cells. To investigate whether SeR inhibits K^+ efflux, this polysaccharide fraction was tested for additive effects on cells pretreated with the K^+ efflux inhibitors glyburide and KCl. These K^+ efflux inhibitors had no effect on untreated cells in the conditions tested (**Figure 9B)**; however, they did reduce loss of viability, ROS accumulation and IL-1β secretion in macrophage-like cells previously exposed to CC, and the presence of SeR (400 µg/mL) enhanced the reduction of ROS accumulation and IL-1β secretion (**Figure 9C)**. These results suggest that SeR inhibited NLRP3 inflammasome activation in CC-pretreated cells through mechanisms other than inhibition of K^+ efflux. Furthermore, the expression of cathepsin B was investigated, but no significant effect was observed when SeR (400 µg/mL) was tested in CC-pretreated cells (**Figure 9D**). Thus, although effects of SeR on

active caspase-1 clearly suggests that this polysaccharide fraction regulates CC-induced NLRP3 inflammasome activation in macrophage-like cells, effects of SeR seems related neither to inhibition of K^+ efflux nor to reduction of cathepsin B levels.

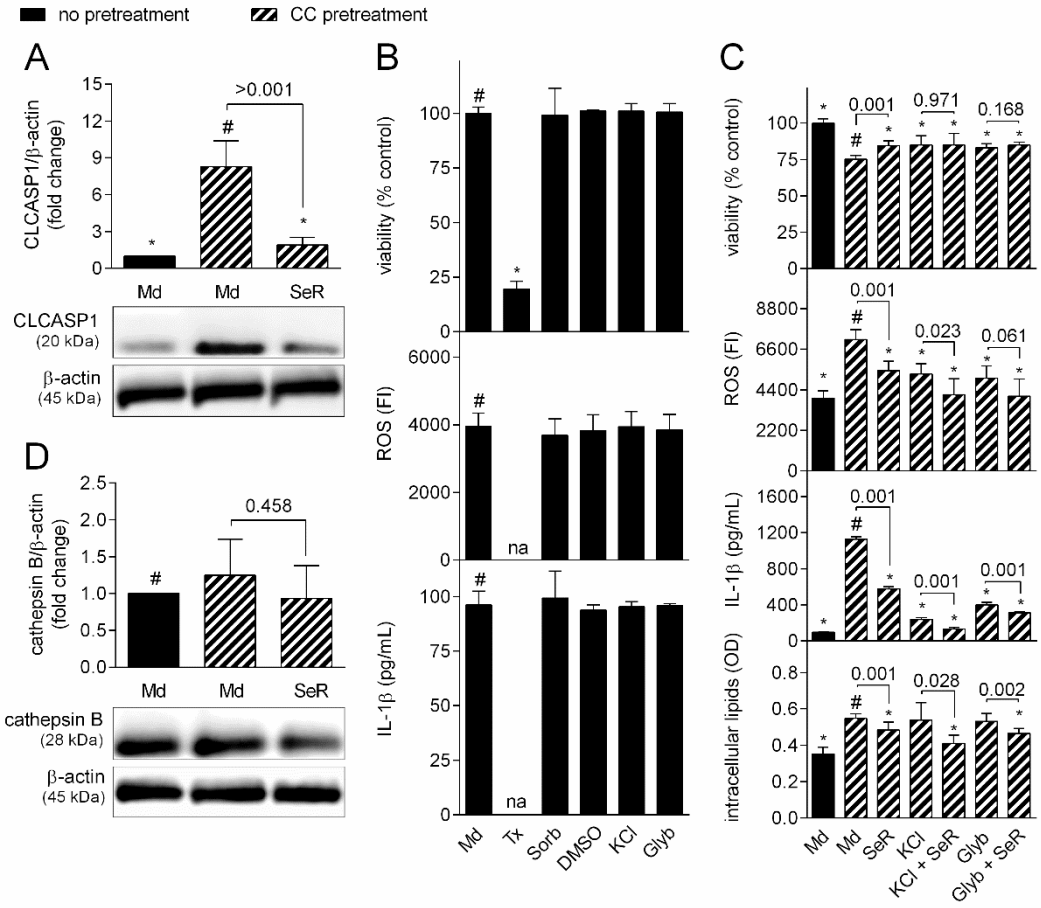

Figure 9. Effects of SeR on NLRP3 inflammasome activation in macrophage-like cells previously exposed to cholesterol crystals (CC). (**A**) active caspase-1 (CLCASP1) from lysate of macrophage-like THP-1 cells treated with CC (1 mg/mL) for 30 min and incubated with polysaccharides from raw chayote (SeR; 400 µg/mL) for a further 12 h. (**B**) Macrophage-like THP-1 cells were treated with K+ efflux inhibitors (130 mM KCl or 200 µM glyburide; Glyb), 260 mM sorbitol (Sorb; osmolarity control) or 0.4% DMSO (solvent control) for 24 h and evaluated for viability, reactive oxygen species (ROS) accumulation and interleukin (IL)-1β release. (**C**) Macrophage-like THP-1 cells were treated with CC (1 mg/mL) for 30 min and with K^+ efflux inhibitors (130 mM KCl or 200 µM glyburide) for a further 30 min. Then, cells were incubated with SeR (400 µg/mL) for 24 h and evaluated for viability, ROS accumulation, IL-1β secretion and intracellular lipid content. (**D**) Cathepsin B from lysate of macrophage-like THP-1 cells treated with CC (1 mg/mL) for 30 min and incubated with SeR (400 µg/mL) for a further 12 h. The density of protein bands was normalised against the levels

of β-actin and expressed as fold change compared to the control. Md: Media. *: Significant difference when compared to control (#) (ANOVA with Dunnett's post hoc test; $p < 0.05$). The number located above the bars represents the p value (Student's t test). Images of gels are representative of three independent experiments. Results represent the mean ± SD of at least three independent experiments.

Since the transcriptional upregulation (e.g. priming) of both IL-1β and the inflammasome sensor NLRP3 are the essential elements for NLRP3 inflammasome assembling (72), and since previous our previous results showed that SeR inhibited pro-inflammatory effects of LPS, which induces NF-κB-dependent IL-1β and NLRP3 priming, the effects of SeR on CC-induced IL-1β and NLRP3 gene expression was tested. Notably, SeR (400 μg/mL) downregulated both IL-1 β and NLRP3 gene expression (**Figure 10A**) in macrophage-like cells previously exposed to CC, suggesting that effects of SeR on CC-induced NLRP3 inflammasome activation is related, at least partly, to the inhibition of priming signals required for NLRP3 inflammasome activation. To confirm effects of SeR on IL-1β and NLRP3 gene expression, SeR (400 μg/mL) was also tested in macrophage-like cells previously exposed to LPS (1 μg/mL). In this test, the NF-κB inhibitor BAY 11-7082 (12 μM) (73) was used to confirm the role of NF-κB on LPS-induced priming of both IL-1β and NLRP3. Confirming our hypothesis, SeR also inhibited NF-κB-induced IL-1β and NLRP3 gene expression in macrophage-like cells previously exposed to LPS (**Figure 10B**).

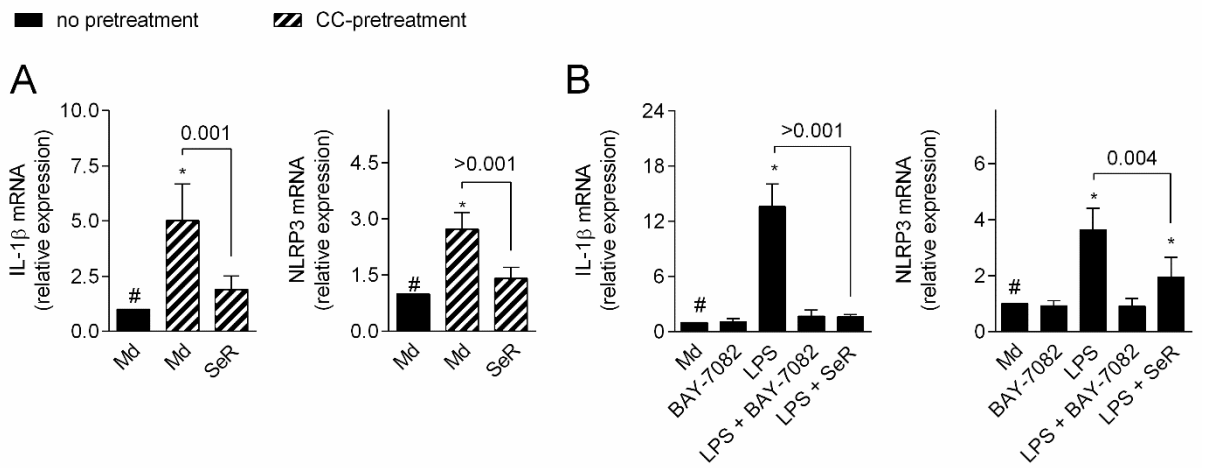

Figure 10. Effects of SeR on priming of the NLRP3 inflammasome in macrophage-like cells previously exposed to cholesterol crystals (CC) or LPS. Relative mRNA expression of interleukin (IL)-1β and NLRP3 in macrophage-like THP-1 cells **(A)** treated with CC for 30 min and incubated with polysaccharides from raw chayote (SeR; 400 μg/mL) for a further 24

h or **(B)** exposed or unexposed to BAY-7082 (12 µM; 30 min), lipopolysaccharide (LPS; 1 µg/mL; 30 min) and incubated with SeR (400 µg/mL) for a further 24 h. Md: Control. The geometrical mean of the cycle threshold (Ct) values of β-actin and ribosomal protein L37 were used to calculate the relative expression of target genes using the ΔΔCt method. The number located above the bars represents the *p* value (Student's t test). *: Significant difference when compared to control (#) (ANOVA with Dunnett's post hoc test; $p < 0.05$). Identical significant differences were observed when ΔCt values was used instead of ΔΔCt. Results represent the mean ± SD of at least three independent experiments performed in quadruplicate.

4.3 Optimization of extraction of polysaccharides from mushroom basidiome

As shown in **Figure 11A**, no differences in the yield and proximate composition of mushroom crude extract were observed after incubation with methanol for 8 h (original method) and chloroform:methanol for 2 h. Furthermore, successive incubations of mushroom crude extract for 8 h were sufficient to achieve similar yields when compared to the original method (24 h) (**Figure 11B**). The use of potassium hydroxide:sodium borohydride instead of sodium hydroxide had no effect on the composition (**Figure 11C**) and size-exclusion chromatography profile of the polysaccharide extracted in hot alkali solution (**Figure 11D**). Notably, when modifications were combined into one procedure, polysaccharide fractions were obtained in half the time and were indistinguishable from those obtained by the original method in terms of yield and monosaccharide composition (**Figure 11E**), protein content (**Figure 11F**), size and homogenity (**Figure 11G**) and conformation (**Figure 11H**). Finally, no differences on size and conformation were observed when polysaccharides obtained by the optimized method were submitted to an additional cycle of extraction (not shown), confirming their stability to the extraction method.

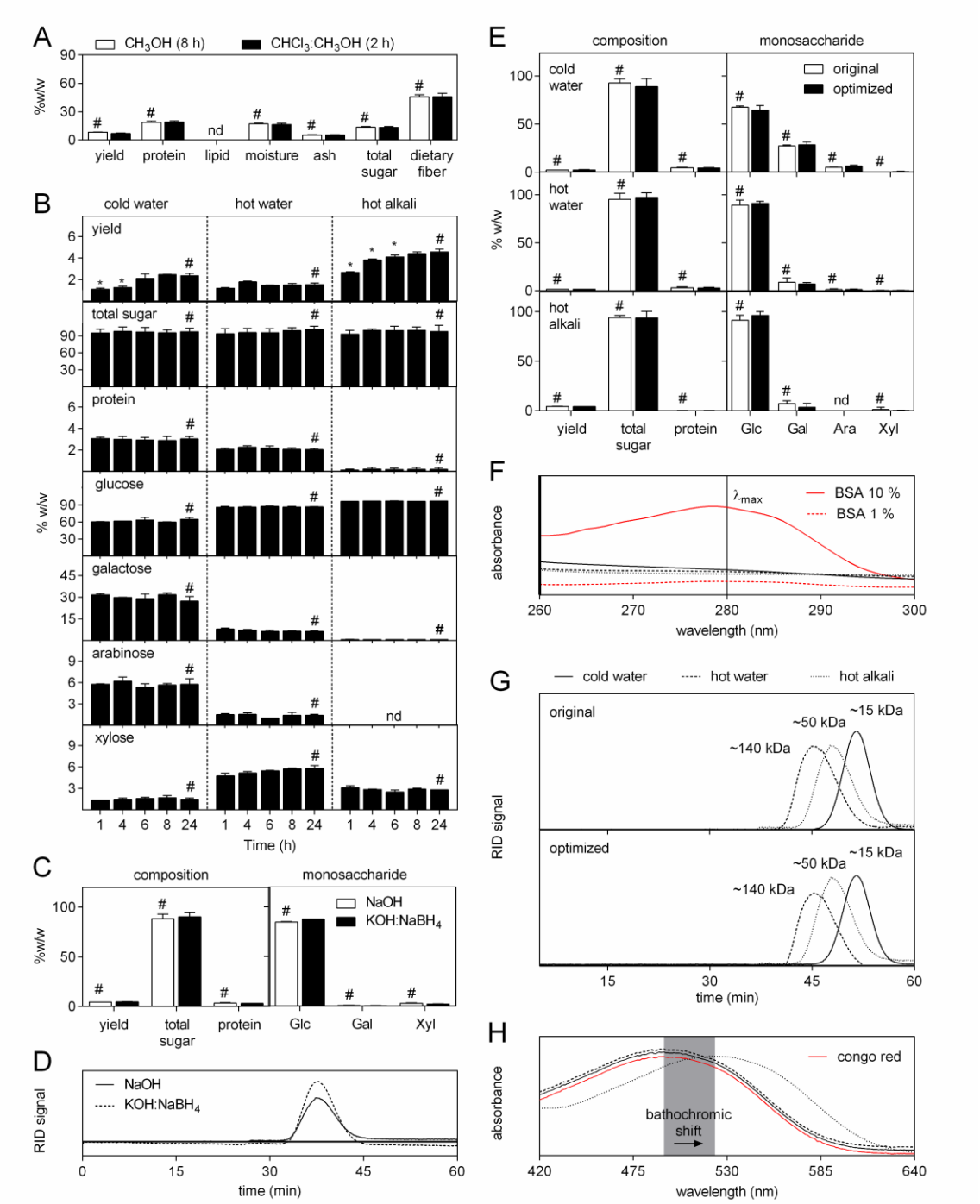

Figure 11. Optimization steps and comparison of polysaccharides obtained with the original and the optimized method. (**A**) Proximate composition of mushroom after extraction with methanol (70 °C; 8 h) or chloroform:methanol (70 °C; 2h). (**B**) Yield and composition of polysaccharides obtained at different extraction times. (**C**) Yield and composition and (**D**) size-exclusion chromatography profile of polysaccharides extracted with sodium hydroxide or potassium hydroxide:sodium borohydride (100 °C; 24 h). (**D**) Yield and composition, (**E**) UV spectra (260-300 nm), (**F**) size-exclusion chromatography profile and

(**G**) conformation of polysaccharides obtained using the optimized method. The yield, composition and conformation were similar to those from polysaccharides obtained by the original method (not shown). RID: Refractive index detector; Glc: Glucose; Gal: Galactose; Ara: Arabinose; Xyl: Xylose; BSA: Bovine serum albumin; nd: Not detected. *: Significant difference when compared to the control (#) (ANOVA with Dunnett's as post hoc test or Student's t-test; $p < 0.05$). Values represent mean ± SD of three independent experiments, except for the yield of extraction, which was performed in duplicate.

4.4 Structure and effects of polysaccharides from the basidiome and submerged culture of *P. albidus* in macrophages

The identity of the basidiome was confirmed as *P. albidus* by both morphological and phylogenetic studies (**Figure 12**).

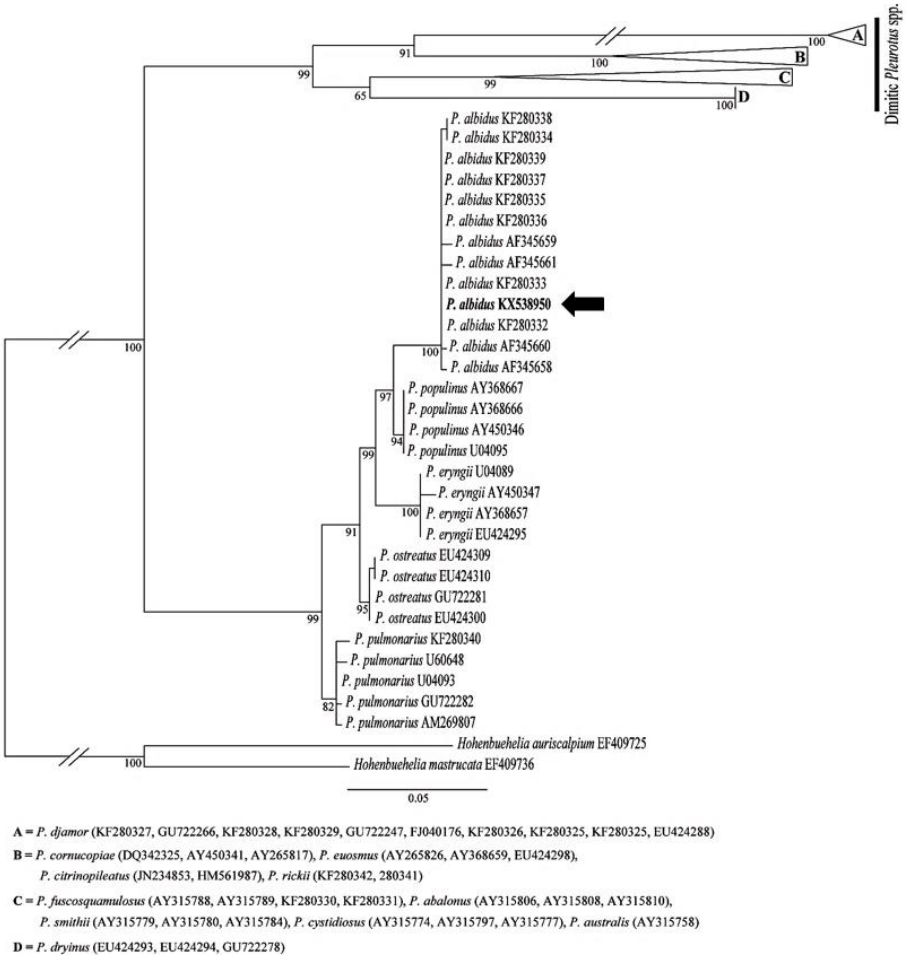

Figure 12. Best tree of maximum likelihood analysis of *Pleurotus* species from Latin America. Bootstrap values < 70% are shown below the node branches. Some root length has

been reduced to facilitate graphical representation. The black arrow indicates the sequence generated in this study (*P. albidus* KX538950).

The production yielded approximately 250 g/kg of fresh basidiome in the substrate (**Figure 13A**) and 9 g/L of biomass in the submerged culture (**Figure 13B**). The basidiome yielded approximately 30 mg/g of BaCW and BaHW and 200 mg/g of BaHA on a dry weight basis, whereas the submerged culture yielded 1.0 of MyEX and 0.5 g/L of MyEN after 10 days of incubation. Carbohydrates were the main constituents of the polysaccharides (> 95%) and glucose was the only monosaccharide detected after hydrolysis of polysaccharides (not shown). Proteins comprised less than 1.0% of the total, and no signals in the size-exclusion chromatography were detected when the multiple wavelength detector was set at 280 nm (not shown). In contrast, when the refractive index detector was used, the size-exclusion chromatography profile revealed only one main peak signal for all fractions, except for PaHA (**Figure 13C**). Moreover, no endotoxin contamination (< 0.01 EU/mL) was detected among the polysaccharides (not shown).

As shown in **Figure 13D**, the infrared spectra of the polysaccharides showed strong and broad bands near 3430 cm^{-1} and 2920 cm^{-1}, which were assigned to the O—H and C—H stretching vibrations (74), respectively. Furthermore, overlapping bands between 1200 and 950 cm^{-1} were assigned to the C—C and C—O stretching vibrations in pyranoid rings, respectively. Bands near 915 and 1110 cm^{-1} were assigned to the D-Glc*p* unit, and a broad band between 1650 and 1610 cm^{-1} was assigned to the bound water. The spectra of PaCW and PaEX also showed a band near 890 cm^{-1} corresponding to a β-configuration, while PaHW and PaEN showed bands near 850 and 760 cm^{-1} suggestive of an α-configuration (75). Notably, PaHA showed both bands near 890 and 760 cm^{-1}.

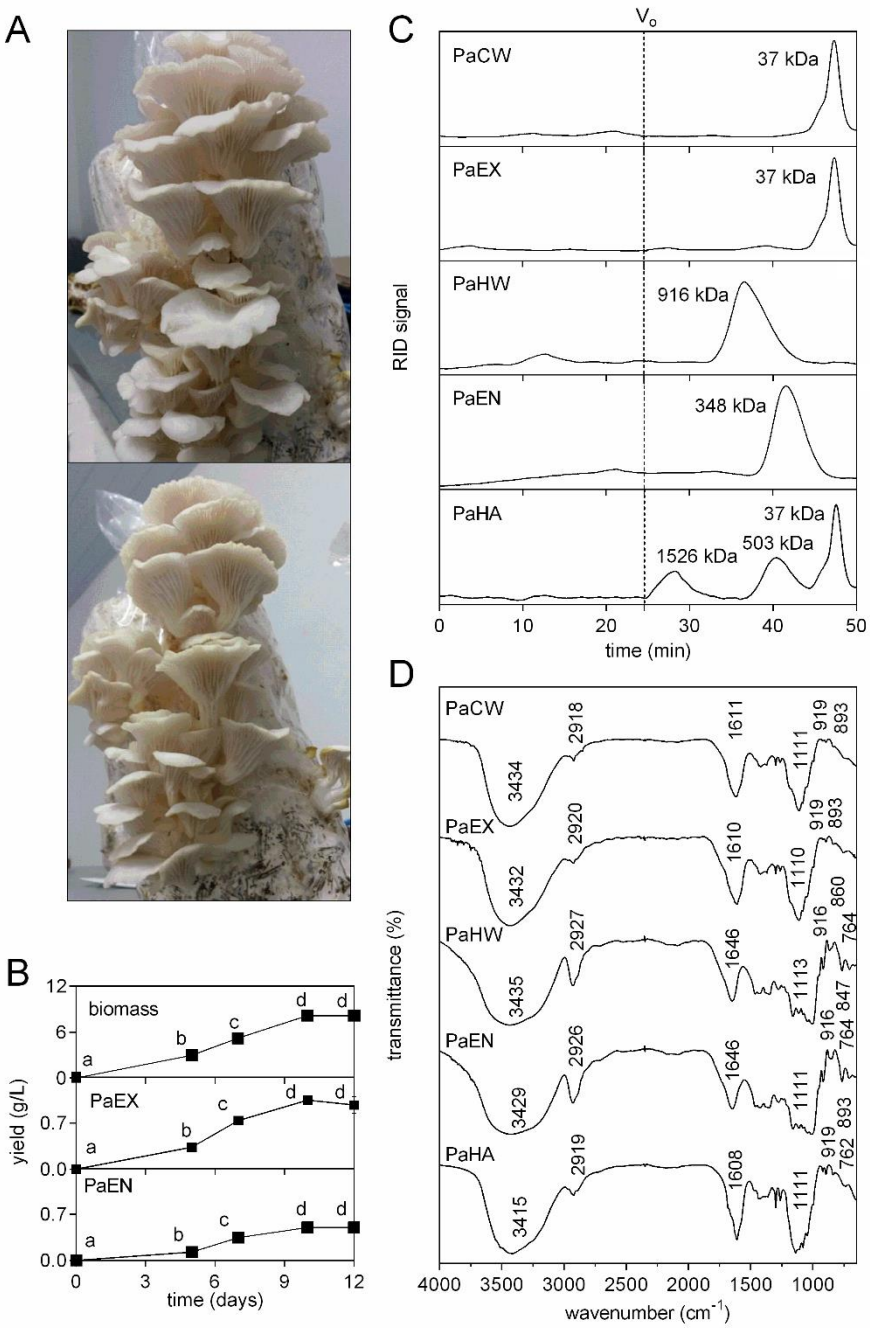

Figure 13. Basidiome, yield of the submerged culture and profile of polysaccharides from *P. albidus.* (**A**) Representative images of the basidiome produced for this study (photos: Daniel Gomes, Sao Paulo Agency for Agribusiness Technology). (**B**) Yield of biomass and exo- (PaEX) and endopolysaccharides (PaEN) from the submerged culture. (**C**) Size-exclusion chromatography profile and (**D**) infrared spectra of PaEN, PaEX and polysaccharides from the cold (PaCW) and hot water (PaHW) and hot alkali (PaHA) extracts from the basidiome. RID: Refractive index detector; V_0: Void volume. Different letters represent significant differences (ANOVA with Tukey's as post hoc test, $p < 0.05$). Results

represent the mean ± SD of three independent experiments, except for the yield of submerged culture, PaEN and PaEX, which was performed in duplicate.

The NMR analyses revealed six anomeric protons in the 1D ^{1}H NMR spectrum of PaCW (**Figure 14A**). Cross-peaks between the protons and carbons in the HSQC spectrum (**Figure 14B**) and correlations between the protons in the COSY spectrum (**Figure 14D**) were typical of an →3)-β-D-Glc*p*-(1→ backbone (76). The TOCSY spectrum of PaCW (**Figure 14E**) allowed the assignment of the others spin systems as (A) a reducing end (β anomer), (B) →6)-β-D-Glc*p*-(1→, (C) →3,6)-β-D-Glc*p*-(1→, (D) β-D-Glc*p*-(1→ and (F) a reducing end (α anomer) (76). An inter-residue connection between (B) →6)-β-D-Glc*p*-(1→ and (C) →3,6)-β-D-Glc*p*-(1→ was confirmed in the HMBC spectrum (**Figure 14F**)**.** Integration of signals in the ^{1}H NMR spectrum showed that PaCW had approximately four →3,6)-β-D-Glc*p*-(1→ units and four →6)-β-D-Glc*p*-(1→ branches for each 100 units of the →3)-β-D-Glc*p*-(1→ backbone.

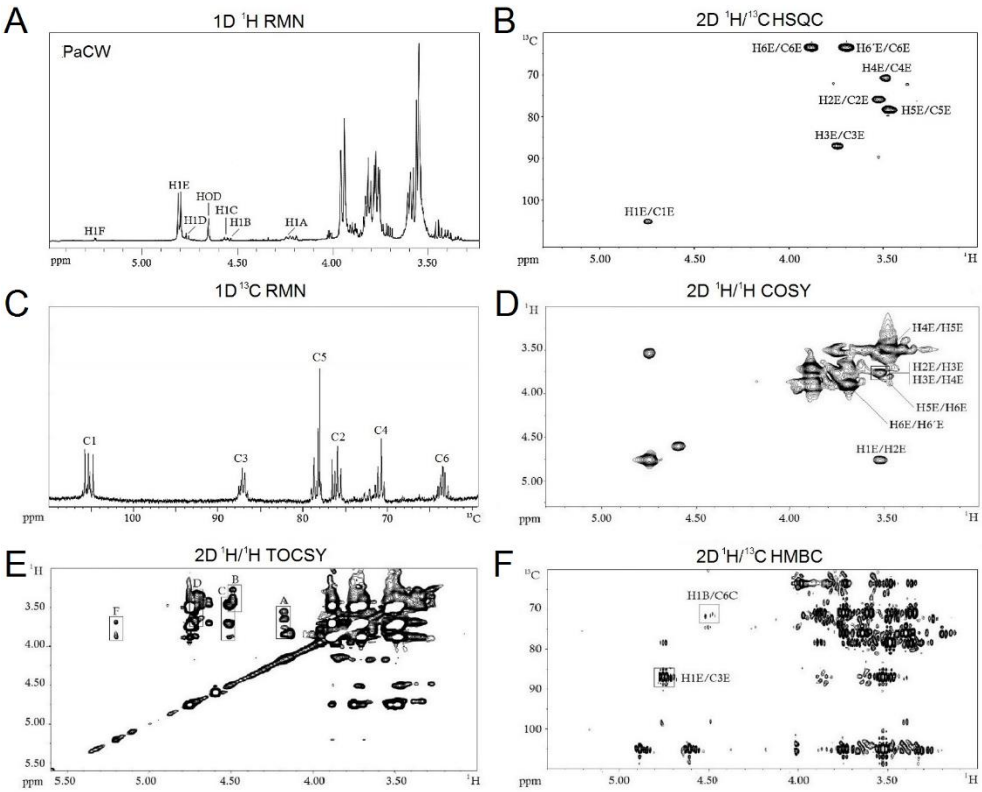

Figure 14. Nuclear magnetic resonance (NMR) spectra of the polysaccharide from the cold water extract (PaCW) from the basidiome of *P. albidus.* (**A**) ^{1}H NMR, (**B**) ^{1}H/^{13}C HSQC, (**C**) ^{13}C NMR, (**D**) 2D ^{1}H/^{1}H COSY, (**E**) ^{1}H/^{1}H TOCSY and (**F**) ^{1}H/^{13}C HMBC spectra (D_2O; 40 °C) of PaCW.

Notably, PaEX showed the same pattern of PaCW in the 1D ^{1}H and ^{13}C NMR, HSQC, COSY, TOCSY and HMBC spectra (**Figure 15**).

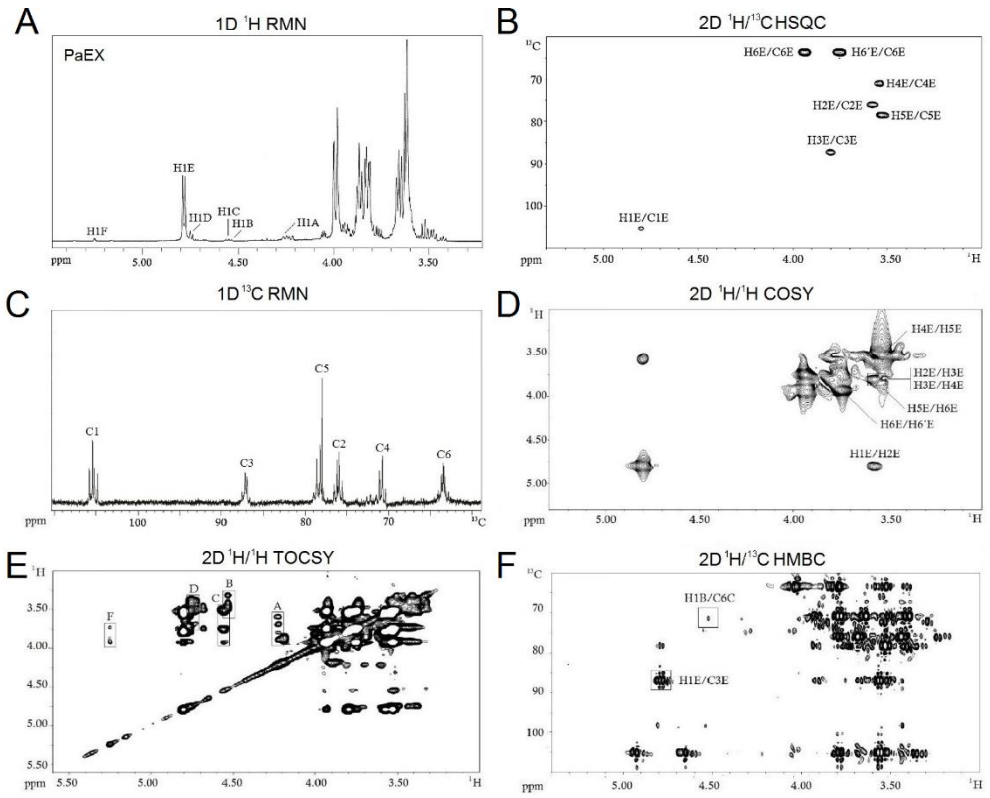

Figure 15. Nuclear magnetic resonance (NMR) spectra of the exopolysaccharide (PaEX) from the submerged culture of *P. albidus.* (**A**) ^{1}H NMR, (**B**) ^{1}H/^{13}C HSQC, (**C**) ^{13}C NMR, (**D**) 2D ^{1}H/^{1}H COSY, (**E**) ^{1}H/^{1}H TOCSY and (**F**) ^{1}H/^{13}C HMBC spectra (D_2O; 40 °C) of PaEX.

The ^{1}H NMR spectrum of PaHW showed five anomeric protons with a main signal (H1B) and an apparent triplet (H1E) typical of (B) a →6)-α-D-Glc*p*-(1→ backbone and (E) →3)-α-D-Glc*p*-(1→ branches (77) (**Figure 16A**). HSQC (**Figure 16B**) and COSY (**Figure 16D**) spectra confirmed the →6)-α-D-Glc*p*-(1→ backbone. The TOCSY spectrum (**Figure 16E**) of PaHW allowed some of the cross-peaks from the others spin systems to be assigned as (A) a reducing end (β anomer), (C) →2)-α-D-Glc*p*-(1→ and (D) a reducing end (α anomer), respectively (78,79). The HMBC spectrum confirmed inter-residue connections between the (E) →3)-α-D-Glc*p*-(1→ branches and the (B) →6)-α-D-Glc*p*-(1→ backbone through H1E and the downshifted C3 from the →3,6)-α-D-Glc*p*-(1→ unit (**Figure 16F**). The presence of a →2)-α-D-Glc*p*-(1→ unit was confirmed in the HSQC-TOCSY spectrum (data

not shown) by low intensity cross-peak signals between δ 5.12 and unbound C6 (δ 61.24) (80).

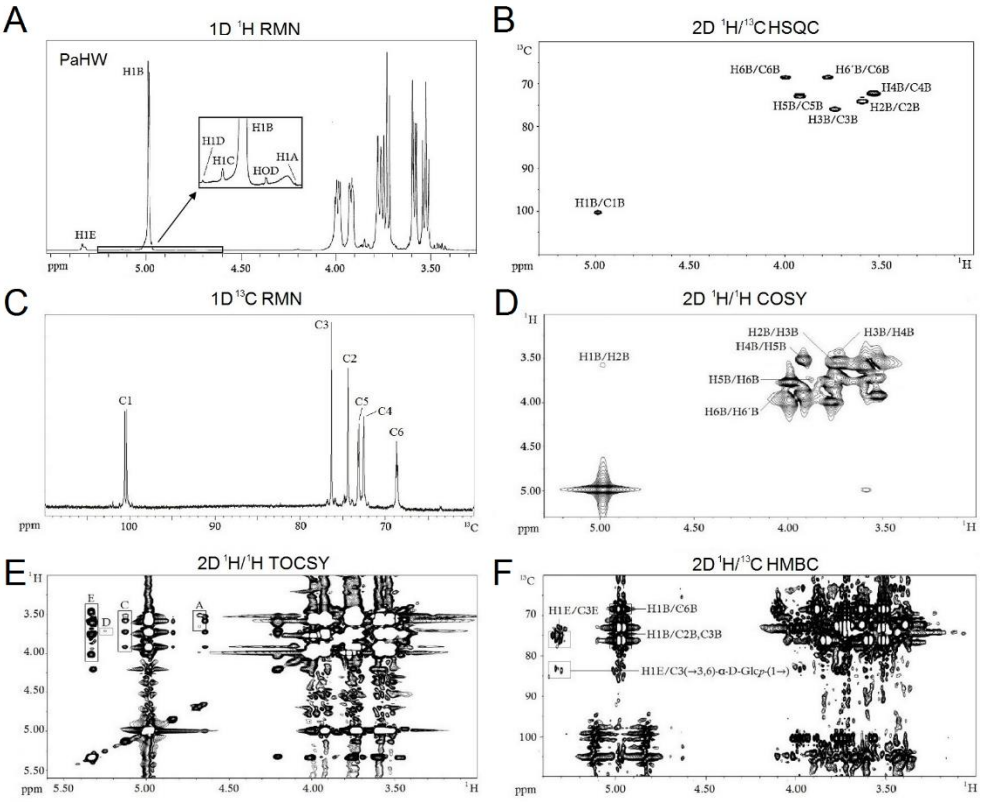

Figure 16. Nuclear magnetic resonance (NMR) spectra of the polysaccharide from the hot water extract (PaHW) from the basidiome of *P. albidus.* (**A**) ^{1}H NMR, (**B**) ^{1}H/^{13}C HSQC, (**C**) ^{13}C NMR, (**D**) 2D ^{1}H/^{1}H COSY, (**E**) ^{1}H/^{1}H TOCSY and (**F**) ^{1}H/^{13}C HMBC spectra (D_2O; 40 °C) of PaHW.

PaEN had similar 1D ^{1}H and ^{13}C NMR, HSQC, COSY, TOCSY and HMBC spectra to those of BaHW (**Figure 17**). However, BaHW had a lower degree of →3)-α-D-Glc*p*-(1→ (5.0% versus 5.5%) and →2)-α-D-Glc*p*-(1→ (0.5% versus 1.0%) branches. Moreover, the TOCSY spectrum of BaHW showed fewer resolved cross-peaks for the reducing ends.

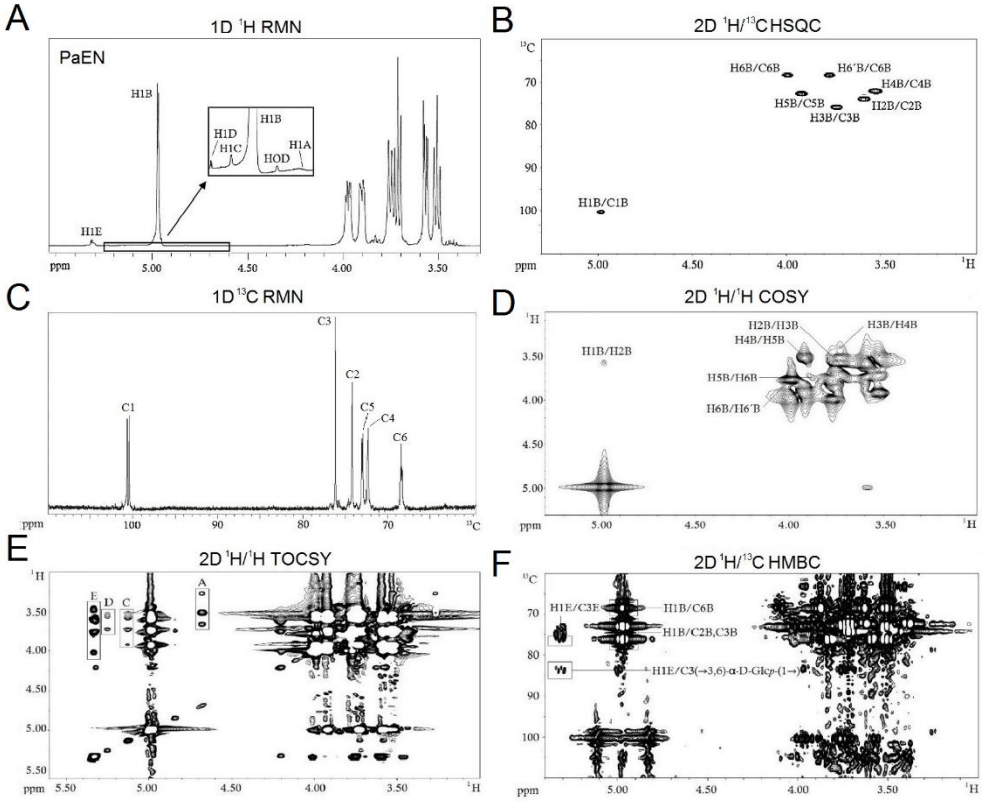

Figure 17. Nuclear magnetic resonance (NMR) spectra of the endopolysaccharide (PaEN) from the submerged culture of *P. albidus.* (**A**) ^{1}H NMR, (**B**) ^{1}H/^{13}C HSQC, (**C**) ^{13}C NMR, (**D**) 2D ^{1}H/^{1}H COSY, (**E**) ^{1}H/^{1}H TOCSY and (**F**) ^{1}H/^{13}C HMBC spectra (D_2O; 40 °C) of PaEN.

The 1D ^{1}H NMR spectrum of PaHA showed each of the chemical shifts assigned to the anomeric regions of the other polysaccharides (**Figure 18A**). The main spin systems were assigned in the HSQC spectrum (**Figure 18B**) as (G) →6)-α-D-Glc*p*-(1→ and (F) →3)-β-D-Glc*p*-(1→ units. The signals from the COSY (**Figure 18D**) and TOCSY (**Figure 18E**) spectra were difficult to assign due to overlapping resonances, However, no connection between the spin systems (G) and (F) was identified in the HMBC spectrum (**Figure 18F**).

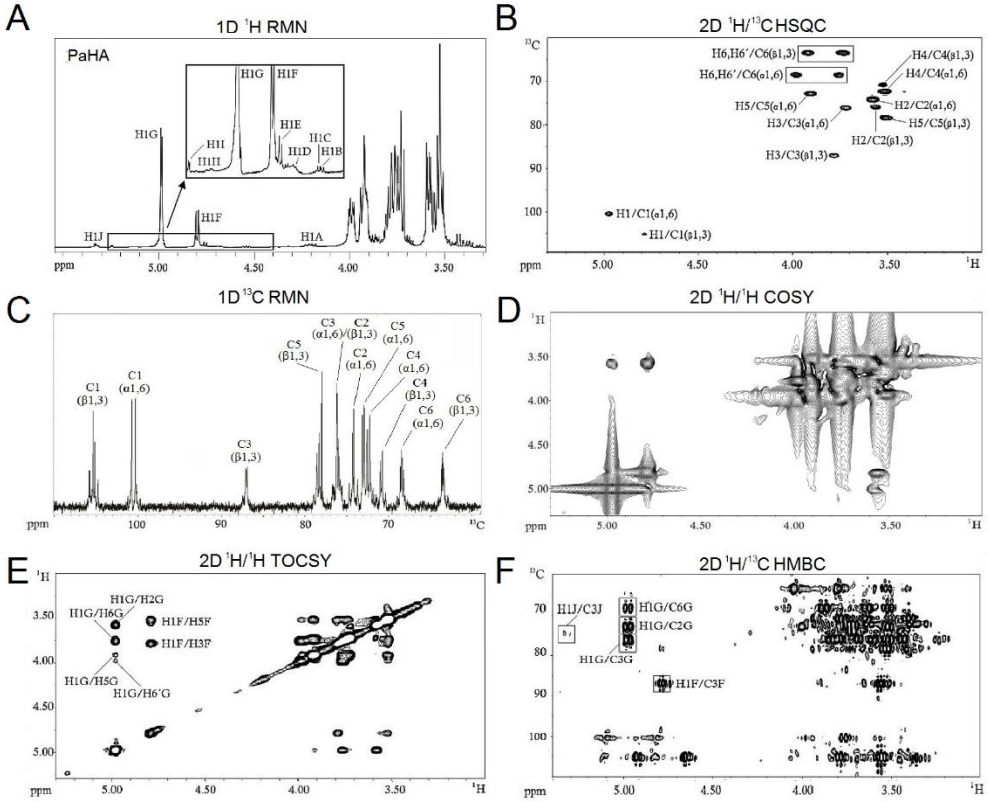

Figure 18. Nuclear magnetic resonance (NMR) spectra of the polysaccharide from the hot alkali extract (PaHA) from the basidiome of *P. albidus.* (**A**) ^{1}H NMR, (**B**) ^{1}H/^{13}C HSQC, (**C**) ^{13}C NMR, (**D**) 2D ^{1}H/^{1}H COSY, (**E**) ^{1}H/^{1}H ROESY and (**F**) ^{1}H/^{13}C HMBC spectra (D_2O; 40 °C) of PaHA.

Treatment with polysaccharides up to 200 µg/mL had no effect on the viability of macrophages when compared to control, as revealed by the MTT and crystal violet assay (**Figure 19A**). Polysaccharide fractions induced TNF-α secretion (**Figure 19B**) and their effects on IL-6 secretion were less evident (**Figure 19C**). PaCW and PaEX had no differences on IL-6 secretion when compared to control, and significant effects of PaHW, PaEN and PaHA were shown only at higher concentrations. Polysaccharides also induced NO secretion (**Figure 19D**). PaCW, PaEX and PaHA induced significant NO secretion at 100 or 200 µg/mL, while PaHW and PaEN induced significant NO production at lower concentration.

The effects of polysaccharides (200 µg/mL) on the phagocytosis of zymosan particles by macrophages previously exposed or not to LPS were also investigated (**Figure 19E**). PaCW and PaEX clearly reduced the phagocytic index, while PaHW, PaEN and PaHA increased the phagocytic index in untreated macrophages. In contrast, in macrophages previously exposed to LPS, PaCW and PaEX did not differ from the control, while PaHW, PaEN and PaHA significantly reduced the phagocytic index.

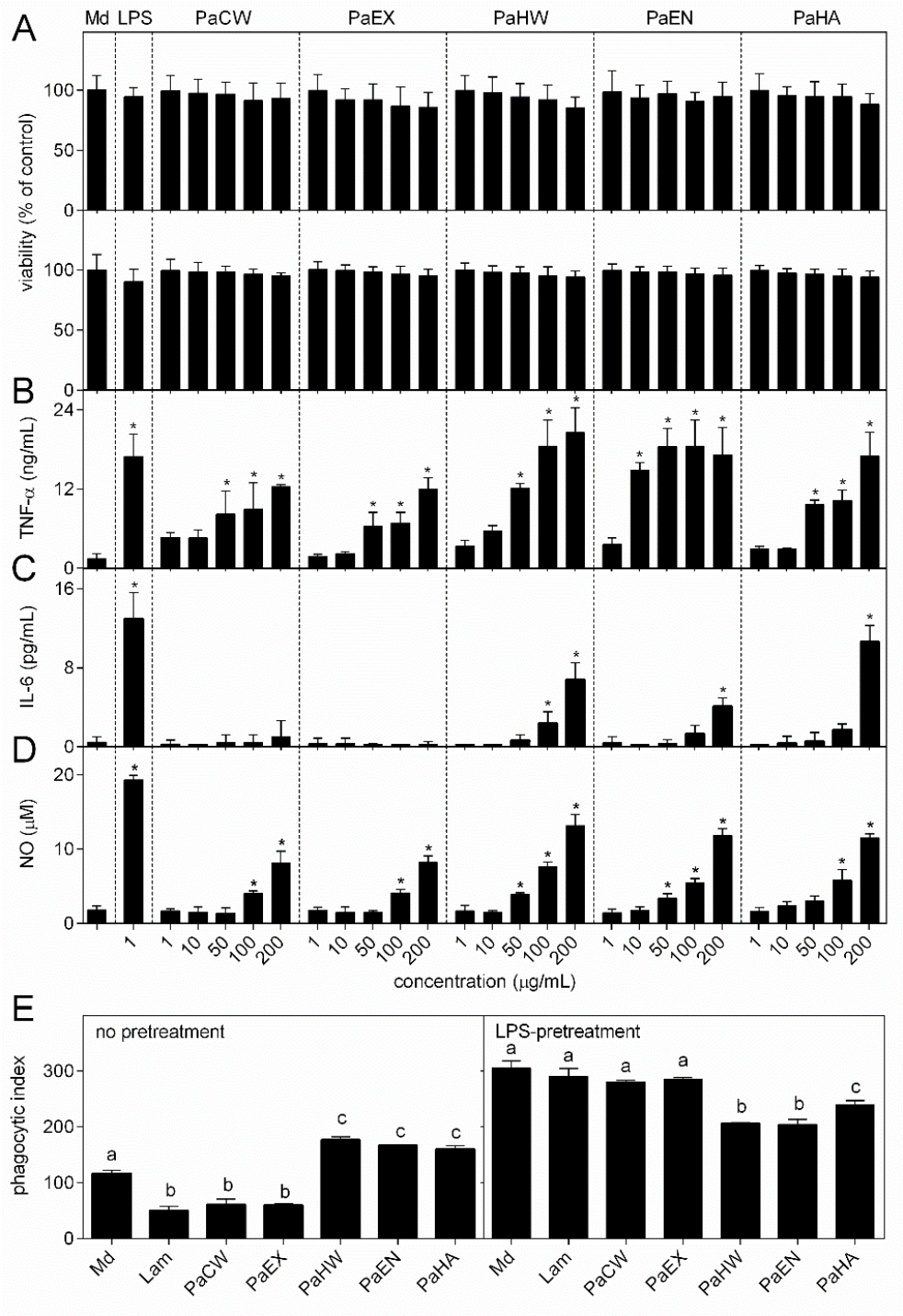

Figure 19. Effects of polysaccharides from *P. albidus* in macrophages. RAW 264.7 macrophages (2.0×10^4 cell/well; 96-well plate) were incubated with polysaccharides from *P. albidus* (1-200 μg/mL; 24 h) and evaluated for (**A**) viability using the MTT (top) and crystal violet assay (bottom) and (**B**) tumor necrosis factor alpha (TNF-α) and (**C**) interleukin-(IL-) 6 secretion. (**D**) RAW 264.7 macrophages (1.0×10^5 cell/well; 24-well plate) were incubated with polysaccharides (1-200 μg/mL; 24 h) and evaluated for nitric oxide (NO) secretion. (**E**)

RAW 264.7 macrophages (1.0×10^5 cell/well; 24-well plate containing coverslips) previously exposed or not to LPS (1 μg/mL; 1 h) were incubated with polysaccharides (200 μg/mL; 24 h) or laminarin from *Laminaria digitata* (Lam; 50 μg/mL; 24 h). Then, phagocytosis of zymosan particles (10 particles/cell) was allowed (37 °C; 1 h). Results represent the phagocytic index (PI = percentage of phagocytosis × mean number of particles per cell). Md: Media. Different letters represent significant differences (ANOVA with Tukey's as post hoc test, $p < 0.05$). *: Significant difference when compared to the control (ANOVA with Dunnett's as post hoc test, $p < 0.05$). Results represent the mean ± SD of three independent experiments.

4.5 Effects of polysaccharides from *P. albidus* on lipid-induced inflammation and foam cell formation

The structural characterization of polysaccharides from the basidiome and submerged culture of *P. albidus* performed **section 4.4** revealed that the exopolysaccharide from the submerged culture (PaEX) and the polysaccharide extracted in cold water from the basidiome (PaCW) had the same structure and therefore biological effects. Furthermore, the polysaccharide extracted in hot alkali solution from the basidiome (PaHA) is a mixture of polysaccharides similar to those of PaCW and those of extracted in cold and hot water (PaHW). Thus, only the endopolysaccharide from the submerged culture (PaEN), PaCW and PaHW were tested for their effects on lipid-induced inflammation and foam cell formation. Furthermore, since glucans were tested for they effects on lipid-induced NLRP3 inflammasome activation, the human monocytic THP-1 cell line was used instead of the RAW 264.7 cell line, which is defective in the expression of the adaptor protein ASC necessary for NLRP3 inflammasome assembling (70).

The glucans from *P. albidus* (50-200 μg/mL) had no effect on the viability of macrophage-like cells; however, they induced TNF-α and IL-1β secretion (**Figure 20A**). PaEN and PaCW also stimulated ROS accumulation at higher concentrations. When the glucans (200 μg/mL) were tested for its effects on lipid-induced foam cell formation, it was noticed that they reduced the intracellular lipid content in macrophage-like cells previously exposed to acLDL (**Figure 20B**). However, only PaCW reduced the lipids in cells previously exposed to CC. PaCW also inhibited TNF-α and IL-1β secretion and ROS accumulation in both acLDL- and CC-pretreated macrophage-like cells, whereas PaEN and PaHW had only a less remarkable inhibitory effect on IL-1β secretion in CC-induced cells.

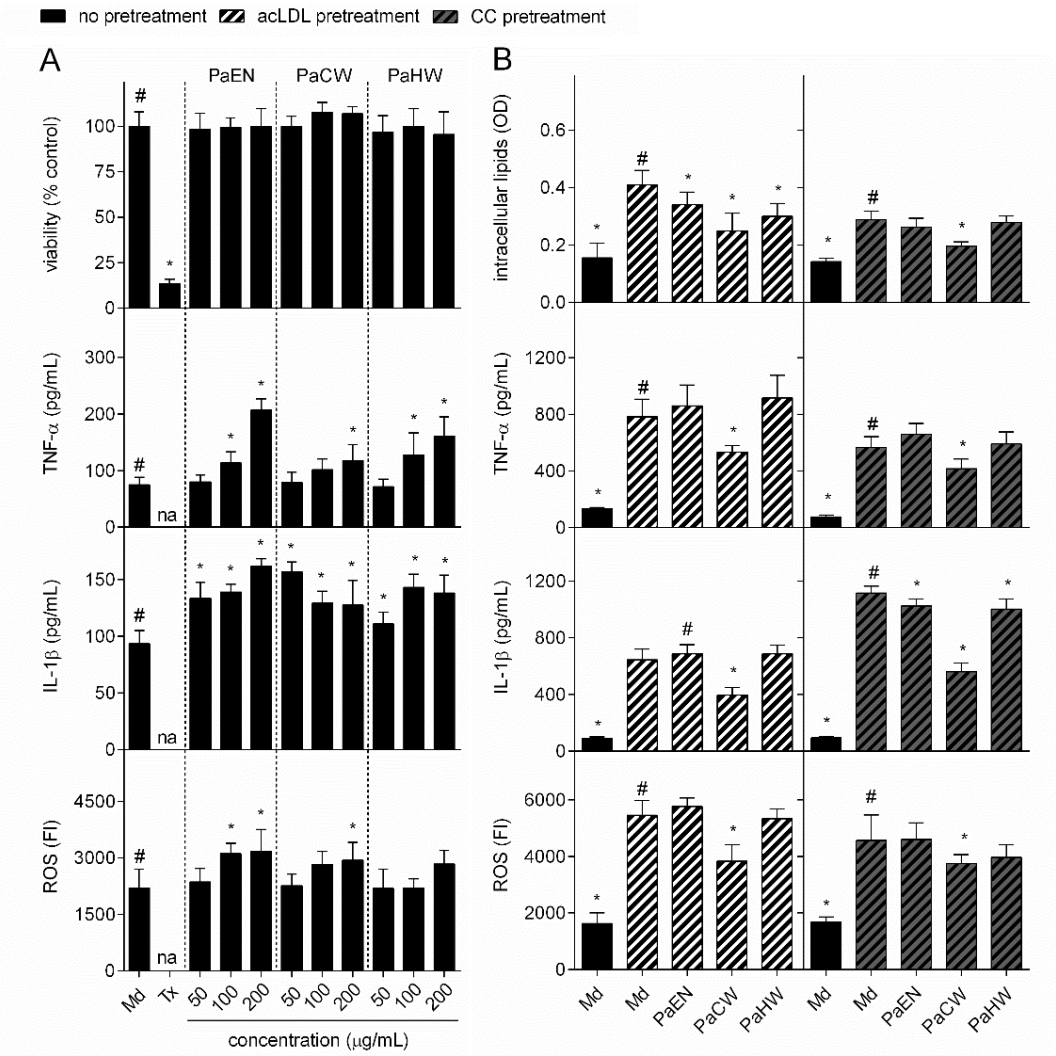

Figure 20. Effects of glucans from *P. albidus* in human macrophage-like cells previously exposed or not to modified LDL (acLDL) or cholesterol crystals (CC). (**A**) THP-1 differentiated cells were incubated with or without glucans (50, 100 or 200 μg/mL) or 0.2% Triton X-100 (Tx; cell death control) for 24 h and evaluated for viability, TNF-α and IL-1β secretion, and reactive oxygen species (ROS) accumulation. (**B**) THP-1 differentiated cells were exposed to acLDL (50 μg/mL) or CC (1 mg/mL). After 30 min, macrophages were incubated with or without glucans (200 μg/mL) for a further 24 h and evaluated for intracellular lipid content, TNF-α and IL-1β secretion and reactive oxygen species (ROS) accumulation. Md: Media; FI: Fluorescence intensity; na: Not analysed; OD: Optical density. *: Significant difference when compared to control (#) (ANOVA with Dunnett's post hoc test; $p < 0.05$). Results represent the mean ± SD of at least three independent experiments.

Since the uptake of modified lipoproteins and formation of CC are early causes of NLRP3 inflammasome activation, it was investigated whether the effects of glucans on lipid-

induced inflammation are related to NLRP3 inflammasome activation. Results revealed that PaCW (200 µg/mL) downregulated NLRP3, caspase-1 and IL-1β gene expression in macrophage-like cells previously exposed to acLDL or CC (**Figure 21A**). In contrast, although PaEN and PaHW (200 µg/mL) downregulated caspase-1 gene expression in acLDL- or CC-pretreated cells, these glucans affected NLRP3 gene expression only in CC-induced cells and had no effect on IL-1β gene expression. To explore whether glucans induce lipid efflux, the expression of PPARγ and LXRα genes was also investigated (**Figure 21B**). Interestingly, only PaCW (200 µg/mL) increased mRNA levels of PPARγ and LXRα in both acLDL- and CC-pretreated macrophages, suggesting that only PaCW induce genes related with lipid efflux among the glucans tested.

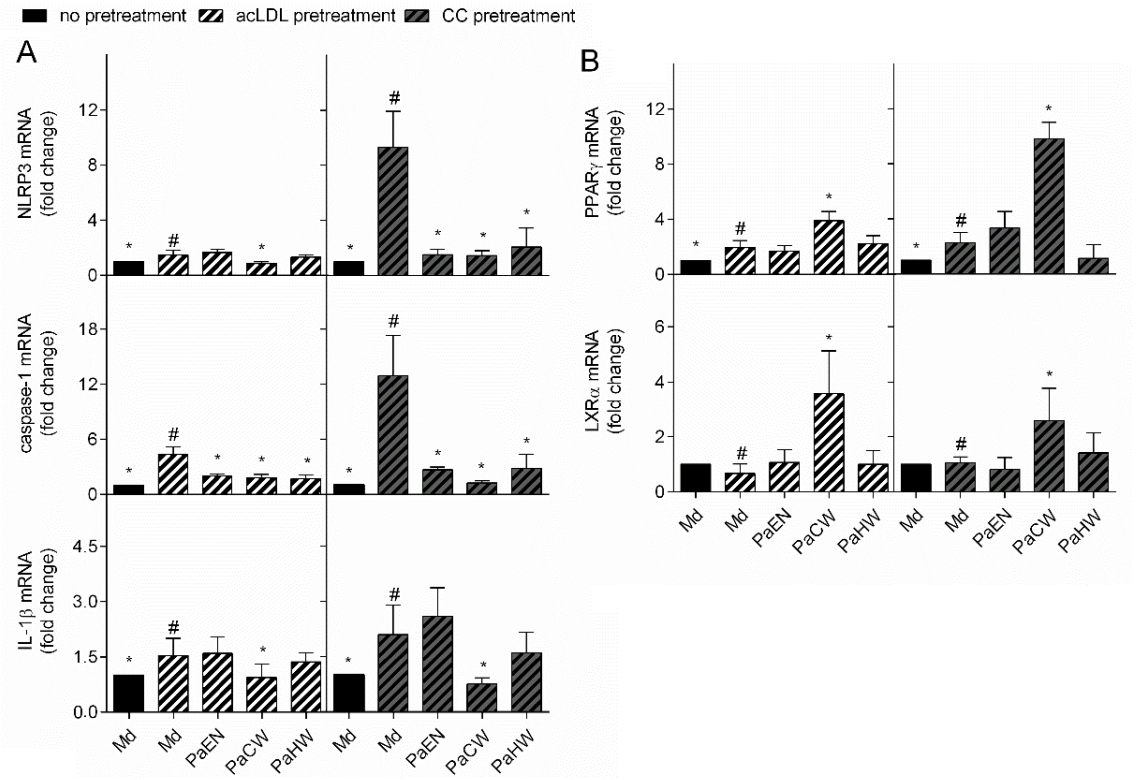

Figure 21. Effects of glucans from *P. albidus* on the expression of genes related to NLRP3 inflammasome activation and lipid efflux in human macrophage-like cells previously exposed to modified LDL (acLDL) or cholesterol crystals (CC). THP-1 differentiated cells were exposed to acLDL (50 µg/mL) or CC (1 mg/mL). After 30 min, macrophages were incubated with or without glucans (200 µg/mL) for a further 24 h and evaluated for the (**A**) relative mRNA expression of NLRP3, caspase-1, IL-1β and (**B**) PPARγ and LXRα. The geometrical mean of the cycle threshold values of β-actin and ribosomal protein L37 genes were used to calculate relative expression using the ΔΔCt method. Md:

media; *: Significant difference when compared to control (#) (ANOVA with Dunnett's post hoc test; $p < 0.05$). Identical significant differences were observed when ΔCt values was used instead of ΔΔCt values. Results represent the mean ± SD of at least three independent experiments.

Since NLRP3 inflammasome activation induces caspase-1-mediated cell death, it was evaluated whether glucans could affect NLRP3 inflammasome-induced cell death in cells previously exposed to acLDL or CC. According to **Figure 22A**, incubation with a relatively low acLDL concentration (50 µg/mL; $acLDL_{Low}$) had no effect on the viability of macrophages and a significant lipid uptake was only noticed after 24 h. Therefore, to avoid this long incubation time, a higher concentration of acLDL (100 µg/mL; $acLDL_{High}$) was tested. However, at this higher concentration, the viability of the macrophages was reduced before the significant increase in lipid uptake (6h), suggesting a lipid toxic effect rather than NLRP3 inflammasome activation. Thus, the effects of glucans on NLRP3 inflammasome-induced cell death were tested only in macrophages previously exposed to CC, since the 2-h incubation did not affect viability and led to significant lipid accumulation. As shown in **Figure 22B**, PaCW—but not PaEN or PaHW—inhibited cell death in macrophage-like cells that had previously been exposed to CC to induce the NLRP3 inflammasome.

The inhibition of NLRP3 inflammasome activation by mushroom glucans was also investigated using active caspase-1 (p20) protein levels. As shown in **Figure 22C**, only PaCW reduced the expression of active caspase-1 in macrophage-like cells previously exposed to CC, confirming that PACW inhibited caspase-1-mediated cell death.

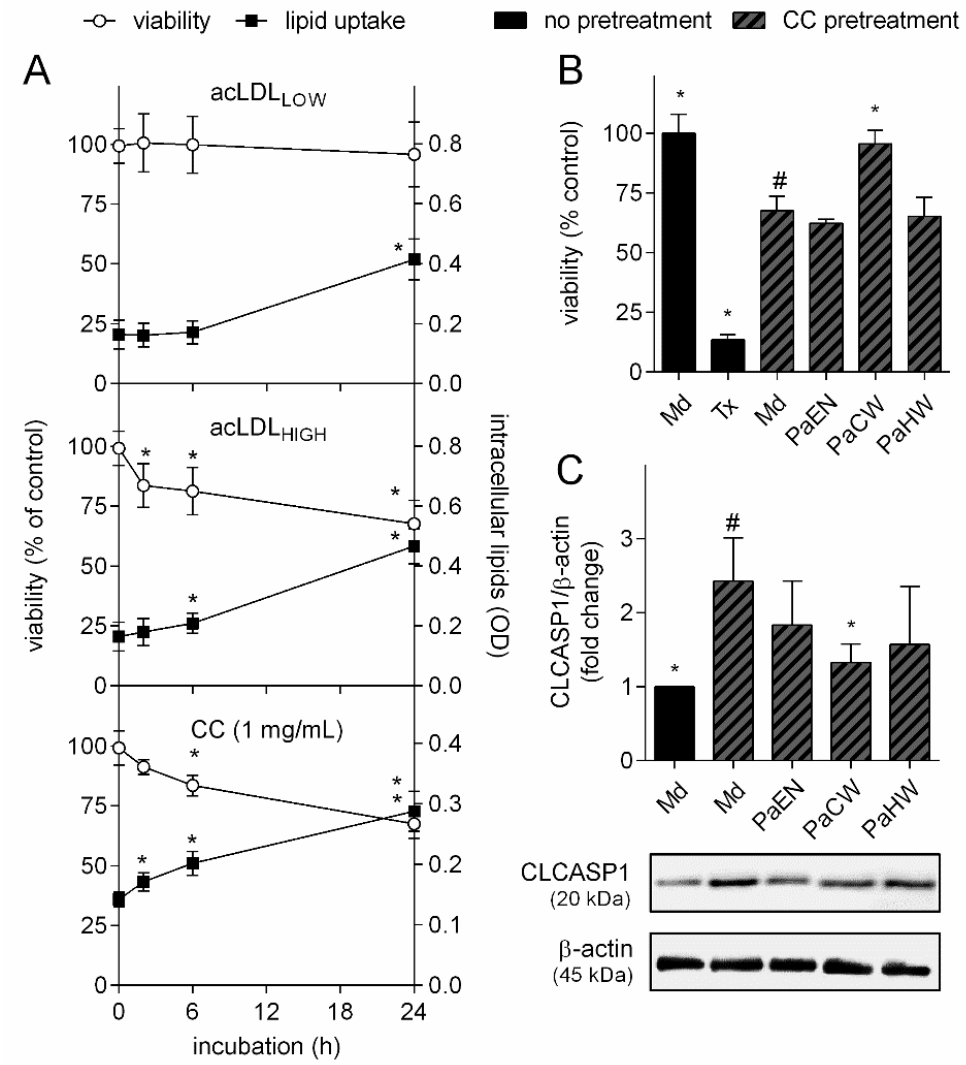

Figure 22. Effects of glucans from *P. albidus* on caspase-1-induced cell death in human macrophage-like cells exposed to cholesterol crystals (CC). (**A**) THP-1 differentiated cells were exposed to modified LDL at low (acLDL$_{Low}$; 50 µg/mL) or high (acLDL$_{High}$; 100 µg/mL) concentrations or CC (1 mg/mL) and evaluated for viability and intracellular lipid content. (**B**) THP-1 differentiated cells were exposed to CC (1 mg/mL). After 30 min, macrophages were incubated with or without glucans (200 µg/mL) or 0.2% Triton X-100 (Tx; cell death control) for a further 24 h and evaluated for viability. (**C**) Protein levels of active caspase-1 (p20) (CLCASP1) from the lysate of THP-1 differentiated cells exposed to CC (1 mg/mL) for 30 min and incubated with glucans (200 µg/mL) for a further 24 h. The densities of the protein bands were normalised against the levels of β-actin and expressed as fold change compared to control (#). Md: Media; OD: Optical density; *: Significant difference when compared to control (ANOVA with Dunnett's post hoc test; $p < 0.05$). Images of gels are representative and results represent the mean ± SD of three independent experiments

5. DISCUSSION

5.1 Effects of polysaccharides from raw and cooked chayote pulp on macrophages

Most of the chayote cell wall polysaccharides remained in the cooked fruit, but a small portion was solubilized in the hot water extract. Since the chayote cell wall structure is composed mainly of highly branched galactans and minor amounts of arabinans and homogalacturonans (27), a high degree of branching of high-MW galactans suggest strong interactions, which might explain why galactan-rich polysaccharides are less prone to solubilization during cooking.

Then, polysaccharides from chayote were evaluated in macrophages. Since the mitochondrial metabolic activity revealed by the MTT assay might be affected by bioactive compounds (81), the results from the MTT assay were confirmed using the crystal violet assay, a nucleus staining-based assay. Notably, differences in the MTT assay was more evident in macrophages previous exposed to LPS than in macrophages without pretreatment. The increased levels induced by SeR and SeH might be the result of an inhibition of LPS-induced activation, since when macrophages become activated by LPS they stop proliferate and adopt a pro-inflammatory phenotype (82). Thus, the relative increase in metabolic activity in macrophages exposed to LPS after incubation with SeR and SeH could be related the inhibition of macrophage activation. Furthermore, no effects were observed on the Caco-2 cell line, supporting the hypothesis of effects in macrophage activation. The effects of polysaccharides on the LDH release by macrophages was also evaluated. Since plasma membrane damage releases LDH into the culture media, the activity of the LDH in the supernatant could be quantified and used as a marker of cytotoxicity. The number of macrophages detached can also give an indication of cell death, as macrophages may detach from the tissue culture plate before undergoing apoptosis (59). Notably, no differences on LDH release and cell detachment were observed between the control and polysaccharides at 100 or 400 µg/mL. Thus, the effects of polysaccharides in the MTT assay might be explained by a decrease in macrophages proliferation rather than cytotoxicity.

Then, it was tested effects of polysaccharides on cytokines and NO secretion by macrophages. Even though the RAW 264.7 mouse macrophage cell line is deficient in the processing IL-1β (70), it exhibits key characteristics of different human macrophage phenotypes (83), being widely used as a model to evaluate the immunomodulatory potential of polysaccharides (6). TNF-α plays an important role in proliferation and differentiation of

macrophages, being considered a central player in inflammatory macrophage activation and recruitment (84). IL-6 is involved in inflammation and infection responses and in the regulation of metabolic and regenerative processes, inducing monocytes recruitment and their differentiation into macrophages (85). NO acts both as an antimicrobial and as a signaling molecule in response to the activation of macrophages (86).

SeR and SeH inhibited TNF-α, IL-6 and NO secretion in macrophages previously exposed to LPS or zymosan. Thus, effects of polysaccharides might be mediated mainly through the toll-like receptors (TLR2 and TRL4), dectin-1 and scavenger receptors, as reported for other botanical polysaccharides (87). The high proportion of arabinose-rich polysaccharides and homogalacturonans and effects on phagocytosis by LPS-pretreated macrophages suggests interaction through TLR4 (88,89). Furthermore, the inhibition of zymosan phagocytosis in macrophages with no pretreatment suggest interaction mainly with dectin-1 and TLR2 (90). Notably, SeC, which showed the highest proportion of high-MW galactan-rich polysaccharides, had no effect on zymosan-induced cytokine secretion or phagocytosis of zymosan particles. These results suggest a minor role for high-MW galactan-rich polysaccharides in dectin-1- and TLR2-mediated responses.

Thus, although the chayote cell wall has been reported to be stable following cooking (27), minor changes in the composition resulting from the solubilization of a small proportion of low-MW polysaccharides, mainly arabinans and homogalacturonans, had impact on their biological effects on macrophages. The complexity of effects of polysaccharides from raw and cooked chayote in macrophages might be attributable both to the complex composition of polysaccharides (91), as well as to the mechanism of recognition by macrophages, with different receptors cooperating with each other and activating redundant signaling pathways (87). In summary, polysaccharides from chayote regulate macrophage function, and minor changes in composition resulting from the solubilization of low-MW polysaccharides during cooking influences their biological effects. The regulation of macrophage activity by chayote polysaccharides appear to be beneficial, because a persistent pro-inflammatory phenotype enhances TNF-α, IL-6 and NO secretion and therefore contribute to the progression of chronic inflammatory diseases. Thus, chayote should be explored as a source of bioactive polysaccharides with immunomodulatory effects.

5.2 Effects of polysaccharides from chayote on lipid-induced inflammation and foam cell formation

In the **section 5.1** it was discussed that SeR is a source of galactan- and arabinan-rich polysaccharides with immunomodulatory effects on macrophages (37). As the effects of SeR were observed in macrophages induced with zymosan, which induces NLRP3 inflammasome activation and impairs reverse cholesterol transport (92,93), we investigated whether SeR modulates CC-induced NLPR3 inflammasome activation and lipid metabolism in human macrophages-like THP-1 cells. Notably, SeR inhibited foam cell formation and pro-inflammatory effects in cells previous exposed to CC.

The observation that SeR inhibited lipid accumulation in CC-pretreated cells led us to explore whether SeR reduces CC phagocytosis or induces lipid efflux in macrophage-like cells. To accomplish this, lipid-laden cells were incubated in CC-free media containing or not SeR to determine if this polysaccharide fraction enhances lipid efflux. Results showed that lipid-laden cells treated with SeR had reduced intracellular lipid content when compared to untreated cells, suggesting that this polysaccharide fraction induces lipid efflux. To confirm this hypothesis, it was assessed if SeR enhances the expression of genes related with lipid metabolism and efflux, and it was observed that SeR upregulated LXRα gene expression in CC-pretreated cells. LXRα acts as a cholesterol sensor, inducing the expression of target genes associated with cholesterol efflux in macrophages—such as the ATP-binding cassette transporter A1 (ABCA1) (94). Despite the levels of the efflux receptors in CC-pretreated cells were not evaluated in this study, the effects of SeR on intracellular lipid content and LXRα gene expression strongly suggests that SeR enhances lipid efflux in macrophage-like cells previously exposed to CC. Furthermore, the effect of SeR on the upregulation of LXRα gene expression was accompanied by the downregulation of both EMMPRIN, a key regulator of lipid-induced inflammation that enhance the expression of NF-κB-related pro-inflammatory molecules (95), and its induced protease MMP-9 (96).

Furthermore, based on the recent finding that the induction of LXR supress NLRP3 inflammasome activation (97) and the observation that SeR also reduced both loss of viability, ROS accumulation and IL-1β secretion in CC-pretreated cells, it was explored whether SeR influences NLRP3 inflammasome activation in macrophage-like cells previously exposed to CC. Since NLRP3 inflammasome assembling induces processing of pro-caspase-1 to active caspase-1 (p20), which, in turn, enhances IL-1β secretion, ROS production (98) and

pyroptosis, an inflammatory form of programmed cell death (99), it was assessed the effects of SeR on CC-induced active caspase-1 levels.

SeR strongly inhibited active caspase-1 levels in macrophage-like cells previously exposed to CC. Then, SeR was assessed for effects on K^+ efflux and cathepsin B levels, which are the common trigger of DAMP-mediated NLRP3 inflammasome activation in cells previously exposed to CC (100). The results revealed that the effects of SeR on CC-induced NLRP3 inflammasome activation are related neither to inhibition of K^+ efflux nor cathepsin B levels. However, although the K^+ efflux and leakage of the lysosomal protease cathepsin B are needed for CC-induced NLRP3 inflammasome activation (61), a priming step that involves the transcriptional upregulation of both IL-1β and the inflammasome sensor NLRP3 are also crucial for NLRP3 inflammasome-induced effects (72).

Since previous study showed that SeR inhibited pro-inflammatory effects in macrophages previously exposed to LPS (37), which induces NF-κB-dependent IL-1β and NLRP3 priming (101), the effects of SeR on CC-induced IL-1β and NLRP3 gene expression was also tested. Confirming our hypothesis, SeR downregulated both IL-1β and NLRP3 gene expression in macrophage-like cells previously exposed to CC. Furthermore, to support the hypothesis that SeR inhibits priming signals required for NLRP3 inflammasome activation, the effect of SeR on both IL-1β and NLRP3 gene expression was also tested in macrophage-like cells previously exposed to LPS, which induces the transcription upregulation of these genes through an NF-κB-dependent manner (101). Notably, NF-κB-dependent transcriptional upregulation of both IL-1β and NLRP3 genes in LPS-pretreated cells were inhibited by SeR, confirming that this polysaccharide fraction inhibits priming signals required for NLRP3 inflammasome activation.

The mechanisms of some widely-used anti-inflammatory compounds have been at least partly ascribed to their effects on NLRP3 inflammasome activation (102). In the present study, we showed that highly branched arabinan- and galactan-rich DF from chayote fruit pulp enhances lipid efflux and regulates priming signals necessary for NLRP3 inflammasome activation in macrophage-like cells previously exposed to CC (**Figure 23**).

Although further study is necessary to define the structure from SeR responsible for the effects and the metabolic pathways modulated in lipid-induced macrophage-like cells, this study expands the current understanding of how a component of the DF present in chayote pulp can promote health benefits not limited to their physical properties on the gastrointestinal tract. This may in turn be useful in exploration of its potential as a functional food ingredient.

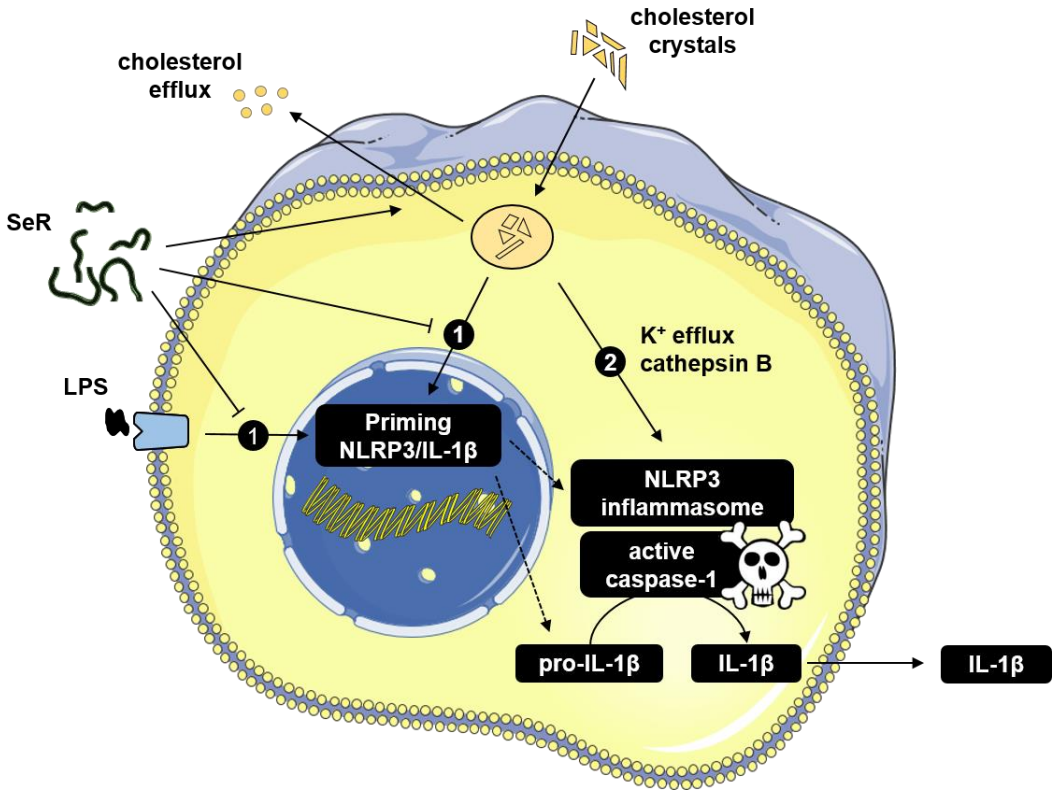

Figure 23. Effects of polysaccharides from raw chayote (SeR) on lipid efflux and NLRP3 inflammasome in macrophage-like cells previously exposed to cholesterol crystals (CC). NLRP3 inflammasome activation requires two steps to induce caspase-1-mediated cell death and interleukin (IL-) 1β secretion: (1) a transcriptional upregulation (e.g. priming) of NLRP3 and IL-1β followed by (2) post-translational regulation responsible for the oligomerization of the NLRP3 inflammasome components. In addition to enhance intracellular lipid content, CC phagocytosed by macrophage-like THP-1 cells induce priming of NLRP3 and IL-1β (step 1), K^+ efflux and lysosomal leakage of cathepsin B, thereby inducing NLRP3 inflammasome oligomerization (step 2). In this work, it was shown that SeR enhance lipid efflux and regulate NLRP3 inflammasome activation through induction of liver X receptor α gene expression and inhibition of priming signals required for NLRP3 inflammasome, respectively.

5.3 Optimization of extraction of polysaccharides from mushroom basidiome

In the original method, the first step is a time consuming incubation in methanol to remove lipids and small molecules. In the optimized method, the use of chloroform:methanol extraction (103) for a short time gave similar results. Furthermore, when crude extracts were submitted to successive extractions with water at 25°C, water at 100°C and 1 M NaOH at

100°C at different incubation times, the minimum time to achieve similar yields when compared to the original method was 8 h, instead of 24 h. The monosaccharide composition of polysaccharides obtained at intermediate times was similar to the original method, but minor differences were observed for galactose and xylose proportions in cold and hot water extracts incubated up to 6 h, which suggests that the cold water-soluble polysaccharide was not entirely extracted and remained in the hot water fraction. Thus, incubation for 8 h at each step seemed to be the minimum for an adequate extraction.

Since sodium hydroxide react with glycosidic linkages in a mechanism called β-elimination or end-wise degradation (104), hot alkali extraction was performed in the presence of sodium borohydride, a reducing agent used to minimize β-elimination. Furthermore, potassium hydroxide was used instead NaOH, since potassium acetate formed during alkali neutralization with acetic acid is more soluble in ethanol than in sodium acetate. Although development of β-elimination reaction was not evaluated, polysaccharide from hot alkali extract from both methods had similar yield, composition and average molecular weight. These results suggest that the original method does not induce β-elimination reaction. Nevertheless, the preventive use of sodium borohydride might be important when extracting polysaccharides more prone to oxidative degradation.

The water-soluble polysaccharides obtained by the optimized method were subject to an additional cycle of extraction to evaluate their stability to the extraction method. Notably, the water-soluble polysaccharides are stable to the method of extraction. In summary, results showed that is possible obtain water-soluble polysaccharides reducing by up to half the extraction time commonly required. Thus, the optimized method could be explored as an inexpensive, efficient and easy reproducible method for the extraction of water-soluble polysaccharides from mushrooms.

5.4 Structure and effects of polysaccharides from the basidiome and submerged culture of *P. albidus* in macrophages

OM are versatile mushrooms with a large number of species and a broad morphological plasticity (44). Therefore, to avoid taxonomic confusion, the mushroom used in the present study was positively identified as *P. albidus* by morphological and molecular methods. Its occurrence in the Serra da Bocaina represents the first record of this species in the state of Rio de Janeiro (Brazil). In addition, the basidiome was collected on *Araucaria*

angustifolia trunk, a substrate previous associated only with the growth of *P. djamor* (Rumph. ex. Fr.) Boedijn, *P. ostreatus* (Jacq.) P. Kumm. and *P. pulmonarius* (Fr.) Quél. (44).

Although *P. albidus* is not recognized as a commercial mushroom, it cultivation under similar conditions as those used for the commercial production of other edible *Pleurotus* yielded relatively high amounts of fresh basidiome and biomass (34,35). Since mushroom polysaccharides are mainly structural—and complex—components of the fungal cell wall, varying conditions were employed to extract the polysaccharides from *P. albidus*. The polysaccharides from the basidiome were extracted using mild-to-strong temperature and pH conditions to break the fungal cell wall from the outer layer to the inner layer. In the case of mycelia from the submerged culture, exopolysaccharides loosely attached to the outer layer of the cell wall were secreted to the extracellular matrix and therefore solubilized in culture broth, whereas endopolysaccharides from the inner layer were extracted after heating.

PaCW and PaEX showed no differences in composition and structure, suggesting the occurrence of the same polysaccharide in both mycelium and the basidiome—as previously been reported for grifolan, another β-D-1,3-glucan substituted at O-6 from *Grifola frondosa* (Dicks.) Gray (105). In contrast, PaHW and PaEN, which are more firmly attached to the fungal cell wall, had NMR spectra typical of α-D-1,6-glucan substituted at O-2 and O-3. Notably, there is only one previous report of glucans from *Pleurotus* substituted at O-2 (106). Furthermore, the stronger condition of pH and temperature during the hot alkali extraction disrupted the cell wall and released the glucans more firmly attached to other components, such as chitin and water-insoluble polysaccharides (10). These results might explain the presence of both α-D-1,6- and β-D-1,3-glucans similar to those of glucans from aqueous extracts.

Since no differences in the MTT were observed between macrophages treated or not with the glucans, the same concentrations were used to evaluate their effects on cytokine secretion. PaCW and PaEX induced TNF-α and NO secretion, but had no effect on IL-6 secretion by macrophages. Furthermore, PaCW and PaEX reduced zymosan phagocytosis by untreated macrophages, but had no effect in macrophages previously exposed to LPS. These effects were similar to that of laminarin, a low MW (~6 kDa) β-D-glucan from *Laminaria digitata* (Hudson) J.V.Lamouroux (brown algae) that acts as a dectin-1 blocker. Laminarin did not affect IL-6 secretion, but induce NO secretion (107), reduced phagocytosis by untreated macrophages and had no effect on LPS-pretreated macrophages (66). In contrast, PaHW and PaEN induced cytokines and NO secretion and had similar phagocytic index on untreated and LPS-pretreated macrophages. Thus, effects of PaHW and PaEN seems—at least partially—

independent of TLR4. In accordance with these results, glucans substituted at O-6 (108) and O-2 (109) interact with macrophages mainly through TLR2 rather than TLR24. Finally, PaHA (mixture of α- and β-D-glucans) had intermediary effect on zymosan phagocytosis in macrophages previous exposed to LPS.

In summary, polysaccharides from *P. albidus* regulate macrophage function, and they have the potential to promote other beneficial effects. PaCW and PaEX are similar to laminarin, which has been demonstrated to regulate gut immunity by controlling T regulatory cell expansion through the modification of microbiota (110). Furthermore, the glucans substituted at O-2 (PaHA and PaEN) are likely resistant to digestive enzymes, which may have the potential to promote the growth of beneficial microorganisms in the human colon. Thus, the *P. albidus* basidiome and submerged culture are promising sources of easily extractable α- and β-D-glucans with potential benefits for human health.

5.5 Effects of polysaccharides from *P. albidus* on lipid-induced inflammation and foam cell formation

Recent studies have shown potential beneficial effects of glucans and other polysaccharides on the reduction of foam cell formation by inhibiting cholesterol influx or by enhancing lipid metabolism and efflux (18–20,111,112). In the **section 5.4**, it was discussed that the glucans from *P. albidus* modulates macrophage function (39). Thus, we investigated the effects of glucans from *P. albidus* on foam cell formation and lipid-induced inflammation in human macrophage-like cells cells.

Although the glucans from *P. albidus* stimulated macrophages without affecting cell viability, they showed inhibitory effects in cells previously exposed to both acLDL or CC, two factors that promote a pro-inflammatory phenotype and lead to lipid-induced inflammation and foam cell formation (24). However, the polysaccharide preparations examined in the present study seemed to act via distinct mechanisms.

PaCW inhibited foam cell formation, pro-inflammatory cytokine secretion and ROS accumulation in macrophages exposed to acLDL or CC. As the intracellular nucleation of acLDL or the presence of extracellular CC are early causes of NLRP3 inflammasome activation in macrophages during hypercholesterolemia (24,113), the reduction of pro-inflammatory cytokine secretion by PaCW could be linked to the downregulation of NLRP3, caspase-1 and IL-1β gene expression in macrophages exposed to acLDL and CC. Furthermore, as PaCW induced LXRα gene expression, which inhibit the transcription of pro-

inflammatory genes, induce ABC transporter-mediated cholesterol efflux through the transcriptional regulation of ABCA1 and ABCG1 and limits cholesterol uptake(114,115), the inhibition of lipid-induced inflammation and foam cell formation would occur mainly through—but would not be limited to—induction of lipid metabolism and efflux.

In contrast, PaEN and PaHW reduced foam cell formation in macrophage-like cells previously exposed to acLDL, but not in macrophages exposed to CC. Although further study to determine by which mechanisms PaEN and PaHW reduce foam cell formation in acLDL-pretreated cells is needed, results suggest that they inhibit scavenger receptor-mediated lipid influx rather than induce lipid efflux. Consistent with this hypothesis, PaEN and PaHW did not induce PPARγ or LXRα gene expression in macrophage-like cells previously exposed to acLDL or CC.

Curiously, PaEN and PaHW downregulated caspase-1 gene expression in macrophage-like cells previously exposed to acLDL, but did not inhibit pro-inflammatory cytokine secretion. Although the transcriptional regulation of caspase-1 enhances NLRP3 inflammasome activation, the transcriptional upregulation of both pro-IL-1β and the inflammasome sensor NLRP3 are the essential elements for NLRP3 inflammasome assembling (116,117). Thus, the absence of effect on pro-IL-1β and NLRP3 gene expression explains why downregulation of caspase-1 by PaEN and PaHW in cells previously exposed to acLDL is insufficient to inhibit pro-inflammatory cytokine secretion. The observation that PaEN and PaHW had only a minor inhibitory effect on IL-1β secretion in macrophages exposed to CC can also be explained by the absence of effect of these polysaccharides on the transcriptional regulation of pro-IL-1β in macrophage-like cells.

As NLRP3 inflammasome-induced cell death is mainly dependent on caspase-1, and as the polysaccharides downregulate caspase-1 gene expression, we explored whether polysaccharides inhibit the loss of viability in macrophage-like cells previously exposed to lipids (99). However, the test was limited to cells exposed to CC, because the negative effect of acLDL on the viability of macrophages suggested a lipid-induced toxic effect rather than NLRP3 inflammasome activation. In this regard, PaCW—but not PaEN or PaHW—inhibited the loss of viability induced by CC, which was in agreement with the inhibition of active caspase-1 protein levels in macrophage-like cells previously exposed to CC.

In summary, the mechanisms by which polysaccharides from *P. albidus* regulate lipid-laden macrophage-like cells may be accounted by their different structures. PaCW, which enhances lipid metabolism and efflux through the PPARγ-LXRα axis, is a low-MW β-1,3-glucan substituted at O-6. In contrast, PaEN and PaHW, which has no effect on PPARγ and

LXRα gene expression and regulate foam cell formation only in cells previously exposed to modified lipoprotein, are relatively high-MW α-1,6-glucans substituted at O-3 and O-2, as previously reported (39).

Recently, it was shown that a heteropolysaccharide containing β-1,3-glucan glycosidic linkage fails to decrease the lipid accumulation in foam cell model after digestion by β-1,3 glucanase, suggesting that this β-1,3-glucan glycosidic linkage is essential to inhibit foam cell formation (21). In the present study, we compared the effects of α-1,6- and β-1,3-glucans with different MW in macrophage-like cells previously exposed to modified LDL or CC. Although it is well know that both the conformation and the MW influences the biological effects of glucans (118,119), this study showed for the first time how these structures affected lipid-induced foam cell formation and inflammation, expanding the understanding of how glucans modulate macrophage function.

Most importantly, the findings revealed that α- and β-glucans from *P. albidus* inhibit lipid-induced inflammation at distinct levels, with significant effects on the priming of the NLRP3 inflammasome. Although a deeper investigation of the regulation of receptors involved in cholesterol influx (e.g., SR-A and CD36) and efflux (e.g., ABCA1 and ABCG1) is needed, the results here clearly showed that α- and β-glucans from *P. albidus* differentially modulate macrophage-like cells function and reduced lipid-induced inflammation and foam cell formation. Since beneficial health effects may be derived from the consumption of these glucans, the edible mushroom and mycelium of *P. albidus* have the potential to be used as a functional food or to be a source for the extraction of biologically-active α- and β-glucans.

6. CONCLUSION

By studying the effects of fungal- and plant-derived NSP in macrophages, we determined the effects of cooking on the composition of water-soluble NSP from chayote pulp, optimized a method for the extraction of NSP from mushrooms, characterized the structure of NSP from *Pleurotus albidus*, and evaluated the effects of both fungal- and plant-derived NSP in macrophages.

The NSP from chayote pulp modulates macrophage function, and minor changes in composition resulting from the solubilization of low-MW NSP during cooking influences their biological effects. Furthermore, NSP regulate lipid metabolism and NLRP3 inflamasome activation in human macrophages, expanding the current understanding of how NSP from chayote pulp can promote health benefits not limited to their physical properties on the gastrointestinal tract.

The optimized method for the extraction of mushroom NSP could be explored as an inexpensive, efficient and easy reproducible extraction method since results showed that is possible obtain NSP from mushrooms reducing by up to half the extraction time commonly required.

In addition, the *P. albidus* basidiome and submerged culture are promising sources of easily extractable α- and β-D-glucans with potential benefits for human health. The α- and β-glucans from *P. albidus* inhibited lipid-induced inflammation at distinct levels, with significant effects on the priming of the NLRP3 inflammasome. Therefore, the basidiome and mycelium of *P. albidus* have potential to be used as a functional food or to be source for the extraction of biologically active glucans.

The integration of the results from this Thesis leads to the conclusion that despite the structural differences between NSP from fungal- and plant-derived sources, both can have effects in macrophages. Although is possible that complex pectin from chayote pulp and glucans from *P. albidus* interact with macrophages through distinct Pattern Recognition Receptors, these NSP can induce similar effects. Notably, the effects of NSP were related not only to the regulation of cytokine secretion, since the NSP from chayote and *P. albidus* regulates the expression of genes crucial for lipid metabolism in human macrophage-like cells. Although further studies are needed, results suggest that the effects in lipid-laden macrophages could be another important mechanism through which the consumption of NSP from fungal- and plant-derived sources is linked with reduced risk of diseases associated with hypercholesterolemia.

REFERENCES

1. Aune D, Keum N, Giovannucci E, Fadnes LT, Boffetta P, Greenwood DC, et al. Whole grain consumption and risk of cardiovascular disease, cancer, and all cause and cause specific mortality: systematic review and dose-response meta-analysis of prospective studies. BJM. 2016;353(i2716):1–14.
2. Jones JM. CODEX-aligned dietary fiber definitions help to bridge the “fiber gap.” Nutr J. 2014;13(1):34.
3. Corrêa-Oliveira R, Fachi JL, Vieira A, Sato FT, Vinolo MAR. Regulation of immune cell function by short-chain fatty acids. Clin Transl Immunol. 2016;5(4):e73.
4. Belkaid Y, Hand T. Role of the Microbiota in Immunity and inflammation. Cell. 2014;157(1):121–41.
5. Ang Z, Ding JL. GPR41 and GPR43 in obesity and inflammation - Protective or causative? Front Immunol. 2016;7:1–5.
6. Ferreira SS, Passos CP, Madureira P, Vilanova M, Coimbra MA. Structure-function relationships of immunostimulatory polysaccharides: A review. Carbohydr Polym. 2015;132(5):378–96.
7. Jenkins SJ, Ruckerl D, Cook PC, Jones LH, Finkelman FD, van Rooijen N, et al. Local macrophage proliferation, rather than recruitment from the blood, is a signature of TH2 inflammation. Science. 2011;332(6035):1284–8.
8. Ginhoux F, Jung S. Monocytes and macrophages: developmental pathways and tissue homeostasis. Nat Rev Immunol. 2014;14(6):392–404.
9. Murray PJ, Wynn T a. Protective and pathogenic functions of macrophage subsets. Nat Rev Immunol. 2011;11(11):723–37.
10. Ruthes AC, Smiderle FR, Iacomini M. D-Glucans from edible mushrooms: A review on the extraction, purification and chemical characterization approaches. Carbohydr Polym. 2015;117:753–61.
11. Gupta PK, Chakraborty P, Kumar S, Singh PK, Rajan MG, Sainis KB, et al. G1-4A, a polysaccharide from Tinospora cordifolia inhibits the survival of Mycobacterium tuberculosis by modulating host immune responses in TLR4 dependent manner. PLoS One. 2016;11(5):e0154725.
12. Skyberg J a, Rollins MF, Holderness JS, Marlenee NL, Schepetkin I a, Goodyear A, et al. Nasal Acai polysaccharides potentiate innate immunity to protect against pulmonary Francisella tularensis and Burkholderia pseudomallei Infections. PLoS Pathog.

2012;8(3):e1002587.

13. Zhang W, Xu P, Zhang H. Pectin in cancer therapy: A review. Trends Food Sci Technol. 2015;44(2):258–71.
14. Chen SN, Chang CS, Hung MH, Chen S, Wang W, Tai CJ, et al. The effect of mushroom beta-glucans from solid culture of Ganoderma lucidum on inhibition of the primary tumor metastasis. Evidence-based Complement Altern Med. 2014;ID 252171, 7 p.
15. Gill SK, Islam N, Shaw I, Ribeiro A, Bradley B, Brien TO, et al. Immunomodulatory effects of natural polysaccharides assessed in human whole blood culture and THP-1 cells show greater sensitivity of whole blood culture. Int Immunopharmacol. 2016;36:315–23.
16. Sun J, Sun J, Song B, Zhang L, Shao Q, Liu Y, et al. Fucoidan inhibits CCL22 production through NF-κB pathway in M2 macrophages: a potential therapeutic strategy for cancer. Sci Rep. 2016;6:35855.
17. Smiderle FR, Baggio CH, Borato DG, Santana-Filho AP, Sassaki GL, Iacomini M, et al. Anti-inflammatory properties of the medicinal mushroom Cordyceps militaris might be related to its linear (1→3)-β-D-glucan. PLoS One. 2014;9(10):e110266.
18. Chen J, Yong Y, Xia X, Wang Z, Liang Y, Zhang S, et al. The excreted polysaccharide of Pleurotus eryngii inhibits the foam-cell formation via down-regulation of CD36. Carbohydr Polym. 2014 Nov;112:16–23.
19. Zha X-Q, Xue L, Zhang H-L, Asghar M-N, Pan L-H, Liu J, et al. Molecular mechanism of a new Laminaria japonica polysaccharide on the suppression of macrophage foam cell formation via regulating cellular lipid metabolism and suppressing cellular inflammation. Mol Nutr Food Res. 2015;59(10):2008–21.
20. Wang Y, Yang X, Cheng B, Mei C, Li Q, Xiao H, et al. Protective effect of Astragalus polysaccharides on ATP binding cassette transporter A1 in THP-1 derived foam cells exposed to tumor necrosis factor-alpha. Phyther Res. 2010;24:393–8.
21. Chen J, Yong Y, Xing M, Gu Y, Zhang Z, Zhang S, et al. Characterization of polysaccharides with marked inhibitory effect on lipid accumulation in Pleurotus eryngii. Carbohydr Polym. 2013;97(2):604–13.
22. Kunjathoor V V., Febbraio M, Podrez EA, Moore KJ, Andersson L, Koehn S, et al. Scavenger receptors class A-I/II and CD36 are the principal receptors responsible for the uptake of modified low density lipoprotein leading to lipid loading in macrophages. J Biol Chem. 2002;277(51):49982–8.

23. Chistiakov DA, Bobryshev Y V., Orekhov AN. Macrophage-mediated cholesterol handling in atherosclerosis. J Cell Mol Med. 2016;20(1):17–28.
24. Sheedy FJ, Grebe A, Rayner KJ, Kalantari P, Carpenter SB, Becker CE, et al. CD36 coordinates NLRP3 inflammasome activation by facilitating intracellular nucleation of soluble ligands into particulate ligands in sterile inflammation. Nat Immunol. 2013;14(8):812–20.
25. Moore K, Sheedy F, Fisher E. Macrophages in atherosclerosis: a dynamic balance. Nat Rev Immunol. 2013;13:709–21.
26. Bekkering S, Quintin J, Joosten LAB, Van Der Meer JWM, Netea MG, Riksen NP. Oxidized low-density lipoprotein induces long-term proinflammatory cytokine production and foam cell formation via epigenetic reprogramming of monocytes. Arterioscler Thromb Vasc Biol. 2014;34(8):1731–8.
27. Shiga T, Peroni-Okita F, Carpita N, Lajolo F, Cordenunsi B. Polysaccharide composition of raw and cooked chayote (Sechium edule Sw.) fruits and tuberous roots. Carbohydr Polym. 2015;130:155–65.
28. Yang L, Hsieh C, Lu T, Lin W. Structurally characterized arabinogalactan from Anoectochilus formosanus as an immuno-modulator against CT26 colon cancer in BALB/c mice. Phytomedicine. 2014;21(5):647–55.
29. Yang LC, Lu TJ, Lin WC. A type II arabinogalactan from A. formosanus G-CSF production in macrophages and leukopenia improvement in CT26-bearing mice treated with 5-fluorouracil. Evidence-based Complement Altern Med. 2013;ID458075, 13 p.
30. Liao W, Luo Z, Liu D, Ning Z, Yang J, Ren J. Structure characterization of a novel polysaccharide from Dictyophora indusiata and its macrophage immunomodulatory activities. J Agric Food Chem. 2015;63:535–44.
31. Corrêa RCG, Brugnari T, Bracht A, Peralta RM, Ferreira ICFR. Biotechnological, nutritional and therapeutic uses of Pleurotus spp. (Oyster mushroom) related with its chemical composition: A review on the past decade findings. Trends Food Sci Technol. 2016;50:103–17.
32. Patel Y, Naraian R, Singh VK. Medicinal properties of Pleurotus species (oyster mushroom): a review. World J Fungal Plant Biol. 2012;3(1):1–12.
33. Lechner BE, Albertó E. Search for new naturally occurring strains of Pleurotus to improve yields: Pleurotus albidus as a novel proposed species for mushroom production. Rev Iberoam Micol. 2011;28(4):148–54.
34. Souza Kirsch L, de Macedo AJP, Teixeira MFS. Production of mycelial biomass by the

Amazonian edible mushroom Pleurotus albidus. Brazilian J Microbiol. 2016;47(3):658–64.

35. Gambato G, Todescato K, Pavão EM, Scortegagna A, Fontana RC, Salvador M, et al. Evaluation of productivity and antioxidant profile of solid-state cultivated macrofungi Pleurotus albidus and Pycnoporus sanguineus. Bioresour Technol. 2016;207:46–51.
36. Sartori SB, Ferreira LFR, Messias TG, Souza G, Pompeu GB, Monteiro RTR. Pleurotus biomass production on vinasse and its potential use for aquaculture feed. Mycology. 2015;6(1):28–34.
37. Castro-Alves VC, Sansone M, Sansone AB, Nascimento JRO. Polysaccharides from raw and cooked chayote modulate macrophage function. Food Res Int. 2016;81:171–9.
38. Castro-Alves VC, Nascimento JRO. Speeding up the Extraction of Mushroom Polysaccharides. Food Anal Methods. 2016;9:2429–33.
39. Castro-Alves VC, Gomes D, Menolli N, Sforça ML, Nascimento JRO. Characterization and immunomodulatory effects of glucans from Pleurotus albidus, a promising species of mushroom for farming and biomass production. Int J Biol Macromol. 2017;95:215–23.
40. FAO/WHO. Draft codex standard for chayotes. In: FAO/WHO, editor. Joint FAO/WHO food standards programme codex alimentarius comission: twenty-third session. 1 st. Rome; 1999. p. 44–9.
41. Lechner BE, Wright JE, Albertó E. The genus Pleurotus in Argentina. Mycologia. 2004;96(4):845–58.
42. White T, Burns T, Lee S, Taylor J. Amplification and direct sequencing of fungal ribosomal RNA genes for phylogenetics. In: Innis M, Gelfand D, Sninsky J, White T, editors. PCR protocols: A guide to methods and applications. San Diego: Academic Press; 1990. p. 315–22.
43. Gardes M, Bruns T. ITS primers with enhanced specificity for basidiomycetes: application to the identification of mycorrhizae and rusts. Mol Ecol. 1993;2(2):113–8.
44. Menolli N, Breternitz BS, Capelari M. The genus Pleurotus in Brazil: a molecular and taxonomic overview. Mycoscience. 2014;55(5):378–89.
45. Yang BK, Jeong SC, Song CH. Hypolipidemic effect of exo- and endo-biopolymers produced from submerged mycelial culture of Ganoderma lucidum in rats. J Microbiol Biotechnol. 2002;12(6):872–7.
46. NEPA/UNICAMP (Center for Studies and Surveys on Food). TACO (Brazilian Table of Food Composition). 4 th. Campinas: NEPA/UNICAMP; 2011. 161 p.

47. Palacios I, García-Lafuente A, Guillamón E, Villares A. Novel isolation of water-soluble polysaccharides from the fruiting bodies of Pleurotus ostreatus mushrooms. Carbohydr Res. 2012;358:72–7.
48. Horwitz W, Latimer G. Official methods of analysis of AOAC International. 18th ed. Horwitz W, Latimer G, editors. Gaithersburg: AOAC International; 2006. 2000 p.
49. Sales-Campos C, Araujo LM, Minhoni MTDA, Andrade MCN De. Physiochemical analysis and centesimal composition of Pleurotus ostreatus mushroom grown in residues from the Amazon. Ciência e Tecnol Aliment. 2011;31(2):456–61.
50. Masuko T, Minami A, Iwasaki N, Majima T, Nishimura S-I, Lee YC. Carbohydrate analysis by a phenol-sulfuric acid method in microplate format. Anal Biochem. 2005;339(1):69–72.
51. Bradford MMM. A rapid and sensitive method for the quantitation of microgram quantities of protein utilizing the principle of protein-dye binding. Anal Biochem. 1976;72:248–54.
52. Nagel A, Sirisakulwat S, Carle R, Neidhart S. An acetate-hydroxide gradient for the quantitation of the neutral sugar and uronic acid profile of pectins by HPAEC-PAD without postcolumn pH adjustment. J Agric Food Chem. 2014;62(9):2037–48.
53. Lorenzen A, Kennedy SW. A fluorescence-based protein assay for use with a microplate reader. Anal Biochem. 1993;214(1):346–8.
54. White A, Hart RJ, Fry JC. An evaluation of the Waters Pico-Tag system for the amino-acid analysis of food materials. J Automat Chem. 1986;8(4):170–7.
55. Shiga TM, Fabi JP, do Nascimento JRO, Petkowicz CLDO, Vriesmann LC, Lajolo FM, et al. Changes in cell wall composition associated to the softening of ripening papaya: evidence of extensive solubilization of large molecular mass galactouronides. J Agric Food Chem. 2009;57(15):7064–71.
56. Morales V, Corzo N, Sanz ML. HPAEC-PAD oligosaccharide analysis to detect adulterations of honey with sugar syrups. Food Chem. 2008;107:922–8.
57. Ogawa K, Tsurugi J, Watanabe T. Complex of gel-forming β-1,3-D-glucan with Congo red in alkaline solution. Chem Lett. 1972;1(8):689–92.
58. Bach E, Schollmeyer E. An ultraviolet-spectrophotometric method with 2-cyanoacetamide for the determination of the enzymatic degradation of reducing polysaccharides. Anal Biochem. 1992;203:335–9.
59. Maxwell E, Hotchkiss AT, Morris VJ, Belshaw NJ. Rhamnogalacturonan I containing homogalacturonan inhibits colon cancer cell proliferation by decreasing ICAM1

expression. Carbohydr Polym. 2015;132:546–53.

60. Delaglio F, Grzesiek S, Vuister GW, Zhu G, Pfeifer J, Bax A. NMRPipe: a multidimensional spectral processing system based on UNIX pipes. J Biomol NMR. 1995;6(3):277–93.
61. Rajamäki K, Lappalainen J, Oörni K, Välimäki E, Matikainen S, Kovanen PT, et al. Cholesterol crystals activate the NLRP3 inflammasome in human macrophages: a novel link between cholesterol metabolism and inflammation. PLoS One. 2010;5(7):e11765.
62. Daigneault M, Preston JA, Marriott HM, Whyte MKB, Dockrell DH. The identification of markers of macrophage differentiation in PMA-stimulated THP-1 cells and monocyte-derived macrophages. PLoS One. 2010;5(1).
63. Mosmann T. Rapid colorimetric assay for cellular growth and survival: Application to proliferation and cytotoxicity assays. J Immunol Methods. 1983;65(1–2):55–63.
64. Sánchez-Miranda E, Lemus Baustista J, Pérez S, Pérez-Ramos J. Effect of Kramecyne on the inflammatory response in lipopolysaccharide-stimulated peritoneal macrophages. Evidence-based Complement Altern Med. 2013;(ID 762020):8 p.
65. Qiu L, Ding L, Huang J, Wang D, Zhang J, Guo B. Induction of copper/zinc-superoxide dismutase by CCL5/CCR5 activation causes tumour necrosis factor-α and reactive oxygen species production in macrophages. Immunology. 2009;128:325–34.
66. Fuentes AL, Millis L, Vapenik J, Sigola L. Lipopolysaccharide-mediated enhancement of zymosan phagocytosis by RAW 264.7 macrophages is independent of opsonins, laminarin, mannan, and complement receptor 3. J Surg Res. 2014;189:304–12.
67. Maeß MB, Sendelbach S, Lorkowski S. Selection of reliable reference genes during THP-1 monocyte differentiation into macrophages. BMC Mol Biol. 2010;11(90):8.
68. Vandesompele J, De Preter K, Pattyn F, Poppe B, Van Roy N, De Paepe A, et al. Accurate normalization of real-time quantitative RT-PCR data by geometric averaging of multiple internal control genes. Genome Biol. 2002;3(7):12.
69. Livak KJ, Schmittgen TD. Analysis of Relative Gene Expression Data Using Real-Time Quantitative PCR and the 2−ΔΔCT Method. Methods. 2001;25(4):402–8.
70. Pelegrin P, Barroso-Gutierrez C, Surprenant A. P2X7 receptor differentially couples to distinct release pathways for IL-1beta. J Immunol. 2008;180(11):7147–57.
71. Warnatsch A, Ioannou M, Wang Q, Papayannopoulos V. Neutrophil extracellular traps license macrophages for cytokine production in atherosclerosis. Science (80-). 2015;349(6245):316–20.

72. Guo H, Callaway JB, Ting JP-Y. Inflammasomes: mechanism of action, role in disease, and therapeutics. Nat Med. 2015;21(7):677–87.

73. Juliana C, Fernandes-Alnemri T, Wu J, Datta P, Solorzano L, Yu JW, et al. Anti-inflammatory compounds parthenolide and Bay 11-7082 are direct inhibitors of the inflammasome. J Biol Chem. 2010;285(13):9792–802.

74. Sun L, Feng K, Jiang R, Chen J, Zhao Y, Ma R, et al. Water-soluble polysaccharide from Bupleurum chinense DC: Isolation, structural features and antioxidant activity. Carbohydr Polym. 2010;79(1):180–3.

75. Synytsya A, Novak M. Structural analysis of glucans. Ann Transl Med. 2014;2(2):17(1-14).

76. Iorio E, Torosantucci A, Bromuro C, Chiani P, Ferretti A, Giannini M, et al. Candida albicans cell wall comprises a branched β-d-(1,6)-glucan with β-d-(1,3)-side chains. Carbohydr Res. 2008;343(6):1050–61.

77. Amari M, Arango LFG, Gabriel V, Robert H, Morel S, Moulis C, et al. Characterization of a novel dextransucrase from Weissella confusa isolated from sourdough. Appl Microbiol Biotechnol. 2013;97(12):5413–22.

78. Cheng HN, Neiss TG. Solution NMR Spectroscopy of Food Polysaccharides. Polym Rev. 2012;52(2):81–114.

79. Dertli E, Colquhoun IJ, Gunning AP, Bongaerts RJ, Le Gall G, Bonev BB, et al. Structure and biosynthesis of two exopolysaccharides produced by lactobacillus johnsonii FI9785. J Biol Chem. 2013;288(44):31938–51.

80. Maina NH, Tenkanen M, Maaheimo H. NMR spectroscopic analysis of exopolysaccharides produced by Leuconostoc citreum and Weissella confusa. Carbohydr Res. 2008;343:1446–55.

81. Wang P, Henning SM, Heber D. Limitations of MTT and MTS-based assays for measurement of antiproliferative activity of green tea polyphenols. PLoS One. 2010 Jan;5(4):e10202.

82. Xaus J, Comalada M, Valledor AF, Cardó M, Herrero C, Soler C, et al. Molecular mechanisms involved in macrophage survival, proliferation, activation or apoptosis. Immunobiology. 2001;204:543–50.

83. Bordbar A, Mo ML, Nakayasu ES, Schrimpe-Rutledge AC, Kim Y-M, Metz TO, et al. Model-driven multi-omic data analysis elucidates metabolic immunomodulators of macrophage activation. Mol Syst Biol. 2012;8(558):558.

84. Parameswaran N, Patial S. Tumor necrosis factor-α signaling in macrophages. Crit Rev

Eukaryot Gene Expr. 2010;20(2):87–103.

85. Scheller J, Chalaris A, Schmidt-Arras D, Rose-John S. The pro- and anti-inflammatory properties of the cytokine interleukin-6. Biochim Biophys Acta. 2011;1813(5):878–88.

86. MacMicking J, Xie Q, Nathan C. Nitric oxide and macrophage function. Annu Rev Immunol. 1997;15(1):323–50.

87. Schepetkin IA, Quinn MT. Botanical polysaccharides: macrophage immunomodulation and therapeutic potential. Int Immunopharmacol. 2006;6(3):317–33.

88. Raghu R, Sharma D, Ramakrishnan R, Khanam S, Chintalwar GJ, Sainis KB. Molecular events in the activation of B cells and macrophages by a non-microbial TLR4 agonist, G1-4A from Tinospora cordifolia. Immunol Lett. 2009;123(1):60–71.

89. Kouakou K, Schepetkin IA, Jun S, Kirpotina LN, Yapi A, Khramova DS, et al. Immunomodulatory activity of polysaccharides isolated from Clerodendrum splendens: beneficial effects in experimental autoimmune encephalomyelitis. BMC Complement Altern Med. 2013;13(1):149.

90. Dillon S, Agrawal S, Banerjee K, Letterio J, Denning TL, Oswald-Richter K, et al. Yeast zymosan, a stimulus fro TLR2 and dectin-1, induces regulatory antigen-presenting cells and immunological tolerance. J Clin Invest. 2006;116(4):916–28.

91. Bae IY, Kim HW, Yoo HJ, Kim ES, Lee S, Park DY, et al. Correlation of branching structure of mushroom B-glucan with its physiological activities. Food Res Int. 2013;51(1):195–200.

92. Malik P, Berisha SZ, Santore J, Agatisa-Boyle C, Brubaker G, Smith JD. Zymosan-mediated inflammation impairs in vivo reverse cholesterol transport. J Lipid Res. 2011;52(5):951–7.

93. Kankkunen P, Teirila L, Rintahaka J, Alenius H, Wolff H, Matikainen S. (1,3)-beta-glucans activate both dectin-1 and NLRP3 inflammasome in human macrophages. J Immunol. 2010;184(11):6335–42.

94. Chawla A, Boisvert WA, Lee CH, Laffitte BA, Barak Y, Joseph SB, et al. A PPARγ-LXR-ABCA1 pathway in macrophages is involved in cholesterol efflux and atherogenesis. Mol Cell. 2001;7(1):161–71.

95. Venkatesan B, Valente AJ, Prabhu SD, Shanmugan P, Delafontaine P, Chandrasekar B. EMMPRIN activates multiple transcription factor pathways in cardiomyocytes, and induces interleukin-18 expression via Rac1-dependent PI3K/Akt/IKK/NF-κ B and MKK7/JNK/AP-1 signaling. J Mol Cell Cardiol. 2010;49(4):655–63.

96. Schmidt R, Bültmann A, Ungerer M, Joghetaei N, Bülbül Ö, Thieme S, et al.

Extracellular matrix metalloproteinase inducer regulates matrix metalloproteinase activity in cardiovascular cells: Implications in acute myocardial infarction. Circulation. 2006;113(6):834–41.

97. Yu S-X, Chen W, Hu X-Z, Feng S-Y, Li K-Y, Qi S, et al. Liver X receptors agonists suppress NLRP3 inflammasome activation. Cytokine. 2017;91:30–7.
98. Lopez-Castejon G, Brough D. Understanding the mechanism of IL-1β secretion. Cytokine Growth Factor Rev. 2011;22(4):189–95.
99. Miao EA, Rajan J V., Aderem A. Caspase-1-induced pyroptotic cell death. Immunol Rev. 2011;243(1):206–14.
100. Muñoz-Planillo R, Kuffa P, Martínez-Colón G, Smith BL, Rajendiran TM, Nuñez G. K+ efflux is the common trigger of NLRP3 inflammasome activation by bacterial toxins and particulate matter. Immunity. 2013;38(6):1142–53.
101. Bauernfeind F, Horvath G, Stutz A, Alnemri ES, Speert D, Fernandes-alnemri T, et al. NF-kB activating pattern recognition and cytokine receptors license NLRP3 inflammasome activation by regulating NLRP3 expression. J Immunol. 2009;183(2):787–91.
102. Latz E, Ts X, Stutz A. Activation and regulation of the inflammasomes. Nat Rev Immunol. 2013;13(6):23702978.
103. Yadav MP, Moreau R a., Hotchkiss AT, Hicks KB. A new corn fiber gum polysaccharide isolation process that preserves functional components. Carbohydr Polym. 2012;87(2):1169–75.
104. Moraes A, Sierakowski M, Amico S. The novel use of sodium borohydride as a protective agent for the chemical treatment of vegetable fibers. Fibers Polym. 2012 Jun;13(5):641–6.
105. Slaven Z, Adelle F, Alessandra R, Corrado F, Massimo R. Medicinal Mushrooms. In: Ray R, Ward O, editors. Microbial Technology in Horticulture: Volume 3. 1 st. Boca Ratón, FL, USA: CRC Press; 2008. p. 390.
106. Pramanik M, Chakraborty I, Mondal S, Islam SS. Structural analysis of a water-soluble glucan (Fr.I) of an edible mushroom, Pleurotus sajor-caju. Carbohydr Res. 2007;342(17):2670–5.
107. Lee JY, Kim YJ, Kim HJ, Kim YS, Park W. Immunostimulatory effect of laminarin on RAW 264.7 mouse macrophages. Molecules. 2012;17(5):5404–11.
108. Bittencourt VCB, Figueiredo RT, Da Silva RB, Mourão-Sá DS, Fernandez PL, Sassaki GL, et al. An α-glucan of Pseudallescheria boydii is involved in fungal phagocytosis

and toll-like receptor activation. J Biol Chem. 2006;281(32):22614–23.

109. Palencia D, Werning ML, Sierra-filardi E, Duen MT, Irastorza A, Corbı AL, et al. Probiotic properties of the 2-substituted (1,3)-β-D-glucan-producing bacterium Pediococcus parvulus. Appl Environ Microbiol. 2009;75(14):4887–91.

110. Tang C, Kamiya T, Liu Y, Kadoki M, Kakuta S, Oshima K, et al. Inhibition of dectin-1 signaling ameliorates colitis by inducing Lactobacillus-mediated regulatory T cell expansion in the intestine. Cell Host Microbe. 2015;18(2):183–97.

111. Wang S, Zhou H, Feng T, Wu R, Sun X, Guan N, et al. β-Glucan attenuates inflammatory responses in oxidized LDL-induced THP-1 cells via the p38 MAPK pathway. Nutr Metab Cardiovasc Dis. 2014;24(3):248–55.

112. Zhang H-L, Cui S-H, Zha X-Q, Bansal V, Xue L, Li X-L, et al. Jellyfish skin polysaccharides: extraction and inhibitory activity on macrophage-derived foam cell formation. Carbohydr Polym. 2014;106:393–402.

113. Duewell P, Kono H, Rayner KJ, Sirois CM, Bauernfeind FG, Abela GS, et al. NLRP3 inflamasomes are required for atherogenesis and activated cholesterol crystals that form early in disease. Nature. 2010;464(7293):1357–61.

114. Li AC, Glass CK. PPAR- and LXR-dependent pathways controlling lipid metabolism and the development of atherosclerosis. J Lipid Res. 2004;45(12):2161–73.

115. Pourcet B, Gage MC, León TE, Waddington KE, Pello OM, Steffensen KR, et al. The nuclear receptor LXR modulates interleukin-18 levels in macrophages through multiple mechanisms. Sci Rep. 2016;6:25481.

116. Patel MN, Carroll RG, Galván-Peña S, Mills EL, Olden R, Triantafilou M, et al. Inflammasome priming in sterile inflammatory disease. Trends Mol Med. 2017;23(2):165–80.

117. He Y, Hara H, Núnez G. Mechanism and Regulation of NLRP3 Inflammasome Activation. Trends Biochem Sci. 2016;41(12):1012–21.

118. Vannucci L, Krizan J, Sima P, Stakheev D, Caja F, Rajsiglova L, et al. Immunostimulatory properties and antitumor activities of glucans (Review). Int J Oncol. 2013;43(2):357–64.

119. Elder MJ, Webster SJ, Chee R, Williams DL, Hill Gaston JS, Goodall JC. β-glucan size controls dectin-1-mediated immune responses in human dendritic cells by regulating IL-1β production. Front Immunol. 2017;8:14–6.

APPENDIX A – Overview of activities (Student's sheet)

Janus - Sistema Administrativo da Pós-Graduação

Universidade de São Paulo
Faculdade de Ciências Farmacêuticas
Documento sem validade oficial
FICHA DO ALUNO

9131 - 7916647/2 - Victor Costa Castro Alves

Email:	castroalves@usp.br
Data de Nascimento:	16/12/1986
Cédula de Identidade:	RG - 2001010203710 - CE
Local de Nascimento:	Estado do Ceará
Nacionalidade:	Brasileira
Graduação:	Farmacêutico - Faculdade de Farmácia, Odontologia e Enfermagem - Universidade Federal do Ceará - Ceará - Brasil - 2011
Mestrado:	Mestre em Ciências - Área: Bromatologia - Faculdade de Ciências Farmacêuticas - Universidade de São Paulo - São Paulo - Brasil - 2014

Curso:	Doutorado
Programa:	Ciência dos Alimentos
Área:	Bromatologia
Data de Matrícula:	21/02/2014
Início da Contagem de Prazo:	21/02/2014
Data Limite para o Depósito:	21/02/2018
Orientador:	Prof(a). Dr(a). João Roberto Oliveira do Nascimento - 21/02/2014 até o presente. Email: jronasci@usp.br
Proficiência em Línguas:	Inglês, Aprovado em 21/02/2014
Data de Aprovação no Exame de Qualificação:	Aprovado em 27/11/2015
Data do Depósito do Trabalho:	
Título do Trabalho:	
Data Máxima para Aprovação da Banca:	
Data de Aprovação da Banca:	
Data Máxima para Defesa:	
Data da Defesa:	
Resultado da Defesa:	
Histórico de Ocorrências:	Primeira Matrícula em 21/02/2014

Aluno matriculado no Regimento da Pós-Graduação USP (Resolução nº 5473 em vigor de 18/09/2008 até 19/04/2013).
Última ocorrência: Matrícula de Acompanhamento em 17/07/2017
Impresso em: 08/09/2017 01:42:33

Janus - Sistema Administrativo da Pós-Graduação

Universidade de São Paulo
Faculdade de Ciências Farmacêuticas
Documento sem validade oficial
FICHA DO ALUNO

9131 - 7916647/2 - Victor Costa Castro Alves

Sigla	Nome da Disciplina	Início	Término	Carga Horária	Cred.	Freq.	Conc.	Exc.	Situação
BMH5760-3/3	Biologia das Mucosas Gástrica e Intestinal (Instituto de Ciências Biomédicas - Universidade de São Paulo)	08/04/2014	13/05/2014	60	4	100	A	N	Concluída
FBA5741-3/2	Química e Bioquímica de Alimentos I	12/09/2014	16/10/2014	60	4	100	A	N	Concluída
FBA5754-1/2	Atualização em Ciências Farmacêuticas	20/10/2014	26/10/2014	30	2	100	A	N	Concluída
FBA5742-2/2	Química e Bioquímica de Alimentos II	31/10/2014	04/12/2014	60	0	-	-	N	Turma cancelada
Atividade do Programa	Participou da Etapa de Estágio Supervisionado em Docência do Programa de Aperfeiçoamento de Ensino junto à Disciplina FBA0413 Química de Alimentos, ministrada aos alunos de graduação do curso de Farmácia e Bioquímica da Faculdade de Ciências Farmacêuticas da Universidade de São Paulo (1)	01/02/2015	30/06/2015	-	3	-	-	-	-
FBA5899-2/4	Biodisponibilidade de Nutrientes e de Substâncias Bioativas em Alimentos e Dietas	02/03/2015	12/04/2015	90	6	100	A	N	Concluída
FBA5756-1/1	Alergia Alimentar	16/03/2015	22/03/2015	30	2	100	A	N	Concluída
FBT5700-3/2	Preparo de Artigos Científicos na Área de Tecnologia Bioquímico-Farmacêutica	08/05/2015	09/07/2015	90	6	100	A	N	Concluída
Atividade do Programa	Trabalho Publicado no Food Analytical Methods, com o trabalho intitulado: "Speeding up the Extraction of Mushroom Polysaccharides", páginas 2429 a 2433, Estados Unidos da América - 2016 (2)	06/02/2016	06/02/2016	-	2	-	-	-	-
Atividade do Programa	Trabalho Publicado no Food Research International, com o trabalho intitulado: "Polysaccharides from raw and cooked chayote modulate macrophage function", páginas 171 a 179, Estados Unidos da América - 2016 (2)	20/02/2016	20/02/2016	-	2	-	-	-	-
Atividade do Programa	Trabalho Publicado no International Journal of Biological Macromolecules, com o trabalho intitulado: "Characterization and immunomodulatory effects of glucans from Pleurotus albidus, a promising species of mushroom for farming and biomass production", páginas 215 a 223, Estados Unidos da América - 2016 (2)	19/11/2016	19/11/2016	-	2	-	-	-	-

	Créditos mínimos exigidos		Créditos obtidos
	Para exame de qualificação	Para depósito de tese	
Disciplinas:	0	20	33
Estágios:			
Total:	0	20	33

Créditos Atribuídos à Tese: 167

Observações:

1) Créditos atribuídos de acordo com o disposto na Portaria GR-3588 e GR-4391 - PAE, de 31.08.09 e aprovados pela Comissão de Pós-Graduação, em Sessão de 08/03/2017.

2) Créditos atribuídos de acordo com o Artigo 64 do Regimento de Pós-Graduação e aprovados pela Comissão de Pós-Graduação, em Sessão de 08/03/2017.

Conceito a partir de 02/01/1997:

A - Excelente, com direito a crédito; B - Bom, com direito a crédito; C - Regular, com direito a crédito; R - Reprovado; T - Transferência.

Um(1) crédito equivale a 15 horas de atividade programada.

Última ocorrência: Matrícula de Acompanhamento em 17/07/2017

Impresso em: 08/09/2017 01:42:33

Janus